

Design and Characterization of Spiral Photonic Crystal Fiber for Wideband Residual Dispersion Compensation

by



(Japatosh Mondal)

A thesis submitted in partial fulfillment of the requirements for the degree of
Master of Science in Electrical and Electronic Engineering



Khulna University of Engineering & Technology
Khulna 9203, Bangladesh
August, 2015

DEDICATION

To My Parents & Honorable Teachers

Declaration

This is to certify that the thesis work entitled "Design and Characterization of Spiral Photonic Crystal Fiber for Wideband Residual Dispersion Compensation" has been carried out by Japatosh Mondal in the Department of Electrical and Electronic Engineering, Khulna University of Engineering & Technology, Khulna, Bangladesh. The above thesis work or any part of this work has not been submitted anywhere for the award of any degree or diploma.



Signature of Supervisor

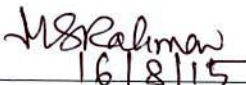


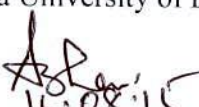
Signature of Candidate


Approval


This is to certify that the thesis work submitted by **Japatosh Mondal** entitled "Design and Characterization of Spiral Photonic Crystal Fiber for Wideband Residual Dispersion Compensation" has been approved by the board of examiners for the partial fulfillment of the requirements for the degree of *Master of Science in Electrical and Electronic Engineering* from the Department of Electrical and Electronic Engineering, Khulna University of Engineering & Technology, Khulna, Bangladesh in August 2015.


BOARD OF EXAMINERS

1. 
16/8/15

Dr. Mohammad Shaifur Rahman
Professor
Department of Electrical and Electronic Engineering
Khulna University of Engineering & Technology
Chairman
(Supervisor)
2. 
16.08.15

Head of the Department
Department of Electrical and Electronic Engineering
Khulna University of Engineering & Technology
Member
3. 

Dr. Md. Rafiqul Islam
Professor
Department of Electrical and Electronic Engineering
Khulna University of Engineering & Technology
Member
4. 

Dr. Mostafa Zaman Chowdhury
Associate Professor
Department of Electrical and Electronic Engineering
Khulna University of Engineering & Technology
Member
5. 
16.08.2015

Dr. S. M. Abdur Razzak
Professor
Department of Electrical and Electronic Engineering
Rajshahi University of Engineering & Technology
Member
(External)

Abstract

This thesis presents modeling and analysis of broadband dispersion compensating photonic crystal fibers (DC-PCFs) for dispersion compensation of standard single mode fibers (SMFs). Nearly Zero Dispersion Fiber (NZDF) is being proposed for zero dispersion wavelengths (ZDW). To get NZDF and DCF, GeO₂ doped defected SiO₂ square in the core with spiral air hole arms (dd-SPCF) and three different PCF models such as three rings spiral photonic crystal fiber (three rings-SPCF), spiral photonic crystal fiber-distribution sunflower seeds (distribution sunflower seeds-SPCF) and spiral photonic crystal fiber-nautilus shell (nautilus shell-SPCF) have been designed and their guiding properties are analyzed. A perfectly matched layer (PML) circular boundary has been used to calculate the confinement loss. The proposed dd-SPCF shows ultrahigh nonlinearity $76.44 \text{ W}^{-1}\text{km}^{-1}$, and dispersion characteristics $-0.0001693 \text{ ps/km-nm}$ with very low effective area $2.6516 \mu\text{m}^2$ at 1550nm . The proposed three rings-SPCF exhibits average dispersion coefficients of $-355.898 \text{ ps/nm-km}$ with a dispersion variation of 11.8 ps/nm-km within the wavelengths of $1450\text{-}1700\text{nm}$. However, nonlinear coefficient of three rings-SPCF is not found so high and particularly in $39.9333 \text{ W}^{-1}\text{km}^{-1}$ at 1550 nm wavelength. In the same way, birefringence is in the order of about 10^{-2} . On the other hand, distribution sunflower seeds-SPCF offers almost flat dispersion profile with average dispersion coefficients of -609.321601 and $-396.32923 \text{ ps/(nm km)}$ with a dispersion variation of 9.34 ps/(nm km) for X and Y-polarization, respectively, within the wavelengths of $1350\text{-}1600$ and $1350\text{-}1800\text{nm}$. Finally, nautilus shell-SPCF achieves average dispersion coefficients of -341.73 ps/nm-km with a dispersion variation of 5.02 ps/nm-km within the wavelengths of $1350\text{-}1700\text{nm}$ with a high birefringence of 0.0231 which is higher than other proposed DC-PCFs. Furthermore, the dispersion slope of the proposed DC-PCFs have been determined and the nautilus shell-SPCF is more appropriate than others for dispersion compensation covering entire E to U band and slope is 0.006195 around 1550nm . Also, this research has explored effective area, confinement losses, and dispersion behavior for fiber's global diameter variations and fiber's structural parameters variation. This work has, at the same time, identified that the structural parameters and global diameter variations do not affect significantly the dispersion accuracy of the proposed DC-PCFs.

ACKNOWLEDGEMENT

First and foremost, I would like to express my sincere and utmost gratitude to my supervisor, Professor Dr. Mohammad Shaifur Rahman. His understanding, encouragement, motivation and expert guidance have provided me with a good basis for this entire research work. His technical and editorial advice has been of tremendous significance for the completion of this dissertation. I am grateful for all his erudite support and cooperation including his precious time and patience.

I would also like to mention with gratitude the support of Dr. S. M. Abdur Razzak, Head of Department of Electrical and Electronic Engineering, Rajshahi University of Engineering & Technology and his research students. With academic commitment they have endowed me with valuable suggestions throughout my research. Further, I extend my thankfulness and sincere appreciation to Dr. Md. Rafiqul Islam (1), Dr. Ashraful Ghani Bhuiyan, Dr. Md. Rafiqul Islam (2), and Dr. Mostafa Zaman Chowdhury. Also, I am greatly indebted to all my faculty colleagues in Bangabandhu Sheikh Mujibur Rahman Science and Technology University (BSMRSTU) for their kind cooperation that helped me enjoy an excellent work environment during past years.

Without the support of all respected teachers and members of the department of EEE, KUET my work would not find any meaningful end. Therefore I earnestly thank them for their help over the years.

Specially, my profound thanks go to the chairman and the members of the dissertation committee for their valuable comments which were supportive in enriching the quality of my thesis.

Finally, thanks to dear friend Nibir Mondol for his strong support, friendship and suggestions before thesis defense. His continuous support helped me for better preparation.

Last but not least, the most sincere thanks go as always, to parents for their strong faith, unconditional love and trust. Thanks for supporting in every step of the way and for constantly being with me.

Author

Contents

Abstract	i
Acknowledgement	ii
List of Figures	vi
List of Tables	xi

1. Introduction

1.1 Background	1
1.2 Motivation	3
1.3 Literature review	4
1.4 Objectives of the thesis	6
1.5 Thesis outline	7
1.6 Summary.....	7

2. Fundamentals of Photonic Crystal Fiber

2.1 Introduction.....	12
2.2 Light spectrum and telecommunication band.....	12
2.3 Construction and basic principles of PCF.....	14
2.4 Classifications of PCF.....	16
2.4.1 Positive core-cladding index difference.....	17
2.4.2 Negative core-cladding index difference.....	18
2.5 Comparison between PCF and conventional fiber.....	20
2.6 Guiding properties of the PCF.....	21
2.6.1 Chromatic dispersion	21
2.6.2 Birefringence	22
2.6.3 Single mode or multimode response	22
2.6.4 Mode field diameter and effective area	23
2.6.5 Confinement loss	24

2.6.6	Bending loss	24
2.7	Fabrication technology of PCFs	25
2.7.1	Extrusion and filling technology	26
2.7.2	Sol-gel technique for fabricating irregular shaped PCF	28
2.7.3	SCF fabrication with soft materials.....	28
2.8	Applications of PCFs.....	29
2.8.1	PCF in fiber optic communication	29
2.8.2	PCF for Super-continuum Generation	30
2.8.3	PCF for Sensing Technology.....	30
2.9	Conclusion	31

3. Numerical Modeling and Analysis of DC-SPCFs

3.1	Introduction.....	34
3.2	Numerical methods.....	34
3.2.1	FEM formulation.....	37
3.2.2	Domain discretization.....	38
3.2.3	Boundary conditions.....	38
3.3	Step by step analysis.....	40
3.4	Determination of the modal properties of PCF.....	40
3.4.1	Chromatic dispersion.....	41
3.4.2	Dispersion length.....	41
3.4.3	Nonlinear length.....	42
3.4.4	Walk off length.....	42
3.4.5	Dispersion slope and RDS.....	42
3.4.6	Effective dispersion.....	43
3.4.7	Confinement loss.....	43
3.4.8	Birefringence.....	44
3.4.9	Effective area.....	45
3.4.10	Numerical aperture.....	45
3.4.11	Single and multimode response.....	45
3.5	Conclusion.....	46

4. Analysis of Spiral Photonic Crystal Fiber	
4.1 Introduction.....	49
4.2 Requirements of nearly zero dispersion fibers (NZDFs) at operating wavelength...	50
4.3 Structure of SPCF with GeO ₂ doped defected SiO ₂ square in the core.....	51
4.4 Numerical simulation using COMSOL Multiphysics 4.2.....	52
4.4.1 Simulation results of GeO ₂ doped defected SiO ₂ square core SPCF.....	52
4.5 Conclusion.....	66
5. Design and Characterization of Broadband DC-SPCF	
5.1 Introduction.....	68
5.2 Requirements for broadband dispersion and dispersion slope compensation.....	68
5.3 Proposed DC-PCF models.....	69
5.3.1 Structure of SPCF with defected elliptical core.....	69
5.3.2 Structure of SPCF (distribution sunflower seeds) with defected elliptical core.....	70
5.3.3 Structure of SPCF (nautilus shell) with defected elliptical core.....	72
5.4 Numerical simulation using COMSOL Multiphysics 4.2.....	73
5.4.1 Simulation results of three rings SPCF.....	74
5.4.2 Simulation results of SPCF (distribution sunflower seeds).....	83
5.4.3 Simulation results of SPCF (nautilus shell).....	92
5.5 Comparison between proposed DC-PCFs and some other DC-PCFs.....	99
5.6 Conclusion.....	102
6. Conclusions and Directions for Future Work	
6.1 Conclusion.....	106
6.2 Directions for future work.....	108

List of Figures

2.1	Electromagnetic spectrum	13
2.2	Optical attenuation characteristics of silica fiber and the telecom windows	13
2.3	(a) Standard hollow capillary (b) PBG based hollow core PCF (c) TIR (Total Internal Reflection) based solid core PCF (Scanning Electron Microscope on the right)	14
2.4	A schematic diagram hollow core PCF cross section	15
2.5	Schematic cross sections and index-profiles of (a) IG-PCFs (the dotted circle in the center indicates an omitted air-hole) and (b) PBG-PCFs (the larger circle in the center represents the core)	16
2.6	Various PCF structures reported in the literature: (a) hexagonal solid-core PCF, (b) cobweb PCF, (c) hexagonal hollow-core PCF, (d) honeycomb PCF and (e) spiral PCF	17
2.7	Types of PCFs (a) PM-PCF, (b) HA-PCF, (c) HNL-PCF, and (d) Bragg Fiber- a special type of HC-PCF	19
2.8	Total internal reflection of light through optical fiber	20
2.9	Schematic cross sections and index-profiles of (a) PCFs (a missing air-hole in the center represents the core) and (b) Ordinary fibers	20
2.10	Dispersion phenomena in an optical fiber	22
2.11	Mode diagram of PCF	23
2.12	Shows the intensity distribution of a light beam inside a fiber	23
2.13	Confinement losses in index-guiding PCF	24
2.14	A bending loss in optical fiber	25
2.15	Conventional setup of fabricating regular shaped PCFs	25
2.16	(a) Sketch of extrusion process and (b) extrusion die concepts with equal and different size feed holes for a target perform structure having 60 holes (4 rings), white filled circles are blocking elements, black and red circles are feed holes	26
2.17	Fig. 2.15 Scanning-electron-micrograph image of a cleaved end-face of a germanium-filled endlessly single mode PCF. Germanium wire is on the right side (dwire = 1.6 μm)	27
2.18	Schematic representation of sol gel fabrication technique	28
2.19	Basic LRFA structure based on Photonic Crystal Fiber	30

2.20	Experimental setup for sensing with Suspended Core Fiber	31
3.1	Summary of the techniques used for the analysis of PCFs	34
3.2	Finite elements in two dimensions	38
3.3	PML region surrounding the waveguide structure	39
3.4	The PCF with 6 circular air holes in its cladding, the FEM mesh and the computational window	40
3.5	Dispersion slope variation	43
4.1	Structure of the proposed SPCF for NZDF	51
4.2	Plots of refractive index as function of wavelength for Silica Glass, GeO ₂ and GeO ₂ doped SiO ₂ square defected core with GeO ₂ doping conc. X= 45.47%	52
4.3	Dispersion curves of the proposed NZDF with circular air holes arrange for optimum design parameters	53
4.4	Contour plot of electric field at (a) 750 nm, and (b) 1550 nm wavelengths	54
4.5	Dispersion properties of dd-SPCF and effects of changing pitch, Λ keeping all others parameters constant	55
4.6	Dispersion properties of dd-SPCF: optimum dispersion and effects of changing a	55
4.7	Dispersion properties of dd-SPCF: optimum dispersion and effects of changing d ₁	56
4.8	Dispersion properties of dd-SPCF: optimum dispersion and effects of changing d ₂	56
4.9	Dispersion properties of dd-SPCF: optimum dispersion and effects of changing d ₃	57
4.10	Dispersion properties of dd-SPCF: optimum dispersion and effects of changing d ₄	57
4.11	Comparison of dispersion properties of dd-SPCF and effects of changing d ₁ , d ₂ , d ₃ and d ₄	58
4.12	Effective area of the proposed dd-SPCF for optimum design parameters and $\pm 2\%$ variation of d ₁	59
4.13	Effective area of the proposed dd-SPCF for optimum design parameters and +2% variation of d ₁ , d ₂ , d ₃ and d ₄	59
4.14	Effective area of the proposed dd-SPCF for optimum design parameters and $\pm 2\%$ variation of a	60
4.15	Effective area of the proposed dd-SPCF for optimum design parameters in changing parameter Λ	60
4.16	Non-linear coefficient of the proposed dd-SPCF for optimum design parameters and $\pm 2\%$ variation of d ₁	61
4.17	Non-linear coefficient of the proposed dd-SPCF for optimum design parameters	61

	and $\pm 2\%$ variation of a	
4.18	Non-linear coefficient of the proposed dd-SPCF for optimum design parameters in changing parameter Λ	62
4.19	Confinement loss of the proposed dd-SPCF for optimum design parameters and $\pm 2\%$ variation of d_1	62
4.20	Confinement loss of the proposed dd-SPCF for optimum design parameters and $\pm 2\%$ variation of d_2	63
4.21	Confinement loss of the proposed dd-SPCF for optimum design parameters and $\pm 2\%$ variation of d_3	63
4.22	Confinement loss of the proposed dd-SPCF for optimum design parameters and $\pm 2\%$ variation of d_4	64
4.23	Confinement loss of the proposed dd-SPCF for optimum design parameters and $\pm 2\%$ variation of a	64
4.24	Confinement loss of the proposed dd-SPCF for optimum design parameters in changing parameter Λ	65
5.1	Structure of the proposed three rings SPCF for broadband dispersion compensation	70
5.2	Structure of the proposed six rings SPCF for broadband dispersion compensation	71
5.3	Elliptical core with circular air holes	71
5.4	Defected elliptical core in central region	71
5.5	Structure of the proposed SPCF (nautilus shell) for broadband dispersion compensation	72
5.6	Dispersion as functions of thickness of PML in core region	74
5.7	Dispersion of the three rings SPCF with a variation of $\pm 2\%$ for all parameters	75
5.8	Chromatic dispersion for X-polarization of variation of r_e of three rings SPCF	75
5.9	Birefringence of three rings SPCF with a variation of $\pm 2\%$ for all parameters	76
5.10	Birefringence variance with respect to r_e of three rings SPCF	77
5.11	Wavelength response of chromatic dispersion of the proposed three rings SPCF for both x- and y-polarization for the optimum design parameters	77
5.12	Electric field for X-polarization and Y-polarization at 1500nm of the proposed three rings SPCF	78
5.13	Effective area of the proposed three rings SPCF for re optimum design parameters	78
5.14	Nonlinear coefficient of the three rings SPCF with a variation of $\pm 2\%$ for all parameters	79

5.15	Influence of r_e on non-linearity of the proposed three rings SPCF	79
5.16	Dispersion slope of three rings SPCF for optimum design parameters	80
5.17	Dispersion compensation ratio of three rings SPCF for optimum design parameters	81
5.18	Variation of effective dispersion against wavelength of 1.825 km long optimized three rings SPCF to compensate for a 40 km long standard SMFs	81
5.19	Confinement loss of the proposed three rings SPCF for the optimum parameters	82
5.20	Variation of effective V-parameter of the proposed three rings SPCF for optimum design parameters	82
5.21	Comparison between chromatic dispersion	84
5.22	Dispersion with respect to thickness of PML of the proposed six rings SPCF	84
5.23	Chromatic dispersion for X-polarization of the proposed six rings SPCF	85
5.24	Chromatic dispersion for Y-polarization of the proposed six rings SPCF	86
5.25	Electric field for X-polarization at r_e of 0.21 μ m and 0.23 μ m	86
5.26	Electric field for Y-polarization at r_e of 0.21 μ m and 0.23 μ m	86
5.27	Birefringence variance with respect to r_e of the proposed six rings SPCF	87
5.28	Effective area of the proposed six rings SPCF for re optimum design parameters	88
5.29	Influence of r_e on non-linearity of the proposed six rings SPCF	88
5.30	Dispersion slope of six rings SPCF for optimum design parameters	89
5.31	Dispersion compensation ratio of six rings SPCF for optimum design parameters	90
5.32	Variation of effective dispersion against wavelength of 1.1427km long optimized six rings SPCF to compensate for a 40 km long standard SMFs	90
5.33	Confinement loss of the proposed six rings SPCF for the optimum parameters	91
5.34	Variation of effective V-parameter of the proposed six rings SPCF for optimum design parameters	91
5.35	Chromatic dispersion for Y-polarization of the proposed nautilus shell-SPCF	93
5.36	Chromatic dispersion for X-polarization of the proposed nautilus shell-SPCF	93
5.37	Birefringence variance with respect to r_e of the proposed nautilus shell-SPCF	94
5.38	Electric field for X and Y-polarization at 1550nm of the proposed nautilus shell-SPCF	94
5.39	Effective area of the proposed nautilus shell-SPCF for re optimum design parameters	95
5.40	Influence of r_e on non-linearity of the proposed nautilus shell-SPCF	95
5.41	Dispersion slope of nautilus shell-SPCF for optimum design parameters	96

5.42	Dispersion compensation ratio of nautilus shell-SPCF for optimum design parameters	96
5.43	Variation of effective dispersion against wavelength of 1.9927 km long optimized nautilus shell-SPCF to compensate for a 40 km long standard SMFs	97
5.44	Confinement loss of the proposed nautilus shell-SPCF for the optimum parameters	97
5.45	Variation of effective V-parameter of the proposed nautilus shell-SPCF for optimum design parameters	98
5.46	Comparison between relative chromatic dispersion for the proposed DC-PCFs	100
5.47	Comparison between birefringence for the proposed DC-PCFs	101
5.48	Comparison between dispersion slope for the proposed DC-PCFs	101
5.49	Comparison between non-linear coefficients for the proposed DC-PCFs	102

List of Tables

Table I	Electromagnetic band	14
Table II	Comparison between properties of the proposed NZDF and other NZDFs	65
Table III	Comparison between properties of the proposed DC-PCFs and other DC-PCFs	99

CHAPTER I

Introduction

1.1 Background

In the history of telecommunication, the innovation of optical fiber is one the most significant achievement in telecommunication systems. Today optical fiber cable is the backbone of the telecommunication system because of its many exclusive and attractive features [1]. The fiber cable provides signal transmission over longer distances with lowest noise and improves data rates which are our main goal in communication system. Moreover, optical fiber is also being used in non-telecommunication systems such as remote sensing, medical imaging, illuminations, sensing temperature or strain in some environment, or generating and amplifying laser light, machining and welding applications because of its small size, light weight, chemically inertness, high bandwidth, long repeater span, invulnerability, less signal degradation and many other laudable properties [2]. This necessarily resulted in application specific fiber design for controlling the near field of an optical mode along the propagation axis. Photonic Crystal Fiber (PCF) is a variant of the micro structured fibers with superior control of guiding properties. Such a vital photonic component has versatile applications in optical communications ranging from nonlinear optical signal processing to high power fiber amplifiers [3]. An optical fiber is an optical waveguide made usually of glass (silica) or plastic and it is used to guide light along its length. It achieves this by exploiting the principle of total internal reflection (TIR) [4] whereby the light is confined within the core of the optical fiber as light travels along its length. The core has a refractive index slightly higher than that of the cladding and this enables the light to be trapped within the core as it travels along the length of the fiber. This type of optical fiber is known as conventional optical fiber. Conventional fibers are used in both telecom and non-telecom applications, but ordinary optical fibers cannot suit certain emerging applications because the properties such as tailoring of conventional optical fiber are very difficult and silica glass are not flexible. To overcome the limitations of conventional optical fibers, photonic crystal fiber (PCF) is an another potential breakthrough in fiber optics technology [5] which is also called the holey optical fiber (HOF) or microstructure optical fiber (MOF). PCF structures can vary according to their applications; the design flexibility is very large and designers can use many different, fascinating and odd air-holes patterns to achieve specific PCF parameters. It also can be designed to carry higher power than conventional fiber and their wavelength dependent

properties can be manipulated to improve their performance in certain applications. Generically PCFs can be defined as optical fibers with a built-in microstructure, in most cases consisting of small air holes in silica (SiO_2). As a result, the entire structure forms silica-air microstructure arranged periodically over much of the cross-section, usually as a "cladding" surrounding a core where light is confined [6] that causes lower refractive index in the cladding region and higher refractive index in the core. Depending on their internal construction, PCF can be divided into different categories where air holes can be arranged in a periodic or an aperiodic fashion as like as photonic band gap (PBG) fiber-PCFs are formed by concentric rings of multilayer film, holey fibers (HFs) -PCFs using air holes in their cross-sections, hole assisted fiber - PCFs guiding light by a conventional higher index core modified by the presence of air-holes, and the Bragg fiber. On the other hand, the core of PCF may be either solid or hollow and the light guiding mechanism within PCF completely depends on the construction of core. In case of solid core PCF, the form of light through the fiber based on the modified TIR mechanism. On the contrary, the PCF with hollow core guides light using photonic band gap (PBG) mechanism where the refractive index of the core is less than the refractive index of the cladding [7]. Band gap fibers with hollow cores can potentially circumvent limits imposed by available materials, for example to create fibers that guide light at wavelengths for which transparent materials are not available because the light is primarily in the air, not in the solid materials. Another potential advantage of a hollow core is that one can dynamically introduce materials into the core such as a gas that is to be analyzed for the presence of some substance [8]. Modulating some parameters of the silica-air microstructure, it is possible to tune the dispersion properties of the PCF which helps to specially design the broadband dispersion compensating fiber (DCF). In addition, it offers a wide variety of possibilities as a result of the variable air-holes arrangements possible. This means it is easier to control the index contrast between the core and cladding unlike in the conventional optical fibers which leads to some unique optical properties like high birefringence [9], very high nonlinearities[10], large mode areas[11], endlessly single mode operation [12], ultra-flattened and nearly zero chromatic dispersion [13], supercontinuum generation [14] and many others. Hence, PCFs can easily outperform conventional fibers in many linear and nonlinear applications of scientific and technological areas due to easy controlling of guiding properties.

1.2 Motivation

Throughout the last two decades, there has been significant activity in the development of photonic crystal fibers that can confine, control and route light to modern electronic devices, namely nanometer scale. So, the design of PCF is a great invention of fiber history. A potentially unlimited range of geometric arrangements such as air hole shape, dimension and position permits control the optical properties, improving some of the characteristics in comparison to conventional optical fibers. The most useful feature of PCFs is that they can be fabricated using one material only in contrast to conventional single-mode fibers which require two or more materials. This unique feature does not only simplify the manufacturing process of the fiber, but it also reduces fiber losses due to material absorption. Already microstructured optical fibers (MOFs) have various significant applications in various scientific domains, like nonlinear optics [15], telecommunications or medical sciences. For example, medical sector requires lasers at new wavelengths or broadband light sources for diagnosis whereas the sensor industry is searching for environmental sensors. Biosensor [16] is another chemical sensing device in which biologically derived recognition entity to develop a quantitative development of some biochemical parameter. It depends on optical fiber, surface plasmon resonance and planar waveguide, but PCF are desirable for their highly sensitive, often non-destructive analyte analysis. Considering the telecommunication sector, PCF has made it to be an attractive optical waveguide in which several important optical properties such as more efficient dispersion compensator [17]-[18], large mode area, high birefringence [19]-[20], high nonlinearity [20], and low-cost fibers. PCF can be made either hollow core or solid core in respect to various emerging sectors [21]. All these crucial tasks are great technological challenges to be solved. However, the fast development of optical fiber network and the boost data rates compels serious chromatic dispersion in elongated transmission distances [22]. The dispersion causes pulse spreading must be compensated in the long distance optical data transmission system to suppress the spreading of pulse. In addition, optical sources of different wavelengths are being widely used nowadays for optical communication. Hence, the best approach is to nullify the positive chromatic dispersion for a large bandwidth of wavelengths. As well as, highly birefringent PCFs are used to eliminate polarization mode coupling and polarization-mode dispersion. In view of the immense growth of broadband communication, this thesis is to contribute in designing more efficient broadband dispersion compensating fiber with high birefringence using PCF.

1.3 Literature review

The research group of Philip St. J. Russell is pioneered in 1990s, have developed the photonic crystal fibers and the exploration of possible applications have been attracted due to its great variety. The first exhibition of the microstructure fiber (MOF) was reported by Knight et al. [23] in 1996, PCF research has been launched and since then, research field on PCF is growing day by day due to its advance facilities in optical properties which are not possible with conventional optical fiber. Knight et al. have established a MOF with periodic air-holes arranged in a hexagonal lattice [24] and exposed that MOF is similar to conventional fiber where light is guided by modified total internal reflection. Nevertheless, the major differences between the conventional fibers and the PCFs were in terms of design space, various controlling parameters and optical properties. In this thesis, focus will be given on broadband dispersion compensation technique with a flattened profile using PCF and nearly zero dispersion fiber (NZDF) with very low effective area. Our aim is to design and characterize of PCFs for nearly zero dispersion fiber (NZDF) with very low effective area, making it very suitable candidate in nonlinear optical applications and for broadband dispersion compensation of single mode fiber (SMF) that will compensate both chromatic dispersion and polarization mode dispersion (PMD) in which polarization states have been maintained using high birefringence PCFs. In order to analyze various types of holey fibers, several techniques have been investigated such as Hermite-Gaussian functions, imaginary-distance beam propagation method, plane-wave expansion method, perturbation approach and numerical techniques. A hermite-Gaussian function is applied to determine such properties as mode-field area and waveguide dispersion in terms of the size or arrangement of the air holes. Steel and Osgood used a plane-wave expansion method to calculate modal fields and dispersion characteristics [25]. The weak point of the method is that only the real part of the propagation constant can be calculated. Ranka et al. utilized an imaginary-distance beam propagation method, which takes into account the polarization effect, to calculate waveguide dispersion and modal field distributions [26]. For the calculation of chromatic dispersion in photonic crystal fibers, Laegsgaard et al. applied a perturbation approach to account for the frequency dependency of dielectric constants [27]. They also investigated how well dispersion curves converge with respect to supercell size for the fundamental defect modes of both index-guiding and photonic band gap fiber structures. Numerical techniques have also been widely used in the analysis and design of holey fibers. In surveying the purpose of micro-structured fiber as zero dispersion wavelength fiber, K. Saitoh and M. Koshiba shows dispersion of 0.304 ps/nm-km at 1550 nm but shows large

effective area [28]. To take even closer to zero dispersion, M. Sajjad Hossain et al. proposed GeO₂ doped SiO₂ square defected core hexagonal PCF that presents dispersion 0.0001787 ps/nm-km at 1550 nm with effective area 3.03 μm^2 [29]. So, the key concern for nearly zero dispersion fiber (NZDF) with very small effective area and high nonlinearity is achieved for soliton pulse and supercontinuum generation (SCG). The weakness point of [28] is that does not describe non-linear coefficient and [29] represents small non-linear coefficient at operating wavelength. However, nearly zero dispersion fiber design can be achieved further. Moreover, small effective area with high nonlinear gain which can be used for Super Continuum Generation, Four Wave Mixing and other nonlinear applications. In exploring the application of holey fiber as a dispersion-compensating fiber, Shen et al. designed photonic crystal fibers which exhibit large negative dispersion up to -474.5 ps/nm-km [30]. Cucinotta et al. utilized the vector finite element method to analyze the effects of hole geometrical variations in propagation properties of holey fibers [31]. Several dispersion management approaches such as fiber Bragg gratings, optical phase conjugation technique and Dispersion Compensating Fibers (DCFs) has been proposed. Among them, DCFs are widely used in commercially to nullify the positive chromatic dispersion for a large bandwidth of wavelengths [32]. In order to reduce the length of DCF, we need high negative dispersion [33]. In addition, high negative dispersion of DCFs is needed to be achieved over a wide range of wavelength for Wavelength Division Multiplexing (WDM) transmissions [34]. Hence, compensation of dispersion and dispersion slope are simultaneously obligatory. However, the major pitfall of conventional DCF is that a high negative dispersion peak is obtained only at a particular wavelength instead of a broad range [35]-[36] which was not flattened profile. So, the key issue for broadband dispersion compensation is to achieve a large negative dispersion over a wide band of wavelength. Recently, Photonic Crystal Fibres (PCFs) have gained attentions in many fields due to its novel properties such as controllable dispersion, birefringence and nonlinearity. Now it has become a promising candidate for addressing the issue of broadband dispersion compensation by serving higher negative dispersion over a wide band of wavelength than that of conventional DCFs [37]. PCF with hexagonal structure is proposed in [38] to compensate dispersion over 1360-1640 nm wavelength range but the negative dispersion with birefringence is not sufficiently large in flattened profile. Modified Octagonal-PCF has been studied in [39] which achieves negative dispersion of only -239.5 ps/(nm.km) at 1.55 μm with 90% slope matching. Although, high negative dispersion is achieved in [40] but available bandwidth for dispersion compensation is narrow and no effort was made to match

RDS. Recently, PCF for dispersion compensation of SMFs have been proposed in [36],[41] using five air-hole rings. Hexagonal PCF [36] shows perfect RDS matching but exhibits insufficient negative dispersion of -130 to -360 ps/(nm.km) in a 1.30-1.60 μm wavelength range. Square-lattice PCF [41] reports a negative dispersion of -204.4 ps/(nm.km) and RDS of 0.003543 nm^{-1} at 1.55 μm wavelength. In particular, nonlinearity can diminish the footprint and power consumption of various optical mechanism which is reported in [42] but dispersion flattened near zero. Spiral photonic crystal fiber (SPCF) [43] shows highly nonlinear and large birefringence which tends to nearly zero-dispersion flattened. Slot spiral silicon photonic crystal fiber [20] reports the property of both high birefringence and high nonlinearity but large negative chromatic dispersion is omitted. In contrast, equiangular spiral photonic crystal fiber (ES-PCF) [18] exhibits a large negative dispersion of -227 ps/(nm.km) with a dispersion variation of 11 ps/nm-km. However, a large negative dispersion with low dispersion variation can be achieved further. Moreover, high birefringence property is required to eliminate the effect of Polarization Mode Dispersion (PMD). Therefore, increasing the birefringence property can also be a good candidate for study. The current studies are purely theoretical, but fiber parameters cannot be controlled precisely in fabrication and sometimes can affect the results rigorously. Previous research indicated that variation of $\pm 2\%$ in the fiber diameter may occur during the fabrication process [44]. So, there is a still need for large negative dispersion with flattened profile, high birefringence and large nonlinearity over a wide range of wavelength with 100% slope matching in fabrication process.

1.4 Objectives of the thesis

The broad aim of the work undertaken in this thesis is the design, characterization and optimization of certain PCFs for potential uses in several practical applications and showing an improvement in performance over that seen with current optical systems. The primary objective of this research is the development of a technique to design the Nearly Zero Dispersion Fiber (NZDF) and Dispersion Compensating Fiber (DCF) in fiber lengths to address the dispersion compensation issues of SMFs in WDM applications. The proposed PCFs structures would be designed to meet the following requirements-

- i. To achieve nearly zero dispersion fiber with small effective area at operating wavelength

- ii. To offer average high negative dispersion over a wide range of wavelengths to compensate the chromatic dispersion of WDM system.
- iii. To achieve a flattened negative dispersion over E+S+C+L+U wavelength bands
- iv. To minimize the effect of PMD by introducing high birefringence property in the proposed dispersion compensating PCF.
- v. To get large nonlinearity by using only one material for dispersion compensating fiber.
- vi. To reduce the length of proposed dispersion compensating PCF by introducing high negative dispersion.
- vii. To investigate the dispersion compensating properties of the proposed PCF considering fabrication tolerance.

The final objective is to show that this technique is conducive to commercial development.

1.5 Thesis outline

Chapter I discusses general introduction of the thesis where optical communications in general starting with looking back at the history of the development over the years and reflects on the applications and advantages of optical communications and Chapter II focuses the discussion on Photonic Crystal Fibres (PCF) which are fundamental concepts of PCF in brief. Chapter III presents a brief discussion about the numerical computational methods for mode solutions of PCF and necessary equations to evaluate the light guiding properties of the designed PCF. Chapter IV concerns analysis of spiral photonic crystal fiber that proposes nearly zero dispersion fibers as a Single Mode Fiber (SMF). Chapter V presents scopes and constrains of designing dispersion compensating PCF, an optimum dispersion compensating PCF design, its modal properties including dispersion, effective refractive index, effective dispersion, relative dispersion slope and birefringence, potential applications. Hence, Chapter IV and Chapter V also include a comparison of properties between the designed PCFs and other similar PCFs in the peer reviewed literature. Finally, Chapter VI includes conclusion and scopes for further study.

1.6 Summary

The general background of PCF research field, factors influencing widespread applicability of these fibers, thesis motivation, literature review, light spectrum and telecom band, objectives and outlines of the thesis has been discussed in brief.

References

- [1] P. S. J. Russell, "Photonic-crystal fibers," *J. Lightwave Technol.*, vol. 24, no. 12, pp. 4729-4749, Dec. 2006.
- [2] J. Hecht, "Understanding fiber optics," *Prentice Hall*, USA, 3rd Edition, 1999.
- [3] C. Lin, "Photonic crystal fibers for nonlinear photonic signal processing and biosensor applications," *Conference on Optical Internet, 2007 and 32nd Australian Conference on Optical Fibre Technology, Joint International*, pp. 1 - 4, 24-27 June 2007.
- [4] G. P. Agrawal, "Fiber-optic communication systems," *John Wiley & Sons Inc.*, USA, 3rd Edition, 2002.
- [5] A. Bjarklev, J. Broeng, and A. S. Bjarklev, "Photonic crystal fibers," *Kulawer Academic Press*, USA, 2003.
- [6] G. P. Agrawal, "Applications of nonlinear fibre optics." *New York, Academic press*, 2008.
- [7] J. C. Knight, "Photonic crystal fibers," *Nature*, vol. 424, pp. 847-851, Aug. 2003.
- [8] Poli, F., A. Cucinotta and S. Seller, "Photonic crystal fibres: properties and applications", *Dorrecht, Springer*. 2007.
- [9] S. Roy, K. Mondal, and P. Roy Chaudhuri, "Modeling the tapering effects of fabricated photonic crystal fibers and tailoring birefringence, dispersion, and supercontinuum generation properties," *Appl. Opt.*, vol. 48, no. 31, pp. G106-G113, Oct. 2009.
- [10] P. Petropoulos, T. Monroe, W. Berlardi, K. Furusawa, J. Lee, and D. Richardson, "2R-regenerative all-optical switch based on a highly nonlinear holey fiber," *Optics Letters*, vol. 26, pp. 1233-1235, 2001.
- [11] M. Y. Chen, "Polarization and leakage properties of large-mode-area microstructured core optical fibers," *Optics Express*, vol. 15, no. 19, pp. 12498- 12507, 2007.
- [12] T. A. Birks, J. C. Knight, and P. St. J. Russell, "Endlessly single-mode photonic crystal fiber," *Optics Letters*, vol. 22, no. 13, pp. 961-963, July 1997.
- [13] A. Ferrando, E. Silvestre, P. Andres, J. Miret, and M. Andres, "Nearly zero ultraflattened dispersion in photonic crystal fibers," *Optics Letters*, vol. 25, pp. 790-792, 2000.
- [14] D. Yeom, E. C. Mägi, M. R. E. Lamont, M. A. F. Roelens, L. Fu, and B. J. Eggleton, "Low threshold supercontinuum generation in highly nonlinear chalcogenide nanowires", *Optics Letters*, vol. 33, no. 7, pp. 660-662, 2008.

- [15] P. St. J. Russell, "History and future of photonic crystal fibers," *Optical Fiber Communication Conference*, USA, March 22-26, 2009.
- [16] Bosch, María Espinosa, Antonio Jesús Ruiz Sánchez, Fuensanta Sánchez Rojas, and Catalina Bosch Ojeda. "Recent development in optical fiber biosensors." *Sensors*, vol. 7, no. 6 pp.797-859, 2007.
- [17] K. Saitoh and M. Koshiba, "Chromatic dispersion control in photonic crystal fibers: Application to ultra-flattened dispersion," *Opt. Exp.*, vol. 11, no. 8, pp. 843–852, Apr. 2003.
- [18] M. A. Islam and M. S. Alam, "Design of a polarization-maintaining equiangular spiral photonic crystal fiber for residual dispersion compensation over $E + S + C + L + U$ wavelength bands," *IEEE Photon. Technol. Lett.*, vol. 24, no. 11, pp. 930–932, Jun. 1, 2012.
- [19] T. P. Hansen, J. Broeng, S. E. B. Libori, E. Knudsen, A. Bjarklev, J. R. Jensen, and H. Simonsen, "Highly birefringent index-guiding photonic crystal fibers," *IEEE Photon. Technol. Lett.*, vol. 13, no. 6, pp. 588–590, 2001.
- [20] T. Huang, J. Liao, S. Fu, M. Tang, P. Shum and D.Liu "Slot spiral silicon photonic crystal fiber with property of both high birefringence and high nonlinearity," *IEEE Photonics Journal.*, vol. 6, no. 3, pp. 628-632, Jun. 2014.
- [21] P. St. J. Russell, "Photonic crystal fibers: A historical account," *IEEE LEOS Newsletter*, vol. 21, pp. 11-15, Oct. 2007.
- [22] B. Zsigri, J. Laegsgaard, and A. Bjarklev, "A novel photonic crystal fiber design for dispersion compensation," *Journal Optics A: Pure Applied Optic*, vol. 6, no. 7, pp. 717-720, Jul. 2004.
- [23] J. C. Knight, T. A. Birks, P. St. J. Russel, and D. M. Atkin, "All-silica single-mode optical fiber with photonic crystal cladding," *Optics Letters*, vol. 21, no. 19, pp. 1547-1549, 1996.
- [24] J. C. Knight, T. A. Birks, D. M. Atkin, and P. St. J. Russell, "Pure silica single mode fiber with hexagonal photonic crystal cladding," *Optical Fiber Communication Conference*, vol. 2, pp. 305-330, 1999.
- [25] M. J. Steel and R. M. Osgood, Jr., "Elliptical-hole photonic crystal fibers," *Optics Letters*, vol. 26, pp. 229-231, Feb. 2001.
- [26] J. K. Ranka, R. S. Windeler, and A. J. Stentz, "Optical properties of high-delta air-silica microstructure optical fibers," *Optics Letters*, Vol. 25, pp. 796-798, June 2000.

- [27] J. Laegsgaard, A. Bjarklev, and S. E. B. Libori, "Chromatic dispersion in photonic crystal fibers: fast and accurate scheme for calculation," *Journal of Opt. Soc. Am. B*, vol. 20, pp. 443-448, Mar. 2003.
- [28] K. Saitoh and M. Koshiba, "Ultra-flattened chromatic dispersion controllability using a defected core photonic crystal fiber with low confinement loss". *Opt. Express* 8365 , vol. 13, no. 21, 2005.
- [29] M. Sajjad Hossain, Kishan Neupane, Md. Shihab Bin Hafiz, and Satya Prasad Majumder, "Dispersion and nonlinear characteristics of a photonic crystal fiber (PCF) with defected core and various doping concentration," *8th International Conference on Electrical and Computer Engineering*, 20-22 December, 2014, Dhaka, Bangladesh.
- [30] L. P. Shen, W. P. Hung, and S. S. Jian, "Design and optimization of photonic crystal fibers for broadband dispersion compensation," *IEEE Photonics Technology Letters*, vol. 15, no. 4, pp. 540-542, Apr. 2003.
- [31] A. Cucinotta, S. Selleri, L. Vincetti and M. Zoboli, "Photonic crystal fibers: perturbation analysis of polarization and dispersion properties," OFC conference, ThS2, Mar. 2002.
- [32] R. R. Musin, and A. M. Zheltikov, "Designing dispersion-compensating photonic-crystal fibers using a genetic algorithm," *Optical Communication*, vol. 281, no. 4, pp. 567-572, Feb. 2008.
- [33] So Eun Kim, Bok Hyeon Kim, Chung Ghu Lee, Sejin Lee, Kyunghwan Oh, and Chul-Sik Kee, "Elliptical defected core photonic crystal fiber with high birefringence and negative flattened dispersion," *Optics Express*, vol. 20, no. 2, pp. 1385-1391 January 2012.
- [34] F. Gerome, J. L. Auguste, S. Fevrier, J. Maury, J. M. Blondy, and L. Gasca, "Dual concentric core dispersion compensating fiber optimized for WDM application," *Electron Lett.*, vol. 41, no. 3, pp. 116-117, February 2005.
- [35] M. Selim Habib, M. Samiul Habib, S. M. A. Razzak, Y. Namihira, M. A. Hossain, and M. A. G Khan, "Broadband dispersion compensation of conventional single mode fibers using microstructure optical fibers," *Optik*, vol.124, no.19, pp. 3851-3855, October 2013.
- [36] M. Mejbaul Haque, M. Shaifur Rahman, M. Samiul Habib, and S. M. A. Razzak, "Design and characterization of single mode circular photonic crystal fiber for broadband dispersion compensation." *Optik-International Journal for Light and Electron Optics*, vol.125, no.11, pp.2608-2611, 2014.

- [37] M. Selim Habib, M. Mejbaul Haque, M. Samiul Habib, M.I. Hasan and M. Shaifur Rahman and S.M.A. Razzak, "Polarization maintaining holey fibers for residual dispersion compensation over S+C+L wavelength bands," *Optik*, vol. 125, pp. 911–915, 2014.
- [38] M. Mejbaul Haque, M. Shaifur Rahman, M. Selim Habib and M. Samiul Habib, "A single mode hybrid cladding circular photonic crystal fiber dispersion compensation and sensing applications," *Photonics and Nanostructures-Fundamentals and Applications*, pp.493-500, January 2015.
- [39] S. F. Kaijage, Y. Namihira, N. H. Hai, F. Begum, S. M. A. Razzak, T. Kinjo, K. Miyayagi, and N. Zou, "Broadband dispersion compensating octagonal photonic crystal fiber for optical communication applications," *J. Appl. Phys.*, vol. 48, 2009.
- [40] M. Chen, Q. Yang, T. Li, M. Chen, and N. He, "New high negative dispersion photonic crystal fiber," *International Journal for Light and Electron Optics*, vol. 121, no. 10, pp. 867-871, June 2010.
- [41] N. Ehteshami, and V. Sathi, "A novel broadband dispersion compensating square-lattice photonic crystal fiber," *Opt. Quant. Electron.*, vol. 44, no. 6, pp. 323-335, July 2012.
- [42] Jianfei Liao, Junqiang Sun, Mingdi Du, and Yi Qin, "Highly Nonlinear Dispersion-Flattened Slotted Spiral Photonic Crystal Fibers," *IEEE Photonics Technology Letters*, vol. 26, no. 4, February 2014.
- [43] S. Revathi, Srinivasa Rao Inbathini, and Rizwan Ali Saifudeen, "Highly nonlinear and birefringent spiral photonic crystal fiber," *Advances in OptoElectronics*, vol. 2014, Article ID 464391, 6 pages, June 2014.
- [44] J. F. Liao, J. Q. Sun, Y. Qin, and M. Du, "Ultra-flattened chromatic dispersion and highly nonlinear photonic crystal fibers with ultralow confinement loss employing hybrid cladding," *Opt. Fiber Technol.*, vol. 19, no. 5, pp. 468–475, October 2013.

CHAPTER II

Fundamentals of Photonic Crystal Fiber

2.1 Introduction

Generically Photonic Crystal Fibers (PCF) can be defined as optical fibers with a built-in microstructure, in most cases consisting of small air holes in glass. In contrast to conventional technology, PCF can be made using a single type of glass where guidance of light is achieved by introducing an air hole lattice that runs longitudinally along the fiber length. Such fibers are also known as microstructured optical fiber (MOF) or holey fiber (HF). For various and outstanding characteristics, the research activity of PCF is increasing dramatically in telecom and non-telecom sector all over the world. For example, PCF is finding application in telecom sector including fiber-optic communications, fiber lasers, nonlinear devices, high-power transmission and then touching non-telecom sector such as biology, sensing, metrology, spectroscopy, microscopy, astronomy and micromachining. The term “Microstructured optical fibers” was coined by Philip Russell, pioneer of this research field were proposed in 1995 and the first demonstration of optical guidance was published in 1996. It is now possible to manufacture the microstructure in air-glass PCF to accuracies of 10 nm on the scale of 1 μm , which allows remarkable control of key optical properties such as dispersion, birefringence, nonlinearity, and the position and width of the Photonic Band Gap (PBG).

2.2 Light spectrum and telecommunication band

An electromagnetic spectrum is defined as is the complete range of the wavelengths of electromagnetic radiation from low to high frequency including radio, infrared, visible light, ultraviolet, X-ray, and gamma ray waves. Wavelengths are about 400 nm (violet light) to 700 nm (red light) is known as visible light spectrum in Fig.2.1, while optical fiber communications typically operate in generally 300 to 1700 nm wavelength region is called “telecom windows” as shown in Fig.2.2. The first window at 800–900 nm was originally used for laser diodes and light-emitting diodes (LEDs) served as transmitters, and silicon photodiodes were suitable for the receivers. The second telecom window utilizes wavelengths around 1.3 μm , where the loss of silica fibers is much lower and the fiber’s chromatic dispersion is very weak but it can increase the effect of optical nonlinearities. The third telecom window, which is now very widely used, utilizes wavelengths around 1.5 μm . The losses of silica fibers are lowest in this

region. Fiber dispersion is usually anomalous but can be tailored with great flexibility. The second and third telecom windows were originally separated by a pronounced loss peak around 1.4 μm wavelengths, this window is rarely used. Nowadays the 1.30 μm window and 1.55 μm window are in extensive use in telecommunication. The range of electromagnetic band is described in Table 1.

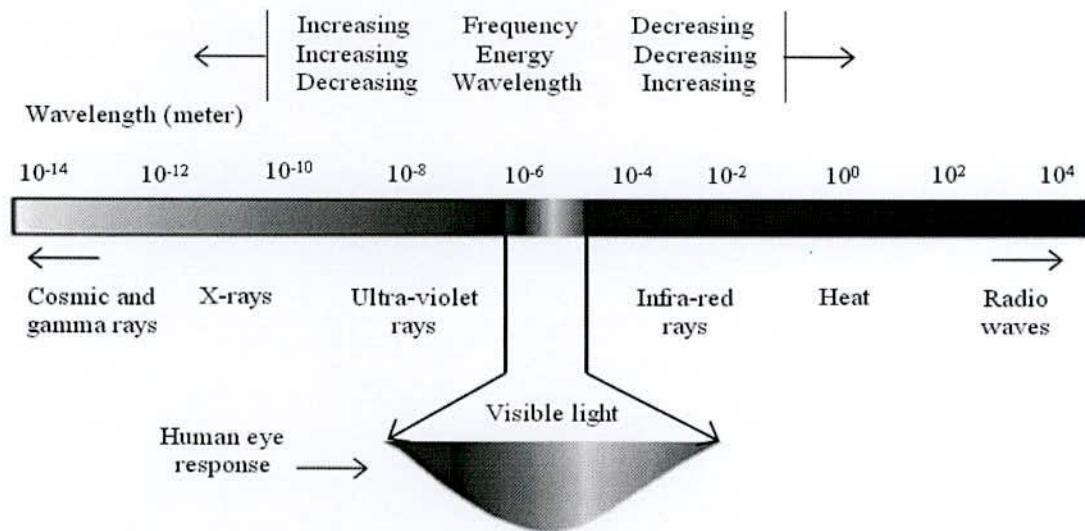


Fig. 2.1 Electromagnetic spectrum

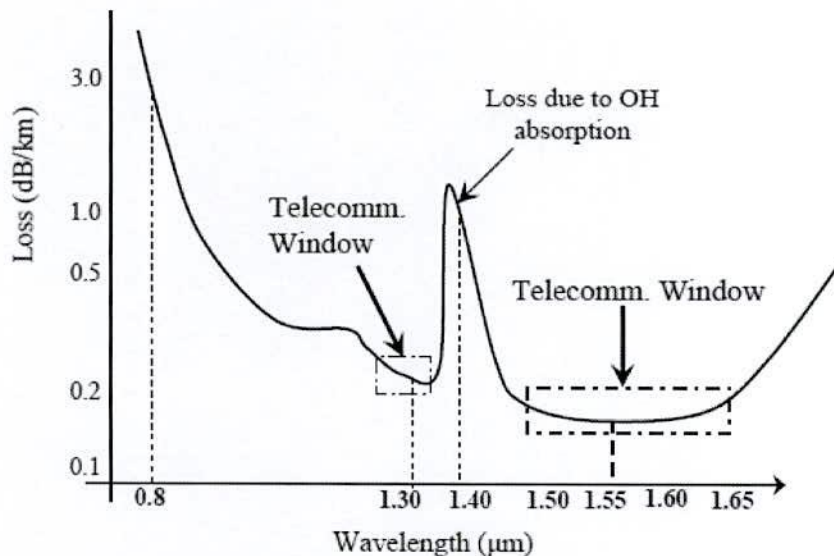


Fig. 2.2 Optical attenuation characteristics of silica fiber and the telecom windows

Table 1: Electromagnetic band

Band name	Range [nm]	Description
O-band	1260-1360	Original
E-band	1360-1460	Extended
S-band	1460-1530	Short wavelength
C-band	1530-1565	Conventional
L-band	1565-1625	Long wavelength
U-band	1625-1675	Ultra-long wavelength

2.3 Construction and basic principles of PCF

PCF consists of microscopic array of air channel run down the entire length of fiber [1]. These air-holes in the silica background represent the cladding and thus make low refractive index profile in cladding. The core is normally formed either by omitting a central air-hole from the whole structure or by organizing a larger air-hole in its position. PCF structure with missing air hole in the core leads to solid core which forms high index profile in the core than cladding. This type of fiber structure is called high index core (HIC) or index-guiding (IG) PCF. Fiber structure with a placement of air hole in the core is called a hollow core (HC) or low index core (LIC) or photonic band gap (PBG) PCF.

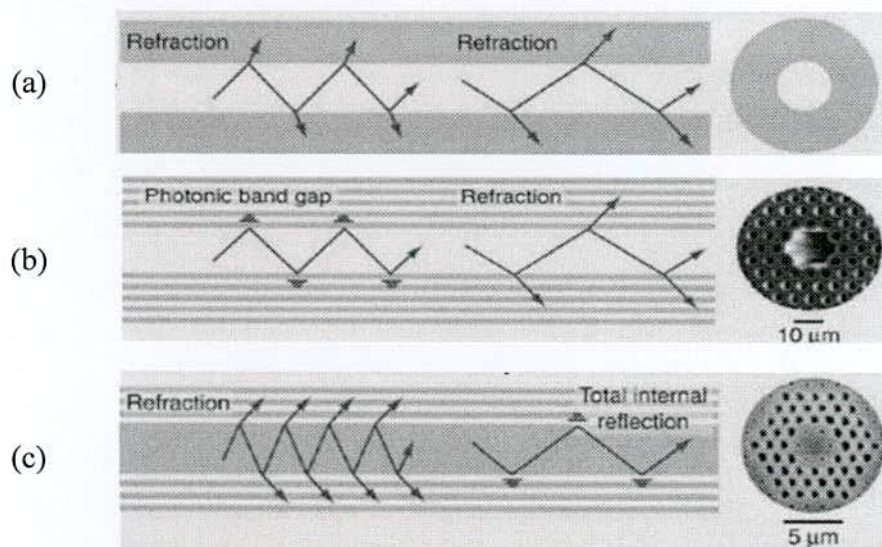


Fig. 2.3 (a) Standard hollow capillary (b) PBG based hollow core PCF (c) TIR (Total Internal Reflection) based solid core PCF.

Fig. 2.3 (a) shows that a hollow capillary refracts light in all angles of incidence. There is no angle at which light can be trapped in the hollow core, so capillaries cannot guide light

under any circumstances. Fig. 2.3 (b) shows a hollow-core photonic crystal fiber with an appropriately formed cladding. This structure can guide light at angles of incidence where a photonic band gap operates, but otherwise refracts like a hollow-core capillary. A solid-core photonic crystal fiber is shown in Fig. 2.3 (c). This structure refracts light at steep angles of incidence on the core-cladding boundary. When the angle is shallow enough, light is trapped in the core and guided.

The typical cross section hollow core PCF with a hexagonal lattice of air holes was first proposed by Philip Russell in 1999 is shown in Fig. 2.4. The key parameter Λ and d/Λ is used to define the structure parameter where d is the hole diameter and Λ is hole-to-hole (pitch) parameter.

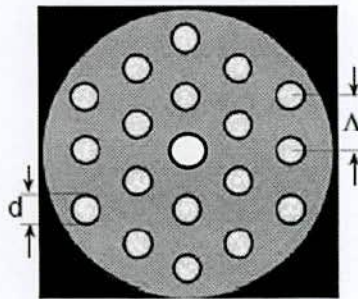


Fig. 2.4 A schematic diagram hollow core PCF cross section

Fig. 2.5(a) shows that IG-PCFs generally omit a single air-hole from the structure. This type of PCFs can also have a high index material (e.g. Ge) doped core. In either case, the core must have a high refractive index ($n_{co} > n_{cl}$) than that (equivalent refractive index) of the of the cladding. Unlike IG-PCFs, PBG PCFs have a hollow core ($n_{co} < n_{cl}$) which is generally created by placing a larger air-hole in the center as shown in Fig.2.5 (b). Thus, PCFs have a number of design freedom namely air-hole diameter, air-hole to air hole distance (the pitch), core radius, and number of rings. Since the guiding properties of optical fibers depend on the refractive index and the refractive index of PCF depends on those design freedoms, application specific guiding properties can be achieved by modulating those parameters [2]. In index-guiding PCFs, similar to conventional fibers, light is guided in a higher index core by modified total internal reflection from a low effective index cladding; in bandgap PCFs, light is confined in a low-index core by reflection from a photonic crystal cladding. Because of their novel guiding mechanism and variety in design, PCF offers a lot of new opportunities not only for applications related to fundamental fiber optics. These opportunities are related to some special properties of the photonic crystal cladding which

are due to the large refractive index contrast and the two-dimensional nature of the microstructure.

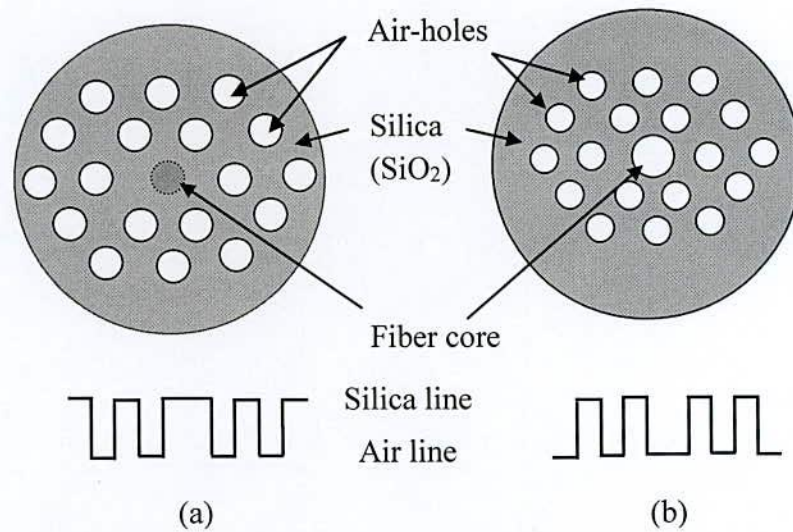


Fig. 2.5 Schematic cross sections and index-profiles of (a) IG-PCFs (the dotted circle in the center indicates an omitted air-hole) and (b) PBG-PCFs (the larger circle in the center represents the core)

For index-guiding PCFs, the properties include endlessly single mode, large mode area, high numerical aperture, high birefringence, high nonlinear coefficient, confinement loss, and dispersion management. Various bandgap PCFs and many significant applications for them have been achieved, such as low-loss air-core bandgap PCFs, all-solid bandgap PCFs, a variety of PCF devices [3] and Bragg PCFs for CO₂ laser transmission [4].

2.4 Classifications of PCF

The most common PCFs reported in the literature have a structure that takes the form of hexagonal, spiral, honeycomb, or cobweb geometry [5], as shown in Fig.2.6. Cobweb microstructures usually have a solid core and honeycomb PCFs usually have a hollow core, whereas PCFs with hexagonal and spiral lattice structures are made with a solid core or a hollow core.

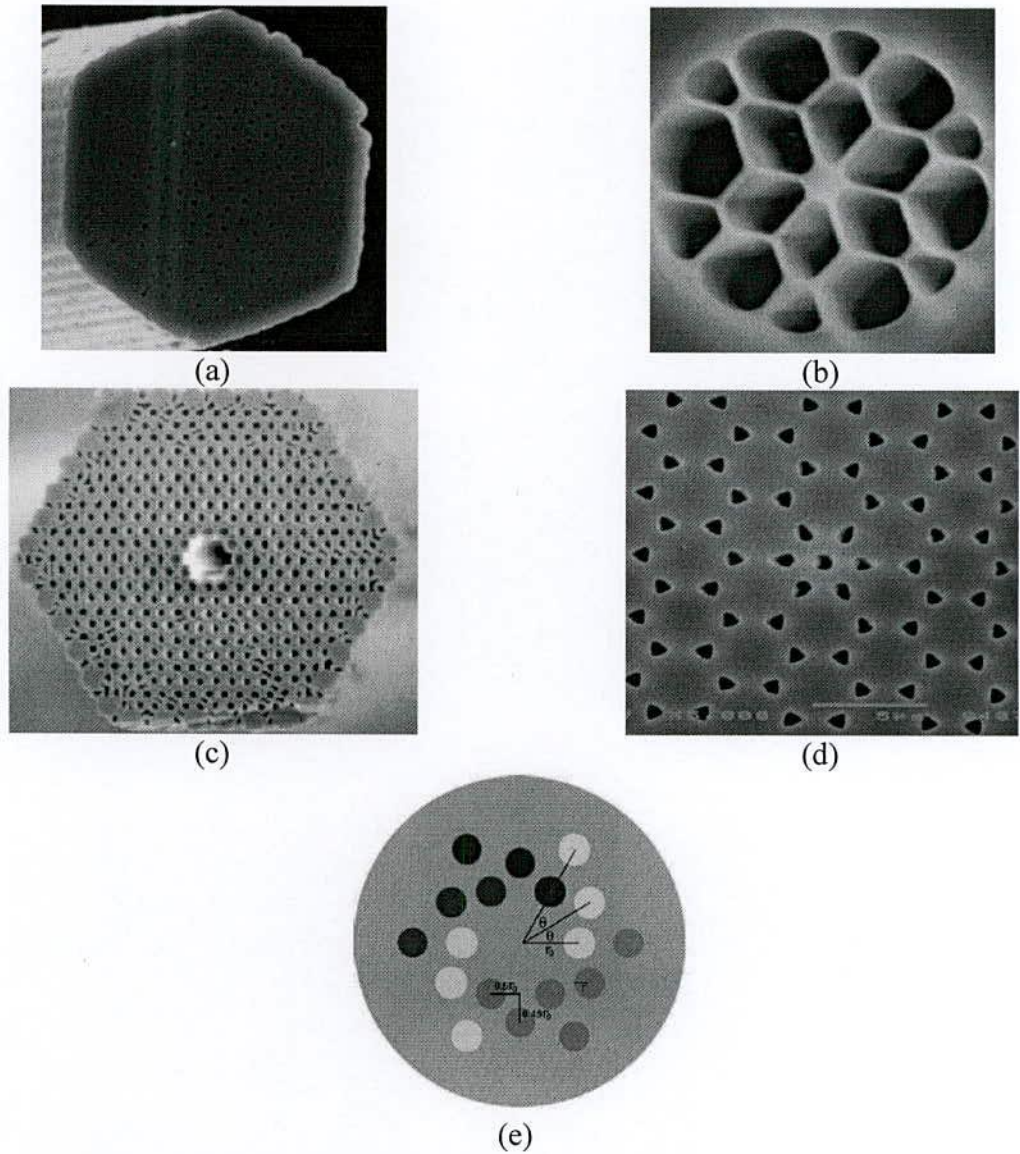


Fig. 2.6 Various PCF structures reported in the literature: (a) hexagonal solid-core PCF, (b) cobweb PCF, (c) hexagonal hollow-core PCF, (d) honeycomb PCF and (e) spiral PCF

However, design of a PCF is highly dependent on its application and choice of certain materials in different bands of wavelengths. We have considered two distinct principles, i.e., total internal reflection (TIR) and PBG mechanism of propagation for analyzing several linear and nonlinear properties of PCF according to [6]. They are:

2.4.1. Positive core-cladding index difference: This type of PCF may be defined as one where the mean cladding refractive index in a certain wavelength is lower than the core index where PCFs will generally maintain TIR-guided. However, index guiding PCF (IG-PCF) guides light through a form of total internal reflection (TIR) called modified TIR

where a two-dimensional photonic crystal works as a fiber cladding and refractive index of core remains higher than refractive index of cladding. The guiding mechanism is defined as “modified” because the cladding refractive index is not a constant value than that of the standard optical fibers rather it changes significantly with the wavelength. Some of the advantages under this principle are:

Controlling the Number of Modes: The number of modes in a waveguide can be controlled easily by using the design of photonic crystal cladding. A fiber can be endlessly single mode (ESM) at all operating wavelengths if carefully designed.

Large mode area (LMA) fiber: This condition is important when a PCF is operated under high power to eliminate undesirable nonlinear effect.

Highly nonlinear (HNL) fiber: Core dimensions of this type of PCF are made very small so as to provide tight mode field confinement.

Hole assisted PCF (HA-PCF): This type of IG-PCF consists of doped core i.e. high index material doped silica surrounded by holey cladding.

Fibers with multiple cores: These fibers find applications in curvature sensing, cladding-pumped lasers, two-photon fluorescence etc.

High numerical aperture (HNA) fiber: It consists of microstructure cladding surrounded by a ring of air-holes with larger dimensions.

Nanoweb Fibers: It does not have a deliberately introduced core but instead relies on a gentle thickness gradient to confine the light. The extremely low loss (0.4 dB/m) in what is essentially a planar glass waveguide with very strong waveguide dispersion makes this an interesting structure for experiments in spatial solitons and nonlinear optics.

2.4.2. Negative core-cladding index difference: Since TIR is not possible here; low loss wave guiding is only possible if PBG exists. Photonic bandgap (PBG) PCF guides light via the mechanism of diffraction rather than total internal reflection [2]. Thus, light of any wavelength within that range cannot escape from the core and in analogy with electronic band-gap materials, cladding structure is called a photonic crystal and the wavelength range over which light is confined within the hollow core is called the band-gap of the material. On the other hand, PBG-PCF is classified as air-guiding (AG), HC fibers, low index core (LIC) fibers, or Bragg fibers. PCF can again be of another type namely polarization maintaining (PM) fibers having either a stress applying part or an asymmetric cladding structure to maintain a linear state of polarization. Again, likewise a conventional fiber, PCF is also classified as single mode or multi-mode fibers depending on the number of modes

supported by a particular PCF either IG or PBG. All these types of microstructure PCF are shown in Fig. 2.7.

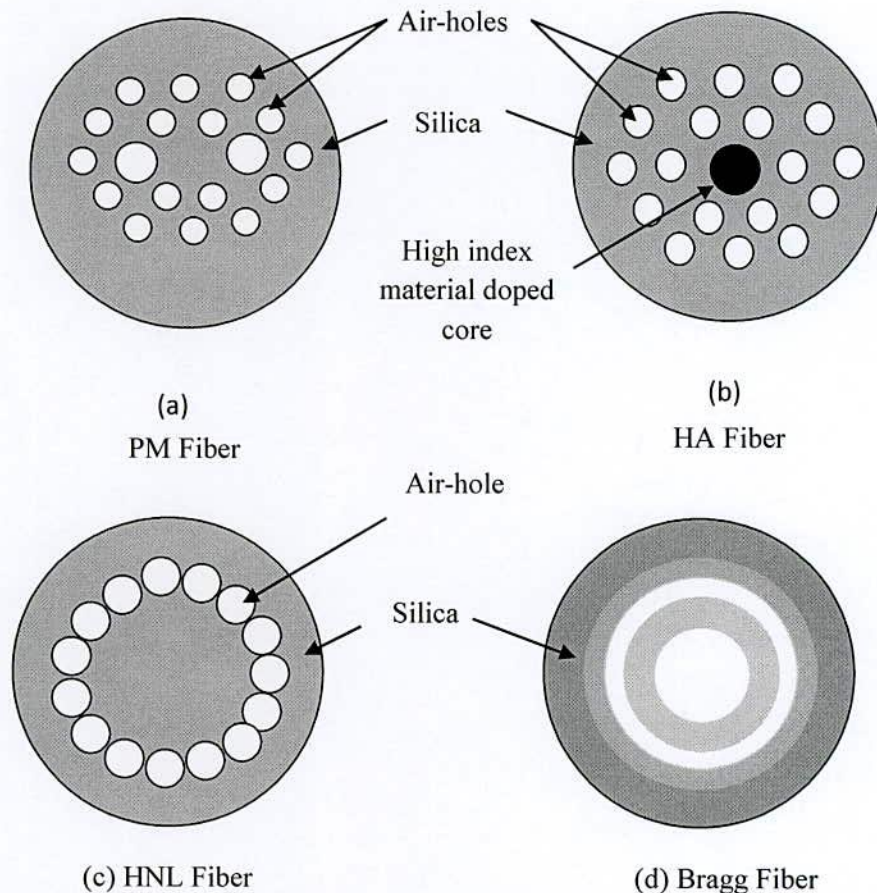


Fig. 2.7 Types of PCFs (a) PM-PCF, (b) HA-PCF, (c) HNL-PCF, and (d) Bragg Fiber- a special type of HC-PCF

Fig. 2.7(a) shows that IG-PCF generally omits a single air-hole from the structure. This type of PCFs can also have a high index material (e.g. Ge) doped core. In either case, the core must have a high refractive index ($n_{co} > n_{cl}$) than that of effective refractive index of the cladding. Unlike IG-PCFs, PBG PCFs have a hollow core ($n_{co} < n_{cl}$) which is generally created by placing a larger air-hole in the center as shown in Fig.2.7 (d).

Hollow core Photonic Band Gap Fiber: A special class of PBG guiding fibers is the hollow core fibers, where the field is confined to an air-filled core. Like other PBG fibers, air-core fibers only guide light in a limited spectral region. For fibers guiding around 1550nm, a typical bandwidth is ~200nm.

Glass of Higher Refractive Index: This kind of PBG fiber may have wider band gap than the low index contrast counterparts. Due to high index contrast, a vectorial method may be required to trace out the accurate band gap region.

All-Solid Structure PBG fiber: In all-solid band gap guiding fibers, the core is made from low-index glass and is surrounded by an array of high-index glass strands. Since the mean core-cladding index contrast is negative, TIR cannot operate, and PBG effects are the only possible guidance mechanism. It is possible to achieve PBG guidance by this mechanism even at index contrasts of 1% with losses as low as 20 dB/km at 1550 nm.

2.5 Comparison between PCF and conventional fiber

Conventional optical fiber is made of a higher refractive index core than that of the lower refractive index cladding. The light is here, confined within the core of the optical fiber by exploiting the principle of total internal reflection as light travels along its length as shown in Fig. 2.8. To increase the refractive index, Germanium is generally used whereas Fluorine is commonly used material for decreasing the refractive index. In contrary, PCF is normally a single material fiber that contains tiny air holes in a silica background as shown in Fig 2.9.

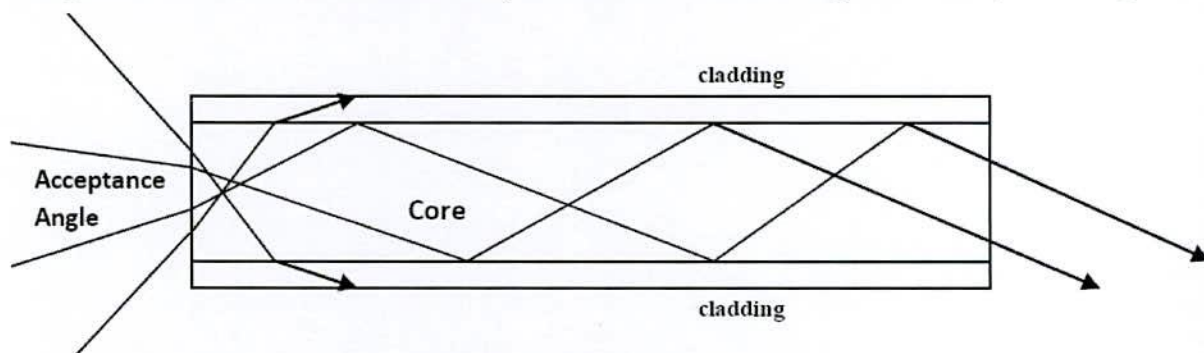


Fig. 2.8 Total internal reflection of light through optical fiber

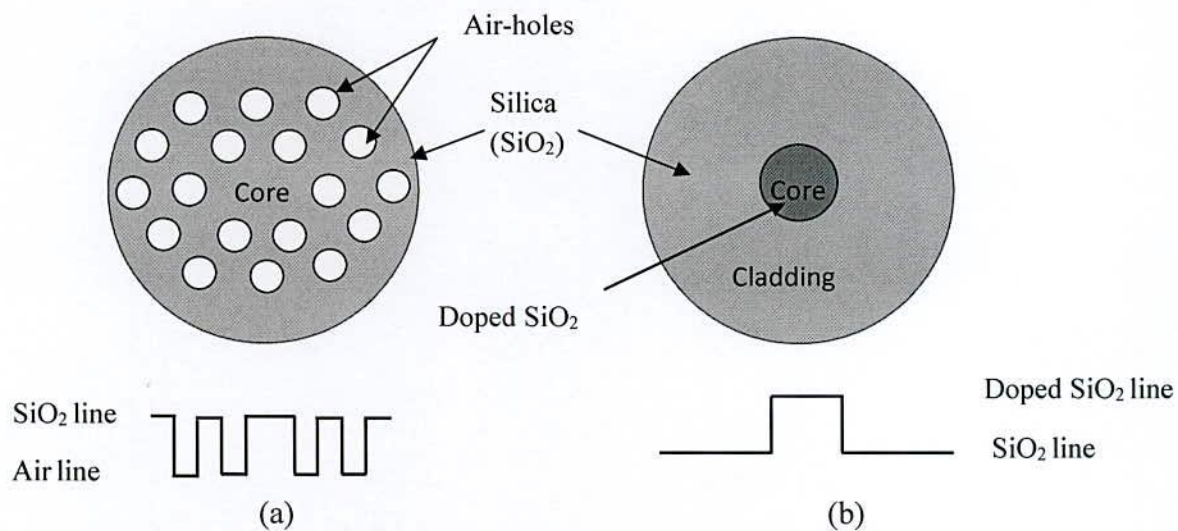


Fig. 2.9 Schematic cross sections and index-profiles of (a) PCFs (a missing air-hole in the center represents the core) and (b) Ordinary fibers

In conventional fibers, Index contrast between the core and the cladding is very low but wide range of controlling the index contrast between core and cladding of PCF is achieved by simply modulating the cladding parameters. Due to high effective index contrast between silica and air, a much broader range of dispersive behavior is accessible with Photonic Crystal fibers than with standard fibers. These design flexibility for tailoring a specific property in the Photonic Crystal Fiber makes it more controllable to fabricate parameters than in single mode fibers. This is the primary difference between the two fibers provides additional degree of freedom because of number of holes, shapes, orientation and placement also make it better than the standard optical fiber properties [7].

2.6 Guiding properties of the PCF

In the following subsections, wavelength dependent response of chromatic dispersion, birefringence, confinement loss, mode field diameter, effective area and single/multi-mode response of PCF are discussed.

2.6.1 Chromatic dispersion

Dispersion is the phenomenon whereby the index of refraction of a material varies with the frequency or wavelength of the radiation being transmitted through it [8]. Dispersion in optical fibers is caused by a variety of factors. For modern glass optical fiber, the maximum transmission distance is limited by dispersion or spreading of optical pulses as they travel along the fiber. Transmission media having such a property are termed dispersive media. When optical pulse passes through dispersive media, this pulse is separated in its component and can overlap each other at receiving end. Thus overlapped optical pulses at the receiver of the may not be recovered and hence the sending data will be lost. Moreover, dispersion is sometimes called 'Chromatic Dispersion' is often used to emphasize this wavelength dependence [9]. The total dispersion in a waveguide or an optical fiber is a function of both the material composition (material dispersion) and the geometry of the waveguide (waveguide dispersion). Material dispersion originates from the frequency or wavelength dependent response of the atoms/molecules of a material to electromagnetic waves and it slightly varies from fiber to fiber. Waveguide dispersion occurs because waveguide geometry variably affects the velocity of different frequencies of light. More technically, waveguide dispersion is caused by the variation in the index of refraction due to the confinement of light an optical mode [10]. However, a similar phenomenon is modal dispersion, caused by a waveguide having multiple modes at a given frequency, each with a

different speed. Polarization mode dispersion, another source of limitation, occurs because although the single mode fiber can sustain only one transverse mode, it can carry this mode with two different polarizations and slight imperfections or distortions in a fiber can alter the propagation velocities for the two polarizations.

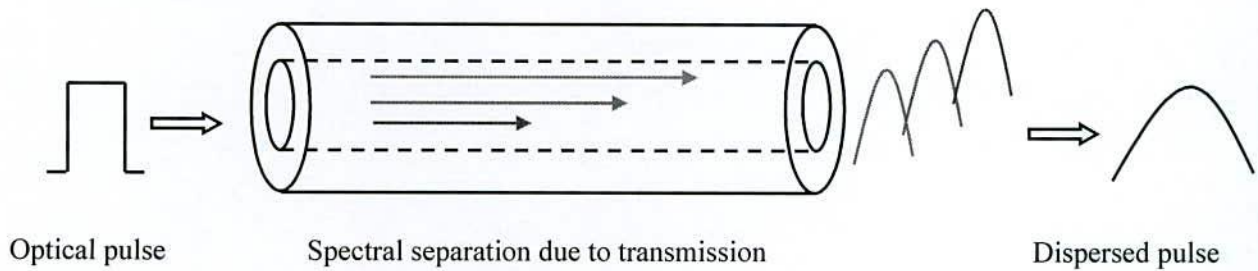


Fig. 2.10 Dispersion phenomena in an optical fiber

2.6.2 Birefringence

Birefringence is a term used to describe a phenomenon that occurs in certain types of materials, in which light is split into two different paths. This phenomenon occurs because these materials have different indices of refraction, depending on the polarization direction of light. A specialty fiber called the Polarization Maintaining (PM) Fiber intentionally creates consistent birefringence pattern along its length. Birefringent photonic crystal fiber (PCF) can be achieved by having asymmetric core. In any design, the geometry of the fiber and the materials used create a large amount of stress in one direction, and thus create high birefringence compared to that generated by the random birefringence. In such a case, intentionally introduced birefringence weakens the random polarization effect thus maintain a single polarization. The birefringence value is normally 10^{-4} of conventional PM fibers but it can be extended to 10^{-1} by using PCFs. In the case of highly birefringent fibers, the propagation constants of the two orthogonally polarized modes are made quite different from each other so that the coupling between the two modes is greatly reduced. Birefringence is used in many optical devices including Liquid crystal displays, light modulators and sensing application.

2.6.3 Single mode or multimode response

The main difference between multi-mode and single-mode optical fiber is that the former has much larger core diameter, typically 50–100 micrometers; much larger than the wavelength of the light carried in it. Because of the large core and also the possibility of

large numerical aperture, multi-mode fiber has higher "light-gathering" capacity than single-mode fiber. Conventional fibers can operate single-mode or multi-mode depending mostly on the dimension of the core. PCFs, on the other hand, can be designed for endlessly single-mode operation by proper choice of air-hole dimension and pitches. For a uniform cladding, PCFs show endlessly single mode response as long as the d/Λ ratio remains within a 0.45, above the value may result in either single-mode or multimode operation. Using the Λ parameter of PCFs, it is possible to determine the single mode response.

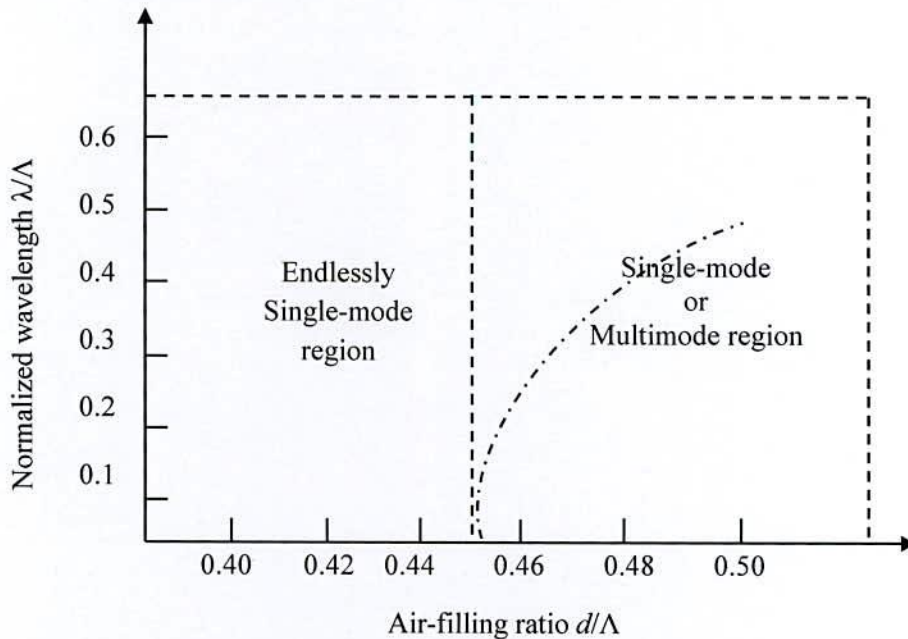


Fig. 2.11 Mode diagram of PCF

2.6.4 Mode field diameter and effective area

A beam of light guided through the fiber does not have strict cross-sectional boundaries. The beam is most intense in the center, with its intensity declining gradually from the center outward.

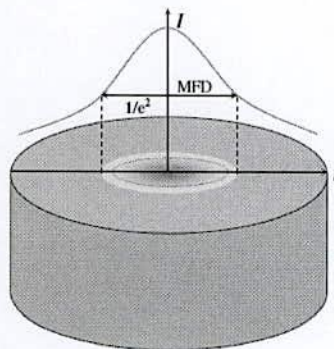


Fig. 2.12 shows the intensity distribution of a light beam inside a fiber

The most popular model used in single mode fibers for the beam intensity is a Gaussian distribution [11-12]. The effective area or simply the effective area is the area where the beam intensity drops to 13.5% of the maximum value and the diameter of which is called the mode field diameter (MFD) and can be calculated directly from the electric field distribution by using the Petermann-II definition [13].

2.6.5 Confinement loss

Confinement losses or leakage losses are present in PCFs due to the fact that there are a finite number of air-holes that can be made in the cross-section of the cladding which results in the PCF guided modes to be leaky [14]. The diameter to pitch ratio (d/Λ) in a particular design of PCF determines how much light leaks from the core into the cladding. The lower the ratio, the more leakage is expected into the cladding. If the confinement loss is higher, then signal will be degraded through the fiber. Actually air-holes in the cladding region limit the optical field penetration in the cladding region. There will be no confinement loss in PCFs if there is infinite number of air-holes in the cladding region.

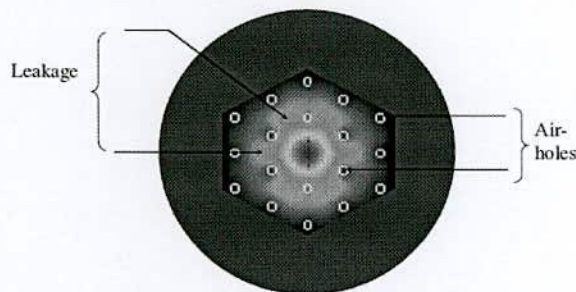


Fig. 2.13 Confinement losses in index-guiding PCF

2.6.6 Bending loss

This is caused by bending of the fiber as shown in Fig. 2.14. This is because internal light paths exceeding the critical angle for total internal reflection, TIR. Theoretically, when the fiber is bent, light propagates outside the bend faster than the inner radius, as is represented in Fig. 2.14. There are two types of bending loss in optical fiber. Macro bending means large scale bending that is visible in which the bend is imposed on optical fiber. The bend region strain affects the refractive index and acceptance angle of the light ray. Whereas micro bending is a small scale bend that is not visible this occurs due to the pressure on the fiber that can be as a result of temperature, tensile stress of force and so forth. It affects refractive index and refracts out the ray of light; thus loss occurs. This is not possible practically and the light is radiated away [15-16].

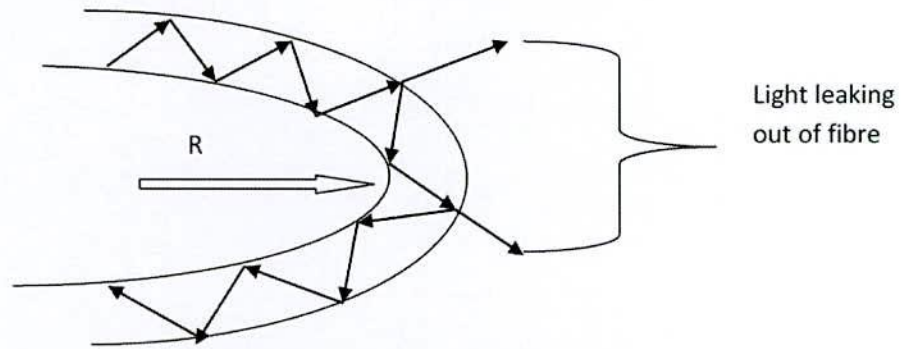


Fig. 2.14 bending loss in optical fiber

2.7 Fabrication technology of PCFs

Fabrication of PCF, like in conventional fiber fabrication, starts with a fiber preform. PCF preforms are formed by stacking a number of capillary silica tubes and rods to form the desired air/silica structure. This way of creating the preform allows a high level of design flexibility as the core size and shape as well as the index profile throughout the cladding region can be controlled. When the desired preform has been constructed, it is drawn to a fiber in a conventional high-temperature drawing tower and hair-thin photonic crystal fibers are readily produced in kilometer lengths. In Fig. 2.15, the overall process has been illustrated.

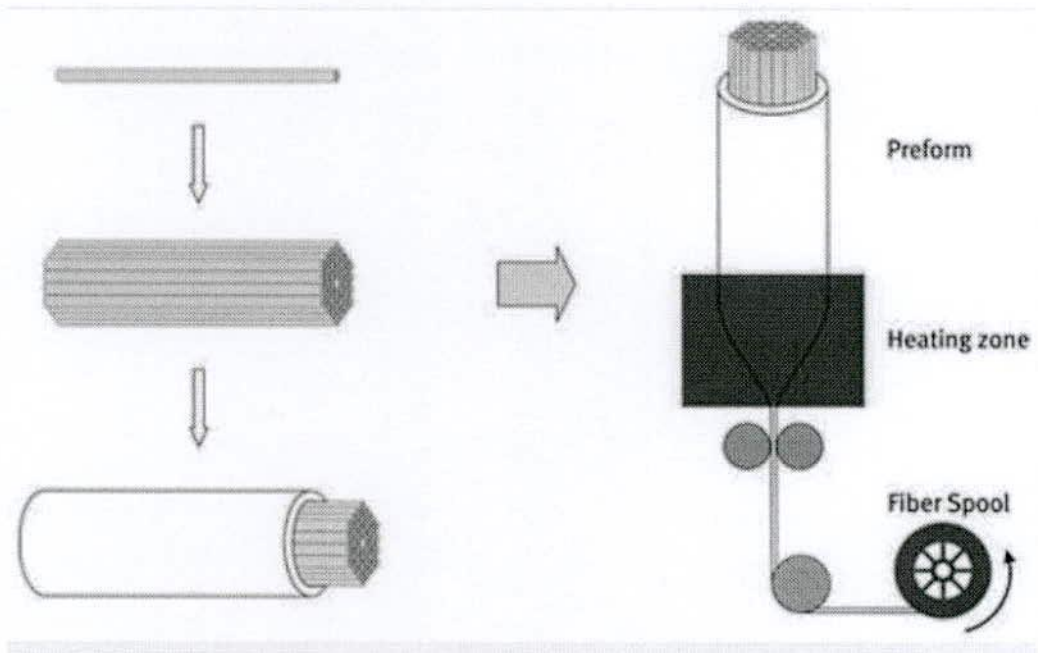


Fig.2.15 Conventional setup of fabricating regular shaped PCFs

Through careful process control, the air holes retain their arrangement all through the drawing process and even fibers with very complex designs and high air filling can be

produced. Finally, the fibers are coated to provide a protective standard jacket that allows robust handling of the fibers. The final fibers are comparable to standard fiber in both robustness and physical dimensions and can be both striped and cleaved using standard tools. In this section, we are reporting three novel fabrication technologies to realize more complex configurations of PCFs. In our thesis, we have characterized PCFs for a wide range of applications which cannot be fabricated by the conventional stack and draw technique mentioned earlier.

2.7.1 Extrusion and filling technology

Extrusions of complex perform:

The successful realization of a range of Micro structured optical fiber (MOF) depends on the use of complex air/glass structures within the fiber cross-section. Stacking, drilling and casting techniques have been used to fabricate structured preforms. These techniques all have limitations in the number of transverse features, hole shapes and configurations that can be achieved. A promising alternative technique is billet extrusion, which has been shown to be a versatile, reproducible single-step approach to fabrication of soft glass and polymer preforms with up to 12 holes. In [17], a new die design concept has been presented along with advances in the extrusion process control, which together overcome these issues to allow the first demonstration of truly complex extruded glass preforms.

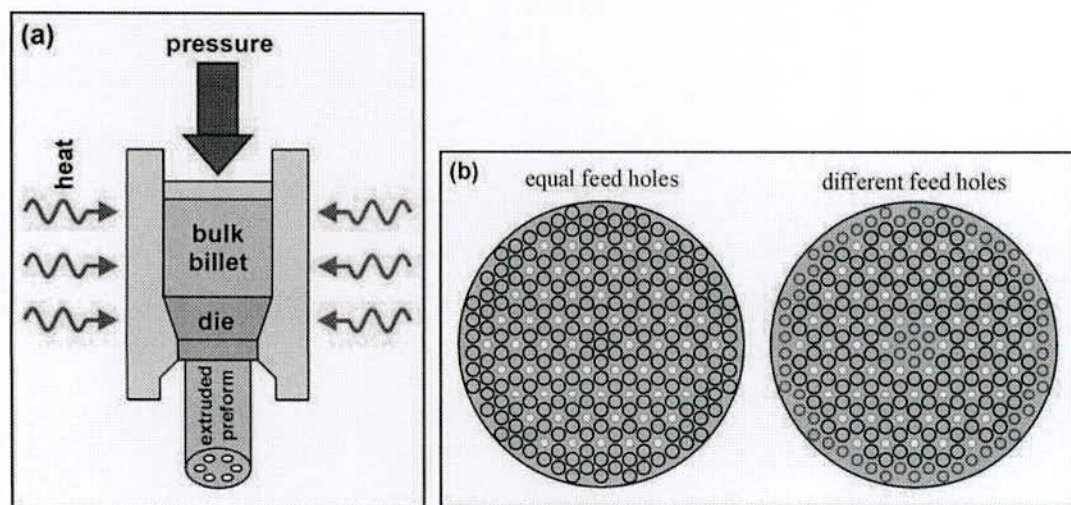


Fig. 2.16 (a) Sketch of extrusion process and (b) extrusion die concepts with equal and different size feed holes for a target perform structure having 60 holes (4 rings), white filled circles are blocking elements, black and red circles are feed holes

The flow of material within the die is explored for a range of structures and materials, and the efficacy of the extruded preforms for low-loss fiber fabrication is demonstrated. In Fig. 2.16, overall process has been shown. This new die design allows great flexibility in the selection of the size, shape and distribution of the feed holes, which provides control of the material flow through the die in a manner that is truly scalable, reconfigurable, easily understood and thus optimized. The die design also offers independent control of the hole shape and configuration within a preform for the first time.

Filling technology for multi-material PCF devices

The optical properties of silica-air photonic crystal fiber (PCF) can be radically altered by filling its hollow channels with materials such as metals, polymers or semiconductors. Various different techniques have been used previously, including high-pressure chemical vapour deposition and pumping in of molten metal at high pressure. Chemical routes have the drawback that the end products of the reaction remain in the channels, often adversely affecting the optical properties. Filling with pure molten material does not suffer from this disadvantage, so that structures of high optical quality can readily be produced. In [18], the optical properties of PCFs in which one two or more holes, adjacent to the core, are filled with semiconductors, glasses or metals by using a pressure cell technique have been reported. In Fig. 2.17, SEM image of fabricated a filled channel of PCF has been shown. This filling procedure allows the core mode to interact strongly with the material of the wire, leading to a strong modification of the light transmission.

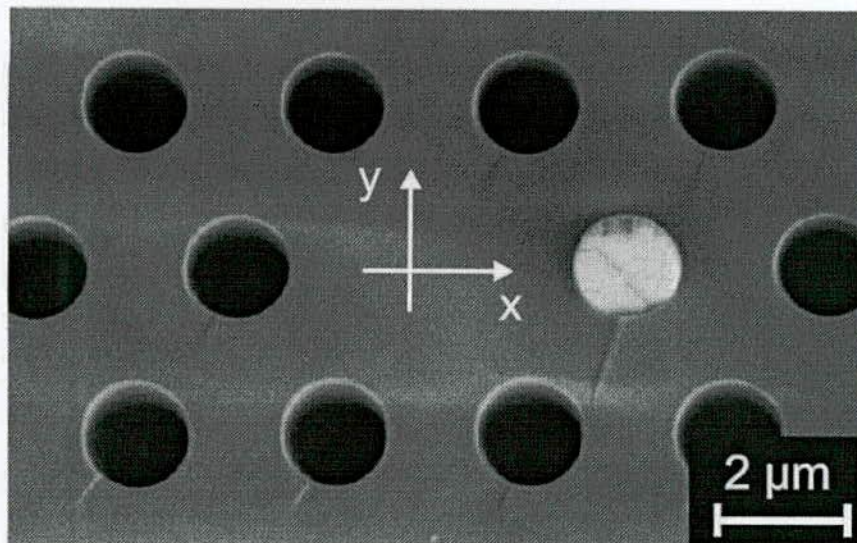


Fig.2.17 Scanning-electron-micrograph image of a cleaved end-face of a germanium-filled endlessly single mode PCF. Germanium wire is on the right side (dwire = 1.6 μm)

2.7.2 Sol-gel technique for fabricating irregular shaped PCF

Microstructured fibers possess an array of air columns embedded within a silica matrix, which extend along the z axis of the fiber. Several methods have been developed for the fabrication of microstructured fibers including the stack and draw of glass capillaries, sol-gel casting, preform drilling, extrusion, and even out gassing of a porous preform during draw. All of the aforementioned methods have various advantages and tradeoffs in terms of ease of fabrication, cost, design flexibility, material contamination, and precision. Here, we like to introduce the sol-gel casting technology towards the fabrication of irregular shaped microstructured optical fibers. The sol-gel casting technique was originally developed for the production of large jacket tubes for optical fiber preforms and has been modified for the fabrication of microstructured fiber [19]. A number of microstructured fibers fabricated using the sol-gel casting method [20]. To maintain uniformity along the length of the preform, the mandrels are individually tensioned and the positioning and spacing is inspected and recorded with a digital camera. The aforementioned process is graphically represented in Fig. 2.18.

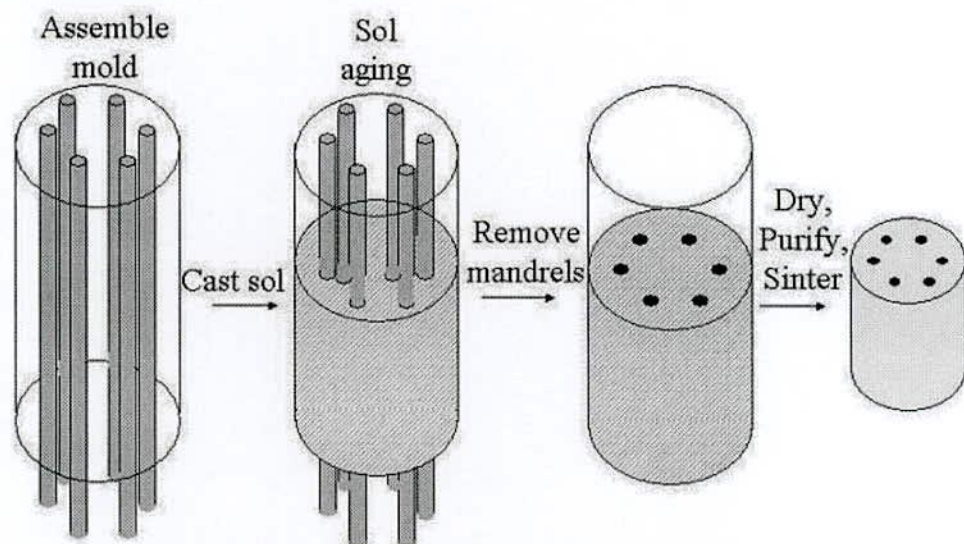


Fig. 2.18 Schematic representation of sol gel fabrication technique

2.7.3 SCF fabrication with soft materials

Fabrication technology is a prime concern in any photonic crystal fiber design, characterization, and implementation. Glass casting, well known stack and draw process, extrusion and ultrasonic drillings are widely used fabrication process for SCF [21]-[24]. Though Stack and draw is suitable for soft glass material, since nanometer dimension of core and very narrow gap between air holes the fiber becomes fragile. Recently new

fabrication technique based on die design and process control has been introduced for sub-wavelength core diameter SCF fabrication [25]. It is shown that by fast-and-cold tapering method micro-structured fiber geometry can be preserved up to 300nm of core diameter [26]. Soft glass like chalcogenide is promising for fabrication of SCF with arbitrary complex air hole geometry and arrangement. Low softening temperature of soft glass plays great role here in shaping air hole arbitrarily in preform formation. Therefore, soft glass has broadened the choice of fabrication methods for SCF fabrication.

2.8 Applications of PCFs

In this section we have discussed on versatile applications of PCF from three different perspectives.

2.8.1 PCF in fiber optic communication

Over the last decade PCF technology has rapidly progressed and been shown to hold significant potential for many important applications in optical fibers communication. Solid core PCF or IG-PCF can be used to serve certain requirement of the optical communication system such as high birefringence, ultrahigh nonlinearities, tailoring dispersion, and LMA fibers. For example, birefringence maintains polarization states in optical device. By re-arranging the air-hole geometry in PCF, birefringence that exceed the performance of conventional birefringent fiber by an order of magnitude which provide different types of sensors including remote environmental sensors and bio-sensors [27]. Chromatic dispersion is another vital issue in communication sector can be changed and controlled largely with the PCF than conventional fiber. For compensating chromatic dispersion, large negative dispersion PCF is designed. HNL-PCF and near zero dispersion flat PCF are being used in optical parametric amplification, all optical signal processing, soliton pulsed systems, and supercontinuum generation. In recent years, Raman amplification has become an increasingly important technique for high performance optical networks, complementing Erbium Doped Fiber Amplifier (EDFA) technology in many applications, and in others supplanting it altogether. The two main advantages of Raman amplification are the ability to use any type of fiber as an amplification medium, and the ability to amplify signals in any wavelength band using an appropriate pumping scheme. Raman amplification can also be applied to lumped amplifiers, in which case the ability to amplify signals in any wavelength band can be used to construct Lumped Raman Fiber Amplifiers (LRFA's) which operate in

wavelength bands where EDFA technology is either inapplicable or relatively inefficient. In Fig. 2.19, a LRFA scheme has been shown.

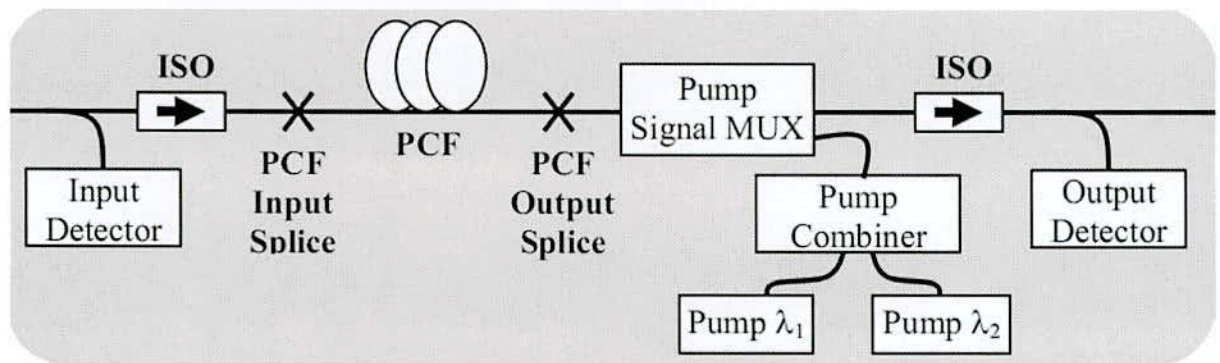


Fig. 2.19 Basic LRFA structure based on Photonic Crystal Fiber

2.8.2 PCF for Super-continuum Generation

Supercontinuum generation (SCG) is a process where laser light is converted to light with a very broad spectral bandwidth (i.e., low temporal coherence), whereas the spatial coherence usually remains high. The spectral broadening is usually accomplished by propagating optical pulses through a strongly nonlinear device, such as an optical waveguide. It is mainly due to their unusual chromatic dispersion characteristics, which can allow a strong nonlinear interaction over a significant length of fiber.

Applications of SC sources

Photonic device testing – Light source for measuring the optical properties of single mode waveguide devices and fibers in the S, C and L bands and at 1310 nm. Using a SC source for these measurements provides the brightness required to overcome a high level of attenuation.

Optical coherence tomography – Powerful, broadband, single mode source for achieving high spatial resolution and scan speed in transverse and longitudinal directions.

Spectroscopy – Fast data acquisition on small-volume samples in biology, chemistry, medicine, physics or environmental monitoring. Due to its high degree of spatial coherence, SC radiation can be focused to a small spot, or collimated to a narrow beam for long path length measurements in low absorbance analytes.

2.8.3 PCF for Sensing Technology

Suspended Core Fiber (SCF) has been widely used in different sensing applications from physical science to life science due to its some discernible properties concerning sensing

applications. Recently, advanced DNA sensing, broadband chemical sensing, and various sensing application has been exploited with SCF[28]-[30].

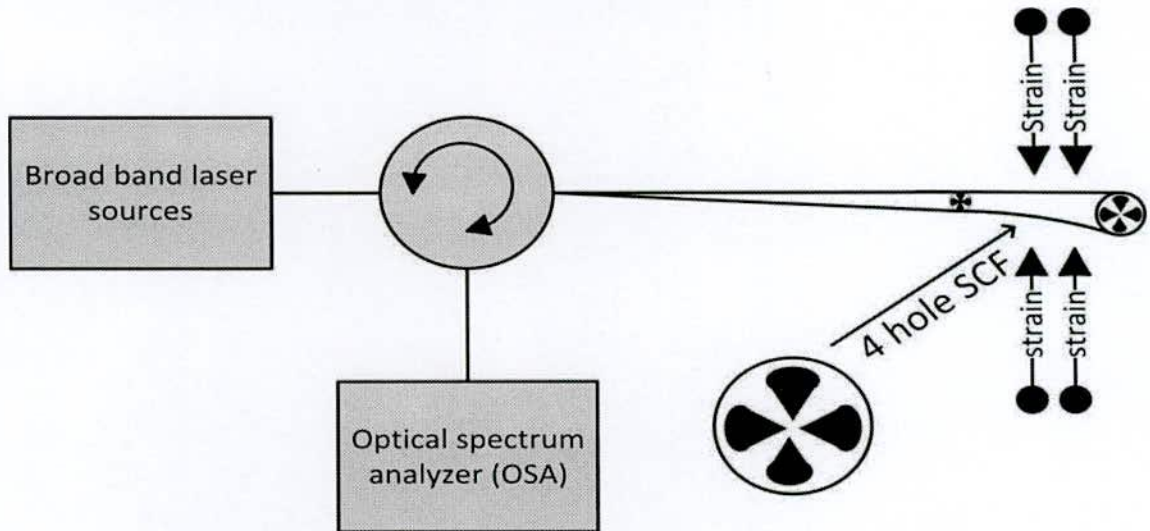


Fig. 2.20 Experimental setup for sensing with Suspended Core Fiber

The air holes of SCF are infiltrated with sample materials and core fields interact with these materials evanescently. Large air hole of SCF helps in speeding up the filling process by sample materials through the air holes in sensing applications. High air filling fraction ensures higher interaction between evanescent field and sample materials. Moreover, broad spectral features have made SCF unparalleled in sensing applications. A typical setup for the sensing application is shown in the below.

2.9 Conclusion

To study the characteristics of PCF as broadband dispersion compensator, some preliminary concepts of PCF has been discussed in brief including PCF construction and basic principles of PCF, refractive index profile, classifications of PCF and difference between conventional optical fiber and PCF. In addition, some guiding properties of PCF have been discussed in details including chromatic dispersion, effective mode area, confinement and bending loss, birefringence, and single and multi-mode response. Considering the fabrication process, various manufacturing technologies have been explained. Finally, application of PCF has been presented.

References

- [1] J. A. Buck, "Fundamentals of optical fibers," *John Wiley & Sons Inc.*, USA, 2nd Edition, 2004.

- [2] J. C. Knight, J. Broeng, T. A. Birks and P. St. J. Russell, "Photonic band gap guidance in optical fibers," *Science*, vol. 282, pp.1476-1478, 1998.
- [3] B. Eggleton, C. Kerbage, P. Westbrook, R. Windeler, and A. Hale, "Microstructured optical fiber devices," *Opt. Express* vol. 9, pp. 698-713, 2001.
- [4] B. Temelkuran, S. D. Hart, G. Benoit, J. D. Joannopoulos, and Y. Fink, "Wavelength-scalable hollow optical fibres with large photonic bandgaps for CO₂ laser transmission," *Nature*, vol. 420, pp. 650-653, 2002.
- [5] P. St. J. Russell, "Photonic crystal fibers," *Science*, vol. 299, no. 5605, pp. 358-362, Jan. 2003.
- [6] P. St. J. Russell, "Photonic crystal fibers", *J. Light w. Technol.*, vol. 24, no. 12, Dec. 2006.
- [7] S. V. Kartalopoulos, "DWDM Networks, Devices, and Technology," *John Wiley & Sons Inc.*, USA, 2003.
- [8] Hect Eugene, "Optics: 4th Ed'," *Addison Wesley* , 2002.
- [9] R. A. Correa and J. C. Knight, "Specialty Fibers: Novel process eases production of hollow core fiber," *Laser Focus World*, vol. 44, no. 05, May 2008.
- [10] Liu Jia-Ming, "Photonic Devices," *Cambridge University Press*, 2005.
- [11] J. C. Knight, "Photonic crystal fibers," *Nature*, vol. 424, pp. 847-851, Aug. 2003.
- [12] L. P. Shen, W. P. Hung, and S. S. Jian, "Design and optimization of photonic crystal fibers for broadband dispersion compensation," *IEEE Photonics Technology Letters*, vol. 15, no. 4, pp. 540-542, Apr. 2003.
- [13] K. Petermann, "Constraints for fundamental-mode spot size for broadband dispersion-compensated single-mode fibers," *Electron. Lett.*, vol. 19, pp. 712-714, Sept. 1983.
- [14] Poli, F., A. Cucinotta and S. Seller, "Photonic crystal fibres: properties and applications," *Dordrecht, Springer*, 2007.
- [15] Goure, J. P. and I. Verrier, "Optical fibre devices," *Cornwall, MPG Books Ltd*, 2002.
- [16] G. P. Agrawal, "Applications of nonlinear fibre optics," *New York, Academic press*, 2008.
- [17] H. Ebendorff-Heidepriem and T. M. Monro, "Extrusion of complex preforms for microstructured optical fibers," *Opt. Exp.*, vol. 15, no. 23, pp. 15086-15092, 2007.
- [18] H. K. Tyagi, M. A. Schmidt, L. P. Sempere, and P. S. Russell, "Optical properties of photonic crystal fiber with integral micron-sized Ge wire," *Opt. Exp.*, vol. 16, no. 22, pp. 17227-17236, 2008.

- [19] Y. DeHazan, J. B. MacChesney, T. E. Stockert, D. J. Trevor, and R. S. Windeler, "U.S. patent," vol.6, 467,312 B1, Oct. 2002.
- [20] R. T. Bise, and D. J. Trevor, "Sol-gel derived microstructured fiber: fabrication and characterization," *Optical Fiber Conference*, OWL6, Mar. 2005.
- [21] H.K.Tyagi, M.A.Schmidt, L.P.Sempere, and P.S.Russell, "Optical properties of photonic crystal fiber with integral micron-sized Ge wire," *Opt. Exp.*, vol. 16, no. 22, pp. 17227-17236, 2008.
- [22] J. Kim, H. K. Kim, U. C. Paek, and B. H. Lee, "The fabrication of a photonic crystal fiber and measurement of its properties," *Journal of Optical Society of Korea*, vol. 7, no. 2, pp. 79-83, Jun. 2003.
- [23] H. Ebendorff-Heidepriem, and T. M. Monro, "Extrusion of complex preforms for microstructured optical fibers," *Opt. Exp.*, vol.15, no. 23, pp. 15086-15092, Oct. 2007.
- [24] K. Mukasa, M. N. Petrovich, F. Poletti, A. Webb, J. Hayes, A. V. Brakel, R. A. Correa, L. Provost, J. Sahu, P. Petropoulos and D. J. Richardson, "Novel fabrication method of highly-nonlinear silica holey fibres," *Conference on Lasers and Electro-Optics, 2006 and 2006 Quantum Electronics and Laser Science Conference. CLEO/QELS 2006*, pp. 1 – 2, 21-26 May 2006.
- [25] H. Ebendorff-Heidepriem, S. C. Warren-Smith, and T. M. Monro, "Suspended nanowires: Fabrication, design and characterization of fibers with nano scale cores," *Opt. Exp.*, vol. 17, no. 4, pp. 2646-2657, Feb. 2009.
- [26] S. G. Leon-Saval, T. A. Birks, W. J. Wadsworth and P. St.J. Russell, "Supercontinuum generation in submicron fibre waveguides," *Opt. Exp.*, vol. 12, pp. 2864-2869, June 2004.
- [27] G. P. Agrawal, "Fiber-Optic Communication Systems," *John Wiley & Sons Inc.*, USA, 2nd Edition, 1997.
- [28] E. Coscelli, M. Sozzi, F. Poli, D. Passaro, A. Cucinotta, S. Selleri, R. Corradini, and R. Marchelli, "Toward a highly specific dna biosensor: pna-modified suspended-core photonic crystal fibers", *J. Quantum Electron.*, vol. 16, no. 4, pp. 967-972, Aug. 2010.
- [29] T. G. Euser, J. S. Y. Chen, M. Scharrer, P. St. J. Russell, N. J. Farrer, and P. J. Sadler, "Quantitative broadband chemical sensing in air-suspended solid-core fibers," *J. Appl. Phys.*, vol. 103, pp. 103-108, 7, May 2008.
- [30] A. S. Webb, F. Poletti, D. J. Richardson, and J. K. Sahu, "Suspended-core holey fiber for evanescent-field sensing," *Opt. Eng. Lett.*, vol. 46, no. 1, pp. 164-70, Jan. 2007.

CHAPTER III

Numerical Modeling and Analysis of DC-SPCFs

3.1 Introduction

In this chapter, various modeling methods and essential equations for the numerical analysis of PCFs modal properties are presented here. A variety of numerical methods have been developed for the electromagnetic analysis of structures with complicated geometries. A summary of all these techniques is shown in Fig. 3.1.

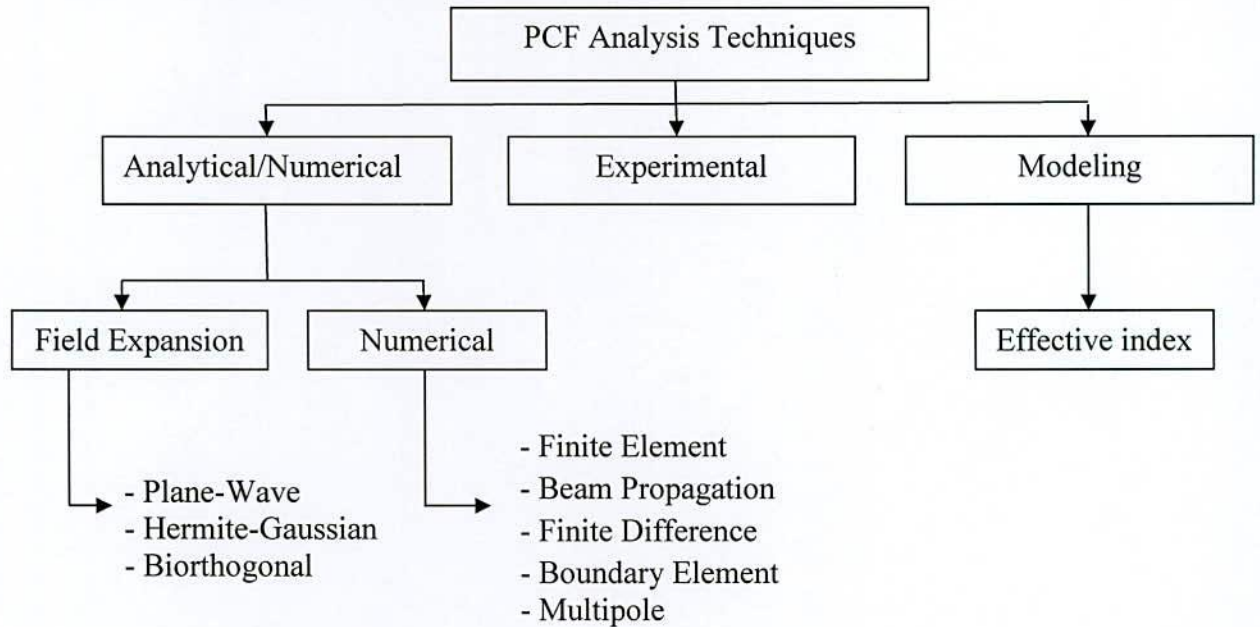


Fig. 3.1 Summary of the techniques used for the analysis of PCFs.

The properties of the various numerical methods used in waveguide can handle arbitrary cross-sectional shapes to analyze guiding properties of the PCF precisely. Moreover, the existence of interfaces with high refractive index-contrast between core and cladding require the use of the vectorial wave equations to accurately model the PCF geometry.

3.2 Numerical methods

In holey fibers or micro-structured optical fibers, index contrast of the materials is generally high, hence the scalar wave analysis methods are not accurate to predict their propagation properties; a full-vector approach is required. Numerical simulations play an important role for the design and modeling of PCFs. Full vectorial methods such as the effective index approach [1], modal decomposition techniques using sinusoidal functions (plane wave expansion method, PWEM) [2], Hermite- Gaussian functions (localized function method,

LFM) [3], beam propagation method (BPM) [4], boundary element method (BEM) [5], finite-element method (FEM) [6]-[9], and finite-difference method (FDM) [10] in time domain or frequency domain has been proposed to date for numerical design tools. Specifically, a highly accurate semi-analytical multi-pole method (MM), has been developed to model fibers with circular air hole inclusions.

The Effective Index method was first proposed by Knox and Toullos in 1970 as an extension to the Marcatili's method (Marcatili 1969) for the fundamental mode of a simple rectangular core waveguide. The advantage of the effective index method is that it can be applied to a wide variety of structures including channel waveguides, strip waveguides and arrays of such waveguides [1] and also for various types of optical fibers and fiber devices [11]. The disadvantage of this method is that it does not give good results when the structure operates near cut-off region.

Another technique based on plane-wave expansion, in which the solution is expressed as a plane-wave modulated by a periodic function that has the same periodicity as that of the photonic crystal structure, was suggested in [12]. However, this technique models the finite PCF structure as well as an infinite structure and, therefore, it is not capable of predicting the confinement loss. Also, it does not take into account the geometry of inclusions, thus not an efficient method.

The localized function method based on Galerkin method has been widely used for waveguide analysis, both scalar and vectorial problems. This method applies a set of localized orthogonal functions, such as Sine, Laguerre-Gauss [13] (for 1D waveguide), and Hermite-Gauss [14] (for 2D problem), to approximate the unknown mode fields of the localized modes. When the mode is far away from cut-off or well confined, the mode fields can be approximated using tens or hundreds of functions. These methods generally involve integrations, which are computation intensive, and the convergence is generally a problem.

The Beam Propagation Method (BPM) describes the evolution of the total field propagating along a waveguide and it is the most widely used tool in the study of light propagation in longitudinally varying waveguides such as tapers, Y-junctions, bends and gratings. The initial BPM is based on the Fast Fourier Transform (FFT) and only solves the scalar wave equations under paraxial approximation. Therefore the FFT-BPM was only developed for the case of weakly guiding structures, neglecting the vectorial properties of the field. But the Vectorial Beam Propagation Methods (VBPMs) are capable of simulating polarized or even hybrid wave propagation in strongly guiding structures.

The Finite Difference Method (FDM) is one of the oldest and perhaps the most commonly used numerical techniques in analyzing dielectric waveguide problems. The finite difference method discretizes the cross section of the device that is being analyzed and it is therefore suitable for modeling inhomogeneous media and complicated boundaries. In FDM, it is necessary to define the finite cross section by enclosing the dielectric guide in a rectangular box. However, if leakage losses need to be calculated, these hard boundaries can be replaced by Perfectly Matched Layer (PML). At that case, the nodes are placed on mesh points so that each node can be associated to a maximum of four or eight neighboring nodes and each node can be of one or more field variables depending on vector, semi-polarized or scalar wave equations that can be approximated in terms of the fields at the neighboring nodes of the mesh. The accuracy of the method depends on the mesh size, the assumed nature of the electromagnetic field (scalar, polarized or vector) and the order of the finite difference scheme used. If a uniform mesh is used then it can result in a very large number of nodes and large matrices and therefore the disadvantages like long run times and high memory requirements may become apparent.

The Boundary Element Method (BEM) is interpreted as a combination technique of the conventional boundary integral equation method and a discretisation technique. The BEM is a boundary solution method and therefore the fields would be required only at the nodes which are on the boundaries of the region. Guan *et al.* [15] used the vector form of the boundary element method (BEM) to examine the guided modal fields of PCFs. In this method, the curved edges between the silica structure and the air holes are modeled as tiny linear segments, and then Green's theorem is used to solve the eigenvalue equation of the unknowns assigned to the segments. Spurious solutions of the BEM were avoided by formulating the eigen value problem using the transverse magnetic field components instead of the longitudinal components of the electric and magnetic fields. Resonances were also suppressed by introducing two observation points for each boundary segment instead of one point. However, the boundary element method can only be applied to homogenous structures. Therefore, the finite element method can be treated as more numerically efficient than the boundary element method.

White *et al.* [16] extended the multipole formulations for multi-core conventional fibers to treat PCFs. In their method, they divide the cross-section of the fiber into homogeneous regions where the wave equation decomposes into two scalar Helmholtz equations that, in turn, lead to a matrix equation which is solved by an iterative technique. This method takes into account the rotational symmetry of PCFs to increase computational efficiency.

The Finite Element Method (FEM) is a well-established numerical method for the solution of a wide range of guided wave problems. It can be very easily applied not only to optical waveguides of any shape but also to optical waveguides with any refractive index distribution, PCF dispersion [17] as well as parametric amplification [18] and to those with any anisotropic materials or nonlinear materials [19]. This method is based upon dividing the problem region into a non-overlapping patchwork of polygons, usually triangular elements. The field over each element is then expressed in terms of polynomials weighted by the fields over each element. This method is solved using iterative techniques to obtain the propagation constants and the field profiles. Then accuracy of the finite element method can be increased by using finer mesh. A number of formulations have been proposed, however, the full vectorial \mathbf{H} field formulation is the most commonly used and versatile method in modeling optical waveguides due to much easier treatment of the boundary conditions. This method can accurately solve the open type waveguide problems near cut-off region and much better results were obtained by introducing infinite elements to extend the region of explicit field representation to infinity. One drawback associated with this powerful vector formulation is the appearance of spurious or non-physical solutions. In order to eliminate the spurious solutions completely, another approach is employed using the edge elements. In addition, the complex FEM formulation has been very useful to evaluate the PCF leakage or confinement losses due to the finite number of air-hole rings in the cladding lattice. In modeling more complex structures, the finite element method is considered to be more flexible than the finite difference method due to the ability of employing irregular mesh. In this thesis, the COMSOL Multiphysics 4.2 software based on the FEM is used for PCF's modal computations.

3.2.1 FEM formulation

COMSOL Multiphysics 4.2 software is used to analyze the various properties of the PCF presented in this thesis which is based on FEM. Through the FEM results, we have studied the leakage loss, dispersion properties, vectorial character, as well as the degeneracy of modes and single-mode of particular kinds of PCFs. Using FEM, the PCF cross section, with the finite number of air holes, is divided into homogeneous subspaces. However, these subspaces are triangles that allow a good approximation of the circular structures of PCF. Afterward, each adjacent sub-space is solved using Maxwell's equations. On the other hand, the leakage loss of a mode can be represented by the imaginary part of its complex

propagation constant. The axial dependence is assumed in the form $e^{-j\beta z}$ and the transverse plane is used for the discretization.

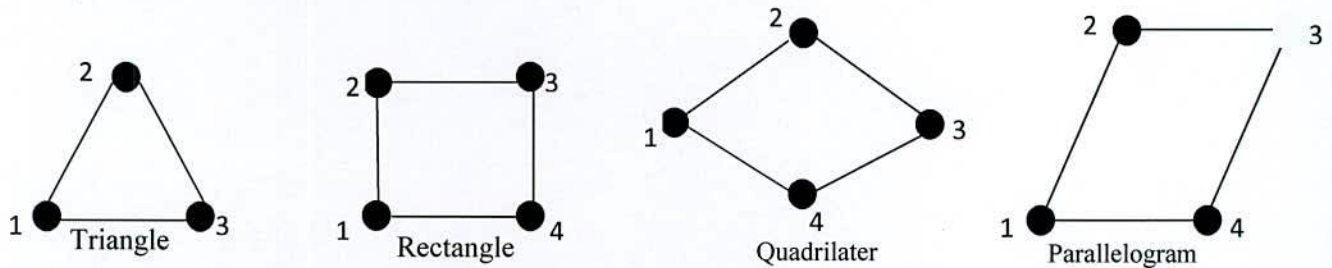


Fig. 3.2 Finite elements in two dimensions

3.2.2 Domain discretization

The discretization of the domain into sub-regions (finite elements) is considered as the initial step in the finite element method. The shapes, sizes, number and configurations of the elements have to be chosen carefully such that the original body or domain is simulated as closely as possible without increasing the computational effort needed for the solution. Each element is essentially a simple unit within which the unknown can be described in a simpler manner. There are various types of elements available for use in finite element formulations. After running the simulations for the numerical experiments, the following parameters are noted down from the program after the simulations concludes:

- Wavelength
- Real propagation constant
- Imaginary propagation constant
- Effective index
- Loss
- H_x field
- H_y field
- H_z field
- Spot size
- Effective area

3.2.3 Boundary conditions

During the numerical analysis, we have considered three types of boundary conditions.

They are:

- Perfect Electric Conductor (PEC): This boundary condition can be expressed as, $\mathbf{n} \cdot \mathbf{B} = 0$

$$\mathbf{n} \times \mathbf{E} = 0 \quad (3.1)$$

Here, \mathbf{n} is the unit normal vector to the boundary. According to this condition, tangential components of \mathbf{E} and normal components of \mathbf{B} is continuous across any interface.

- Perfect Magnetic Conductor (PMC): This boundary condition can be expressed as,

$$\mathbf{n} \cdot \mathbf{D} = 0$$

$$\mathbf{n} \times \mathbf{H} = 0 \quad (3.2)$$

According to this condition, tangential components of \mathbf{H} and normal components of \mathbf{D} is continuous across any interface.

- Perfectly Matched Layer (PML):

A perfectly matched layer is an artificial boundary condition implying perfect absorption of incident electric field. This boundary condition is required for approximating infinite zone beyond the waveguide outer edge to a finite domain of numerical analysis. Through the adjusting of the PML parameters so as to have a wave impedance of exactly the same as inside the computational domain, the PML can offer a reflection less boundary to the outgoing radiation whatever its strength or angle it hits the PML computational domain interface. The PML boundary condition effectively absorbs the unwanted radiation waves without reflection. However, the optimized conductivity is calculated from certain sets of equations. In our work, we have considered cylindrical PML available in the commercial COMSOL Multiphysics 4.2 software.

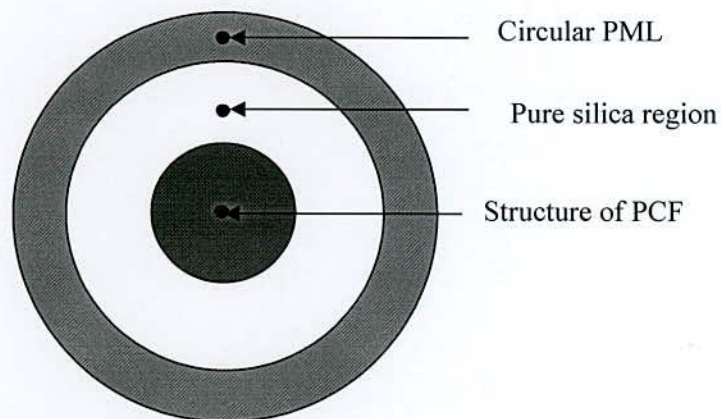


Fig. 3.3 PML region surrounding the waveguide structure

Formulation of wave equations in the PML region can be done after rigorous analysis,

$$\begin{aligned}\Delta \times \bar{H} &= j\omega n^2 s \bar{E} \\ \Delta \times \bar{E} &= -j\omega \mu_0 s \bar{H} \\ s &= 1 - j \frac{\sigma_e}{\omega n^2 \epsilon_0} = 1 - j \frac{\sigma_m}{\omega \mu_0}\end{aligned}\quad (3.3)$$

3.3 Step by step analysis

The most widely used kind of PCFs are those with cladding made up of circular holes arranged in a triangular lattice with core residing in the region at the center formed by missing of hole(s) Fig.3.4 shows the fiber cross sections together with the FEM mesh and size of computational window. By the help of the boundary conditions, the computation can be carried out in a relatively small computational domain. Also by taking advantages of the structure mirror symmetry, we only need a quarter of the structure as the computational domain.

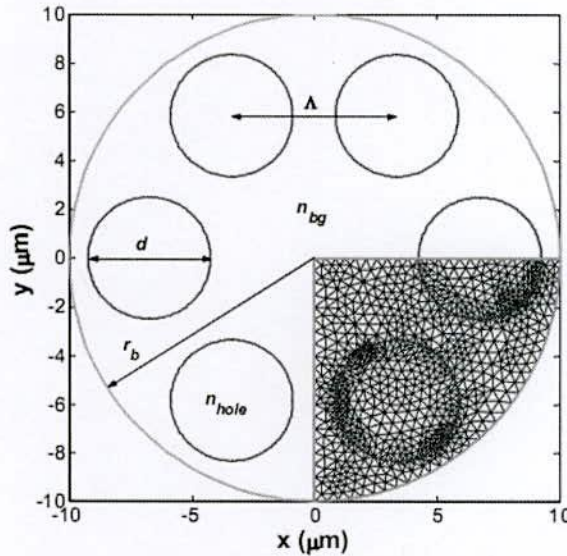


Fig. 3.4 PCF with 6 circular air holes in its cladding, the FEM mesh and the computational window

3.4 Determination of the modal properties of PCF

The designed PCF is simulated to find the effective refractive index, n_{eff} using COMSOL Multiphysics 4.2 based on FEM. After taking the effective refractive index, n_{eff} is obtained, the modal properties of the PCF such as chromatic dispersion, dispersion slope and relative dispersion slope (RDS), effective dispersion, confinement loss, birefringence,

effective area and effective V-parameter can be easily calculated using the following equations.

3.4.1 Chromatic dispersion

The higher-order dispersion terms depend on both waveguide dimensions and material dispersion. Material dispersion occurs due to variation of speed of light inside the material for different wavelengths. Wavelength dependence of refractive index is responsible for material dispersion. To account this effect, *Sellmeier formula* (also called *Sellmeier equation* or *Sellmeier dispersion formula*, after W. Sellmeier) is normally used. It is an empirical relationship between refractive index and wavelength for a particular transparent medium. The usual form of the equation for glasses is,

$$n^2(\lambda) = 1 + \frac{B_1\lambda^2}{\lambda^2 - C_1} + \frac{B_2\lambda^2}{\lambda^2 - C_2} + \frac{B_3\lambda^2}{\lambda^2 - C_3} \quad (3.4)$$

where n is the refractive index, λ is the wavelength, and $B_{1,2,3}$ and $C_{1,2,3}$ are experimentally determined Sellmeier coefficients. These coefficients are usually quoted for λ in micrometers and λ is the vacuum wavelength.

The chromatic dispersion of the PCF is calculated from the following differential equation formulated in [20].

$$D(\lambda) = -\frac{\lambda}{c} \frac{d^2 \text{Re}[n_{eff}]}{d\lambda^2} \text{ ps/(nm.km)} \quad (3.5)$$

In above equation, is the real part of effective refractive index, λ is the wavelength, c is the velocity of light in vacuum. The total dispersion is algebraic summation of material dispersion and waveguide dispersion $\text{Re}[n_{eff}]$. Moreover, the waveguide dispersion strongly depends on the silica-air structure itself [21] and can be altered significantly by modulating some parameters like geometry of the air holes, pitch, and air-hole diameters. Hence, the chromatic dispersion of PCFs is related to those additional design parameters and by optimizing these parameters, suitable guiding properties can be achieved for dispersion compensation of SMF.

3.4.2 Dispersion length

In order to determine the effects of higher order dispersions on pulse propagation, some characteristics length scales are needed to be defined. By comparing these length scales to each other or the actual device length L , one can obtain a rough estimate of which terms

need to be taken into account in order to construct an accurate model. Important dispersion length parameters are:

$$L_{D3} = \frac{T_0^3}{\beta^3} \quad (3.6)$$

$$\gamma = \frac{2\pi}{\lambda} \times \frac{n_2}{A_{eff}} \quad (3.7)$$

$$L_{D4} = \frac{T_0^4}{\beta^4} \quad (3.8)$$

Here T_0 is the pulse width of the source excitation operating at a certain central wavelength.

3.4.3 Nonlinear length

Nonlinear length is the minimum length of the device necessary for occurrence of nonlinear effects. It is defined as below,

$$L_{NL} = \frac{1}{\gamma P_0} \quad (3.9)$$

where P_0 is the peak power of the source laser.

3.4.4 Walk off length

The characteristic walk-off length represents the distance over which the pump and probe pulses pass through each other's envelope. It is defined as below,

$$L_w(\lambda) = \frac{T_0}{|\beta_{1p}(\lambda) - \beta_{1s}(\lambda)|} \quad (3.10)$$

where T_0 is the width of the pulse (at 1/e intensity), and $\beta_{1p}(\lambda)$ and $\beta_{1s}(\lambda)$ are the first-order dispersion coefficients of the pump and probe wavelengths, respectively.

3.4.5 Dispersion slope and RDS

Dispersion slope $D(\lambda)$ describes the amount of change in chromatic dispersion as a function of wavelength, λ . Chromatic dispersion is the derivative of relative pulse delay and dispersion slope is the derivative of chromatic dispersion values, whereas the RDS is found by taking the ratio of dispersion slope to dispersion. The equations of DS and RDS are given as follows [22].

$$DS(\lambda) = \frac{dD(\lambda)}{d\lambda} \text{ ps}/(nm^2 \cdot km) \quad (3.11)$$

$$RDS = \frac{DS(\lambda)}{D(\lambda)} nm^{-1} \quad (3.12)$$

$$RDS_m = RDS_n = \frac{DS_m(\lambda)}{D_m(\lambda)} = \frac{DS_n(\lambda)}{D_n(\lambda)} \quad (3.13)$$

The RDS is used to judge dispersion compensating capability of a DCF over a range of wavelengths. Once the RDS of the DCF is close to that of the SMF, the design of the broadband DCF will be accomplished. However, the RDS of SMF is 0.0036nm^{-1} at 1550 nm.

Lower dispersion slopes result in fewer dispersion changes throughout the wavelength and thus chromatic dispersion remains constant as a function of wavelength is shown in Fig.3.5. For high speed multichannel DWDM network, lower dispersion channel enable more uniform, optimal performance across the DWDM wavelength.

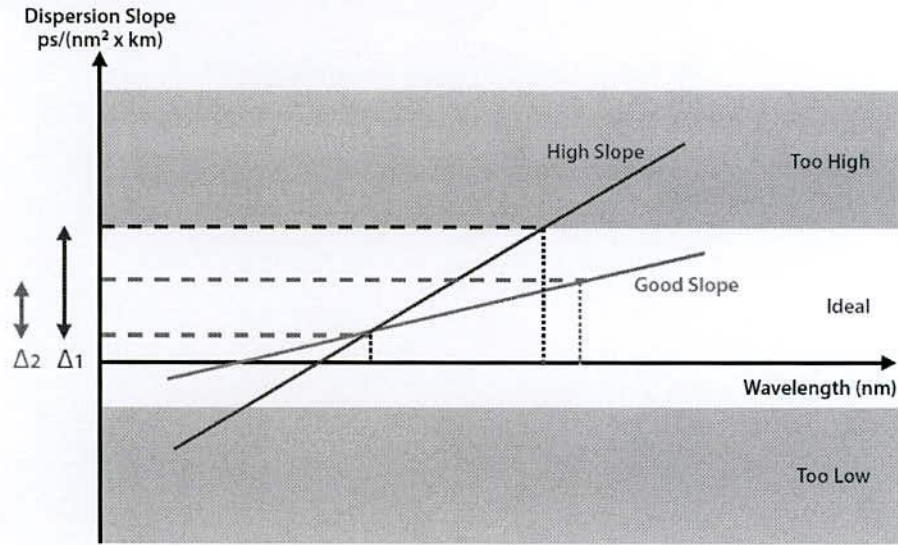


Fig. 3.5 Dispersion slope variation

3.4.6 Effective dispersion

A fiber link consists of transmission fiber mainly SMF of length L_m with the dispersion of $D_m(\lambda)$ and a dispersion compensating fiber (DCF) of length L_n , with the dispersion of $D_n(\lambda)$. The effective dispersion $D_e(\lambda)$, on the fiber link after compensating the SMF of length, can be calculated using the following equation [22].

$$D_e(\lambda) = \frac{D_m(\lambda)L_m + D_n(\lambda)L_n}{L_m + L_n} \text{ ps}/(\text{nm.km}) \quad (3.14)$$

It should be noted that the effective dispersion of DCF should be lower than ± 0.8 ps/(nm.km) for higher data transmission rate [20, 22].

3.4.7 Confinement loss

Confinement losses or leakage losses are present in PCFs due to the fact that there are a finite number of air-holes that can be made in the cross-section of the cladding which results

in the PCF guided modes to be leaky [23] The diameter to pitch ratio (d/Λ) in a particular design of PCF determines how much light leaks from the core into the cladding. The lower the ratio, the more leakage is expected into the cladding.

On the other hand, there is a design freedom in PCF to choose the suitable number of air-hole rings to keep the confinement loss within the desired value. However, the confinement loss in dB/m can be defined as [22]

$$L_c = 8.686 \times \frac{2\pi}{\lambda} \times I_m[n_{eff}] \quad (3.15)$$

where $I_m[n_{eff}]$ represents the imaginary part of the wavelength dependent refractive index and λ is the wavelength in the free space.

3.4.8 Birefringence

When installing a new fiber optic network or upgrading an existing network to higher bit rate, the quality and the properties of the optical fiber determine the suitability of this network to carry a defined transmission speed. Polarization mode dispersion (PMD) may pose severe limits on the transmission of higher data rates over existing fiber infrastructure. As a result, PMD measurements have become an essential part of the fiber characterization process.

PMD is caused by local birefringence (or double refraction) in the fiber, which may arise from a combination of material and waveguide birefringence. If a fiber exhibits different indexes of refraction (IOR) based on polarization states (rotational orientation with respect to the fiber axis) of the transmission signal, then this fiber is said to be birefringent. The different IORs lead to different velocities of propagation of the modes.

The birefringence is defined as [22].

$$B = [n_x - n_y] \quad (3.16)$$

Where, n_x and n_y are the mode indices of the two orthogonal polarization fundamental modes. It should be mentioned that, the conventional PM fiber exhibits a modal birefringence of about 5×10^{-4} and is insufficient to eliminate the effect of PMD. Hence, birefringence of the DCF should be higher to eliminate the PMD of SMF.

In silica optical fibers, material birefringence is typically the result of internal or external stress in fiber core, introduced in the fiber manufacturing process or in fiber cabling through bending and twisting. Breaking the symmetry of the PCF core can increase the birefringence of the PCF.

3.4.9 Effective area

The effective area A_{eff} in μm^2 of the proposed PCF is obtained from [20] and is given

$$A_{eff} = \frac{(\iint |E|^2 dx dy)^2}{(\iint |E|^4 dx dy)} \quad (3.17)$$

where E is the electric field vectors in the medium. Small effective areas are indicative of significant nonlinear effects inside the core of the fiber. Effective area is also related to confinement loss, micro-bending loss, macro-bending loss, and splicing loss of the fiber [24].

3.4.10 Numerical aperture

Rays that meet the core-cladding boundary at an angle (measured relative to a line normal to the boundary), greater than the critical angle for this boundary, are completely reflected. The critical angle (minimum angle for total internal reflection) is determined by the difference in index of refraction between the core and cladding materials. Rays that meet the boundary at a low angle are refracted from the core into the cladding and do not confine light and hence information along the fiber. The critical angle also determines the acceptance angle of the fiber, often related to the numerical aperture. A high numerical aperture allows light to propagate down the fiber in rays both close to the axis and at various angles, allowing efficient coupling of light into the fiber. However, this high numerical aperture increases the amount of dispersion as rays at different angles have different path lengths and therefore take different times to traverse along the fiber. A low numerical aperture may therefore be desirable.

3.4.11 Single and multimode response

Optical fibers with large core diameters, that are greater than $10\mu m$, may be analyzed by geometric optics. Such optical fibres are more likely to be multimode fibers from the electromagnetic analysis. This is because the V parameter (which is the normalized optical frequency) is likely above 2.405. As an optical waveguide, the fiber may support one or more confined transverse modes by which light can propagate along the fiber. Fiber supporting only one mode is called single mode or mono mode fiber. The behavior of larger core multimode fiber can also be modeled using the wave equation which shows that such fiber supports more than one mode of propagation.

However, the tradition of determining single and multimode response from V parameter stems from analysis of the step-index fiber (SIF). In contrast, due to the constructional

difference between SIF and PCF, the equation to find the V parameter should be different from that of SIF and the equation of effective V parameter is given by [25].

$$V_{eff} = k\Lambda F^{\frac{1}{2}}(n_{eff}^2 - n_a^2) \quad (3.18)$$

where $k = \frac{2\pi}{\lambda}$ is the wave number in the vacuum, F is the air-filling fraction, Λ is the pitch, n_{eff} is the effective index, and n_a is the refractive index of the air. Once the normalized effective parameter, V is obtained as $V_{eff} < \pi$ for certain wavelength bands, then the fiber will act as a single mode fiber (SMF) over that wavelength band.

The most common type of single mode fiber has a core diameter of 8 to 10 μm , with refractive index difference between core and cladding around 0.36% and is designed for use in the near infrared. Multimode fiber by comparison, is manufactured with core diameters as small as 50 micrometers and as large as hundreds of micrometers [25].

In a graded index fiber, the refractive index in the core decreases continuously between the axis and the cladding. This causes light rays to bend smoothly as they approach the cladding rather than reflecting abruptly from the core-cladding boundary. The resulting curved paths reduce multipath dispersion because high angle rays pass more through the lower index periphery of the core rather than the high index centre.

3.5 Conclusion

To analyze the numerical modeling of PCF, there are numerous modeling techniques have been explained. But FEM has been widely used due its novel features which are already discussed in this thesis. For simulating the PCF, COMSOL Multiphysics 4.2 software based on FEM has been used in this thesis. As well as, important and necessary equations for numerical computations have been presented to study the properties of PCF as broadband dispersion compensator.

References

- [1] Chiang, K. S., K. M. Lo and K. S. Kwok, "Effective-index method with built-in perturbation correction for integrated optical waveguide," *J. Lightwave Technol.* vol.14, no.2, pp.223-228, 1996.
- [2] A. Ferrando, E. Silvester, J. J. Miret, P. Andrés, and M. V. Andrés, "Full vector analysis of a realistic photonic crystal fiber," *Optics Letters*, vol. 24, no. 5, pp. 276–278, Mar. 1999.

- [3] D. Mogilevtsev, T.A. Birks, and P.St.J. Russell, "Localized function method for modeling defect modes in 2-D photonic crystals," *J. Lightwave Technol.*, vol. 17, no. 11, pp. 2078–2081, Nov. 1999.
- [4] F. Fogli, L. Saccomandi, and P. Bassi., "Full vectorial BPM modeling of index guiding photonic crystal fibers and couplers," *Optics Express*, vol. 10, no. 1, pp. 54–59, Jan. 2002.
- [5] T. L. Wu and C. H. Chao, "Photonic crystal fiber analysis through the vector boundary-element method: Effect of elliptical air hole," *IEEE Photonics Technology Letters*, vol. 16, no. 1, pp. 126–128, Jan. 2004.
- [6] F. Brechet, J. Marcou, D. Pagnoux, and P. Roy, "Complete analysis of the characteristics of propagation into photonic crystal fibers, by the finite element method," *Opt. Fiber Technol.*, vol. 6, no. 2, pp. 181–191, Apr. 2000.
- [7] S. Guenneau, A. Nicholet, F. Zolla, and S. Lasquellec, "Modeling of photonic crystal optical fibers with finite elements," *IEEE Trans. Magn.*, vol. 38, no. 2, pp. 1261–1264, Mar. 2002.
- [8] M. Koshiba, "Full-vector analysis of photonic crystal fibers using the finite element method," *IEICE Trans. Electron.*, vol. 85-C, no. 4, pp. 881–888, Apr. 2002.
- [9] A. Cucinotta, S. Selleri, L. Vincetti, and M. Zoboli, "Holey fiber analysis through the finite-element method," *IEEE Photon. Technol. Lett.*, vol. 14, no. 11, pp. 1530–1532, Nov. 2002.
- [10] Z. Zhu and T. G. Brown, "Full-vectorial finite-difference analysis of microstructured optical fibers," *Optics Express*, vol. 10, no. 17, pp. 853–864. Aug. 2002.
- [11] Van de Velde, K., H. Thienpont and R. Van Green. "Extending the effective index method for arbitrarily shaped inhomogeneous optical waveguides." *J. Lightwave Technol.* vol. 6, no.6, pp.1153-1159, 1988.
- [12] J. Broeng, T. Sondergaard, S. E. Barkou, P. M. Barbeito, and A. Bjarklev, "Waveguidance by the photonic bandgap effect in optical fibers," *J. Opt. A: Pure Appl. Opt.*, vol. 1, no. 4, pp. 477–482, 1999.
- [13] D. Marcuse, "Solution of the vector wave equation for general dielectric waveguides by the Galerkin method," *IEEE J Quantum Electron.*, vol. 28, pp. 459-465 1992.
- [14] A. Weisshaar, J. Li, R. L. Gallawa, I. C. Goyal, "Vector and quasi-vector solutions for optical waveguide modes using efficient Galerkin's method with Hermite-Gauss basis functions," *J. Lightwave Technol.*, vol. 13, pp. 1795-1780, 1995.

- [15] N. Guan, S. Habu, K. Takenaga, K. Himeno, and A. Wada, "Boundary element method for analysis of holey optical fibers," *J. Lightwave Technol.*, vol. 21, no. 8, pp. 1787–1792, 2003.
- [16] T. P. White, B. T. Kuhlmeiy, R. C. McPhedran, D. Maystre, G. Renversez, C. M. de Sterke, and L. C. Botten, "Multipole method for microstructured optical fibers. I. Formulation," *J. Opt. Soc. Amer.*, vol. 19, no. 10, pp. 2322–2330, 2002.
- [17] F. Poli, A. Cucinotta, S. Selleri, and A. H. Bouk, "Tailoring of flattened dispersion in highly nonlinear photonic crystal fibers," *IEEE Photonics Technology Letters*, vol. 16, pp. 1065–1067, Apr. 2004.
- [18] A. Cucinotta, F. Poli, and S. Selleri, "Design of erbium-doped triangular photonic crystal fiber based amplifiers," *IEEE Photonics Technology Letters*, vol. 16, pp. 2027–2029, Sept. 2004.
- [19] M. Fuochi, F. Poli, S. Selleri, A. Cucinotta, and L. Vincetti, "Study of Raman amplification properties in triangular photonic crystal fibers," *IEEE Journal of Lightwave Technology*, vol. 21, pp. 2247–2254, July 2003.
- [20] F. Begum *et al.* "Novel broadband dispersion compensating photonic crystal fibers: Applications in high speed transmission," *Optics and Laser Technology*, vol. 41, no. 6, pp. 679–686, Sep. 2009.
- [21] A. Bjarklev, J. Broeng, and A. S. Bjarklev, "Photonic crystal fibres," *Kluwer Academic Publishers, USA*, 2003.
- [22] S. F. Kaijage, Y. Namihira, N. H. Hai, F. Begum, S. M. A. Razzak, T. Kinjo, K. Miyayagi, and N. Zou, "Broadband dispersion compensating octagonal photonic crystal fiber for optical communication applications," *Japanese Journal of Applied Physics*, vol. 48, 2009.
- [23] Poli, F., A. Cucinotta and S. Seller, "Photonic crystal fibres: properties and applications," *Dordrecht, Springer*, 2007.
- [24] N. Mortensen, "Effective area of photonic crystal fibers," *Opt. Express*, vol. 10, no. 7, pp. 341–348, 2002.
- [25] Goure, J. P. and I. Verrier, "Optical fibre devices". *Cornwall, MPG Books Ltd*, 2002.

CHAPTER IV

Design of Zero-Dispersion Spiral Photonic Crystal Fiber

4.1 Introduction

To analyze the various properties of Spiral Photonic Crystal Fiber (SPCF), nearly zero dispersion fibers (NZDFs) with high nonlinearity and dispersion compensating fibers (DCFs) is our desirable characteristics in this thesis. To do this, various design methodologies have been described sequentially in chapter IV and chapter V. A novel NZDF at operating wavelength with low effective area has been discussed in this chapter and design of dispersion compensating fibers (DCFs) have been explained in chapter V. The supercontinuum generation (SCG) by using micro structured (MS) PCF has become a topic of intense research since it is reported by Rank et al. 2000 [1]. In SCG, tailoring the dispersion to achieve flat, anomalous dispersion with small slope and a zero crossing near/at the pump wavelength is an extremely important aspect [2]. Pumping near zero dispersion wavelengths (ZDW) with higher nonlinearity not only reduces its power requirement but also smoothes the generated supercontinuum (SC) power spectra [3]. Therefore, the researchers are working on hexagonal, octagonal and various irregular design architectures towards highly nonlinear dispersion flattened PCF [4]. It has already been reported that silica PCF with asymmetrical hole distribution provides the maximum possible nonlinearity, whereas a very small improvement over the symmetric case may be obtained [5]. A soft glass equiangular spiral PCF has already been reported to be a suitable candidate for SCG pumped at near infrared wavelength of 1064 nm due to its higher nonlinearity ($\approx 5250 \text{ W}^{-1}\text{km}^{-1}$) [6]. However, the SCG being pumped at visible region should be an important phenomenon due to its embedded application in nanoscopy, confocal microscopy, and flow cytometry [7]. But, SCG in highly nonlinear soft glass, schott SF6, bismuth oxide, and tellurite PCFs using long pump pulses (ns) in visible region is difficult possibly because of the low damage threshold of these glasses. Silica is superior in the visible region due to its few orders of magnitude higher damage threshold than the above mentioned nonlinear materials [8]. Therefore, in this work, we have engineered the spiral PCF design architecture [6] in silica material to achieve nearly zero dispersion fiber (NZDF) with higher nonlinearity in the visible region. In recently silica host PCF with GeO_2 doped SiO_2 square defected core exhibits dispersion characteristics (0.0001787ps/km-nm) with very low effective area ($3.03 \mu\text{m}^2$) at 1550nm has been reported [9]. To improve the above result, a PCF containing GeO_2 doped defected SiO_2 square in the core with spiral air hole arms(dd-

SPCF) is proposed. The simulation for the structure shows ultrahigh nonlinearity ($76.44 \text{ W}^{-1}\text{km}^{-1}$ at 1550nm), and dispersion characteristics $-0.000169 \text{ ps/km-nm}$ with very low effective area $2.6516\mu\text{m}^2$. So, the proposed dd-SPCF may be a suitable candidate for SCG in ultraviolet to infrared regions. The analysis of this work has been carried out using a full-vector FEM [10], which allow the determination of the optical mode field distributions of the pump signal over the entire cross section of the fiber.

4.2 Requirements of nearly zero dispersion fibers (NZDFs) at operating wavelength

The fiber is simulated by a Finite Element Method (FEM) with Perfect Matched Layers (PMLs) absorbing boundary condition. The COMSOL software 4.2 version is used as a simulation tool. The FEM directly solves the Maxwell equations to best approximate the value of the effective refractive index. Once the modal effective refractive index, n_{eff} is obtained by solving an eigen value problem drawn from Maxwell equations using the COMSOL software 4.2, chromatic dispersion, effective area and confinement loss of PCFs can be easily calculated.

The finite element method transforms the magnetic field vector wave equation as

$$([A] - (k_0^2 - n^2)[B])\{h\}=0 \quad (4.1)$$

where $[A]$ and $[B]$ are algebraic matrix, $\{h\}$ is magnetic field vector distributing of cross section.

The dispersion of microstructured fibers can also be divided into two types, one is material dispersion $D_m(\lambda)$ expressed as

$$D_m(\lambda) = -\lambda/c (d^2\text{Re}[n_{\text{eff}}]/d\lambda^2) \quad (4.2)$$

Where $\text{Re}[n_{\text{eff}}]$ is the real part of effective refractive index n_{eff} , λ is the wavelength, c is the velocity of light in vacuum. Refractive index of SiO_2 and GeO_2 can be found from Sellmeier's equation [11].

$$n^2 = 1 + \sum_{i=1}^3 \frac{A_i \lambda^2}{\lambda^2 - l_i} \quad (4.3)$$

where A_i and l_i are the oscillator strength and oscillator wavelength respectively. The refractive index of GeO_2 doped SiO_2 can be computed from the following equation [11].

$$n^2 = 1 + \sum_{i=1}^3 \frac{[SA_i + X(GA_i - SA_i)]\lambda^2}{\lambda^2 - [Sl_i + X(Gl_i - Sl_i)]^2} \quad (4.4)$$

where SA , Sl , GA , Gl are the Sellmeier coefficients for the SiO_2 and GeO_2 glasses and X is the doping concentration of GeO_2 and the material dispersion based on Sellmeier's equation

has been taken into account explicitly in the effective index of the PCF. The effective area A_{eff} is calculated as follows [12].

$$A_{eff} = \left(\int_{-\infty}^{\infty} \int_{-\infty}^{\infty} |E|^2 dx dy \right)^2 / \int_{-\infty}^{\infty} \int_{-\infty}^{\infty} |E|^4 dx dy \quad (4.5)$$

Then using effective area we calculate the nonlinearity parameter by [13].

$$\gamma = \frac{2\pi n_2}{\lambda A_{eff}} \quad (4.6)$$

where nonlinear refractive index, n_2 for GeO₂ doped SiO₂ can be calculated as [13].

$$n_2 = 2.507 + 0.505\Delta \quad (4.7)$$

4.3 Structure of SPCF with GeO₂ doped defected SiO₂ square in the core

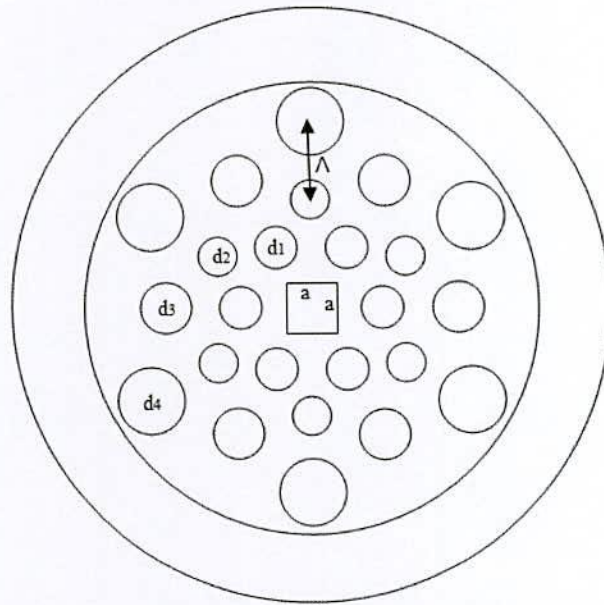


Fig. 4.1 Structure of the proposed SPCF for NZDF

The cross section of the proposed GeO₂ doped defected SiO₂ square core SPCF structure is shown in Fig.4.1. It has 6 arms and the starting air holes of each arm form a single spiral of radius r_0 with equal angular displacement from previous one is increased by θ . The radii of subsequent rings enhance by geometric progression of following manner ($r_0, r_0+2p, r_0+4p, \dots$); where p represents the distance factor to control the pitch. The air-hole pitch is labeled Λ . Each arm contains 4 air holes which are denoted by d_1, d_2, d_3 and d_4 respectively. The central core region is perturbed by a GeO₂ doped SiO₂ square with side a . The host material is regular silica. The insertion of the extra GeO₂ doped SiO₂ square in the core region is the novel concept of the present design. The existence of the central defected air-

hole has the function to control the waveguide dispersion properties of the fiber as will be demonstrated later on. The NZDF can be fabricated by the sol-gel method [14] which gives well-arranged air holes. To analyze, $\Lambda=1.4$, $r_0=1.3\mu\text{m}$, $\theta =60^\circ$, $a=1\mu\text{m}$, $d_4=0.6\mu\text{m}$, $d_3=0.48\mu\text{m}$, $d_2=0.32\mu\text{m}$ and $d_1=0.416\mu\text{m}$ are reported for the optimized structure.

4.4 Numerical simulation using COMSOL Multiphysics 4.2

COMSOL Multiphysics (formerly FEMLAB) 4.2 is a versatile simulation software based on FEM. It is a flexible platform that allows even novice users to model all relevant physical aspects of their designs. COMSOL Multiphysics also offers an extensive interface to MATLAB. Simulation of a dd-SPCF model using COMSOL Multiphysics 4.2 software requires a high configuration computer. In this thesis, all simulations are performed with a notebook of HP brand (ProBook 4440s). The detail configuration of used notebook is as follows:

Processor	Intel(R) core(TM) i5, 3230M CPU@2.60GHz
RAM (Installed)	4GB
Operating System	Windows 7 Ultimate, 64 bit
Cache memory RAM, (built into the processor)	3MB

4.4.1 Simulation results of GeO₂ doped defected SiO₂ square core SPCF

The wavelength dependence of Silica glass, GeO₂ and GeO₂ doped SiO₂ based on sellmeier's equation is shown in Fig.4.2.

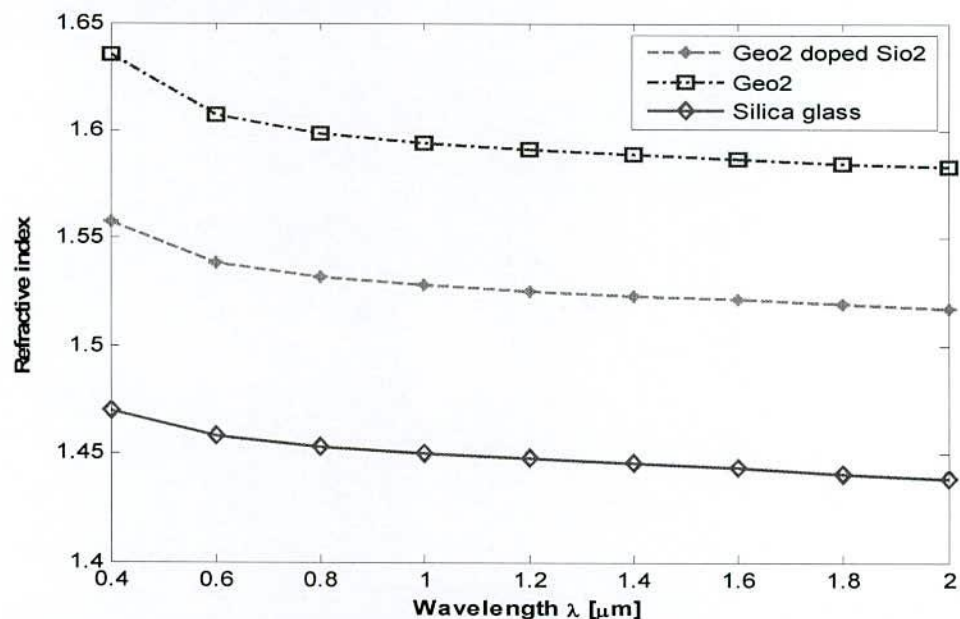


Fig.4.2 Plots of refractive index as function of wavelength for Silica Glass, GeO₂ and GeO₂ doped SiO₂ square defected core with GeO₂ doping conc. $X=45.47\%$

From Ref.[9], it is clearly seen that the continuous increment of the doping concentration of GeO_2 in the defected core downshift the chromatic dispersion to negative values. Fig. 4.3 shows wavelength dependence of chromatic dispersion of the proposed NZDF for optimum design parameters.

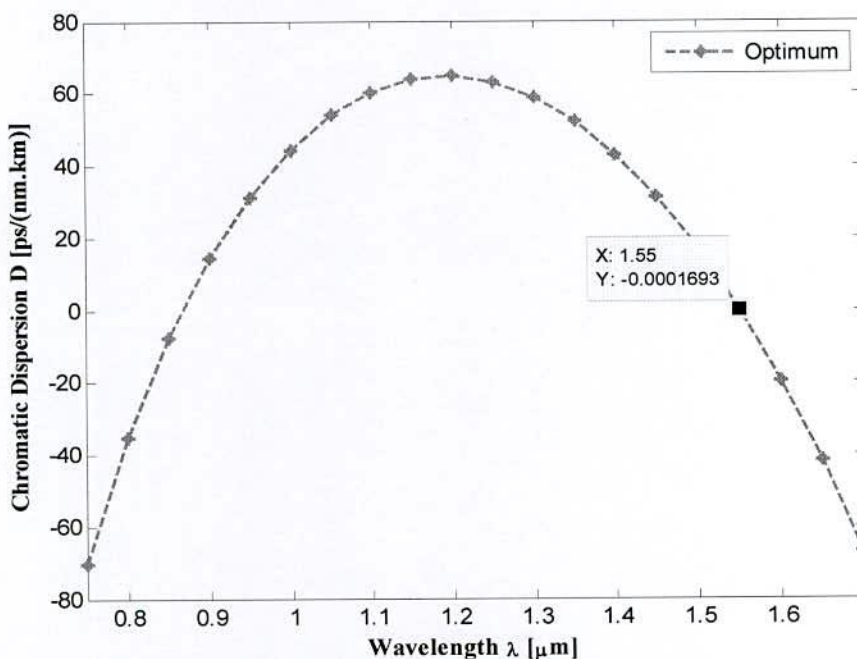


Fig.4.3 Dispersion curves of the proposed NZDF with circular air holes arrange for optimum design parameters

To interpret the dispersion curve, contour plot of electric field distribution over the dd-SPCF cross section shown in Fig. 4.4 can be used. At lower wavelengths (at 750nm) the field is fully confined in the core and interacts solely with the material shown in Fig. 4.4(a). Therefore, at lower wavelengths dispersion is totally dominated by the material dispersion. The dispersion curve remains almost same before the first ZDW even though the core size varies. As shown in Fig. 4.4(b), as the wavelength increases, field interacts with the first ring of air holes and waveguide dispersion starts increasing. Afterwards, waveguide dispersion nullifies the material dispersion and yields first ZDW. For further increase in wavelength, material dispersion starts dominating again while the field distribution interacts with the upper portion of the first air hole ring and finds more silica material in between the two successive holes of the second ring. Therefore, the increasing pattern of dispersion is turned into a flat portion and then curved down being dominated by the material dispersion.

However, the smaller the core size, the higher the nonlinearity due to its small effective area. But, excessive reduction of the core size crawl down its group velocity dispersion (GVD) curve to normal dispersion region without any ZDW. As the core size increases the GVD curve stretches up and gives higher bandwidth of anomalous dispersion but the nonlinearity decreases. Therefore, a tradeoff between high value of nonlinearity and larger bandwidth of anomalous dispersion is needed towards a highly nonlinear dispersion flattened PCF.

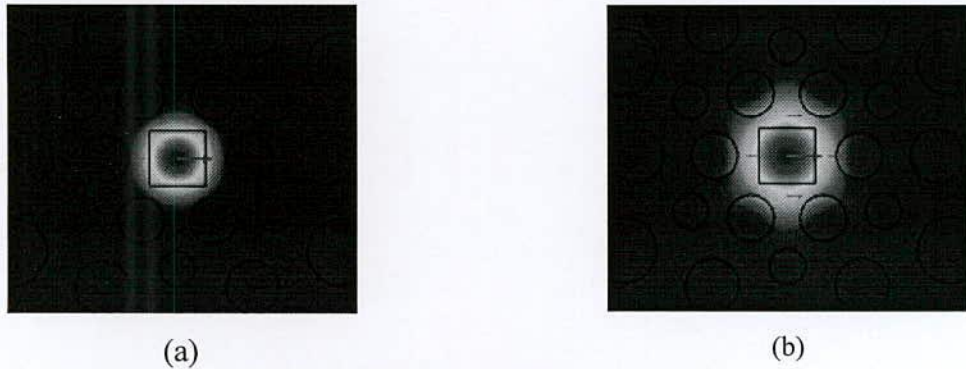


Fig.4.4 Contour plot of electric field at (a) 750 nm, and (b) 1550 nm wavelengths

In Fig 4.5-4.11 we show the variation of the design parameters Λ , d , a to the total dispersion curve of the PCF to investigate the parameter dependence of the dispersion, effective area nonlinear properties and confinement loss of proposed PCF keeping the doping concentration of GeO_2 doped SiO_2 defected core constant at 45.47%. Dispersion accuracy of the proposed fiber for variation in pitch, Λ and a while keeping all others parameter constant is shown in Fig. 4.5 and Fig. 4.6 respectively. It is found that the proposed dd-SPCF shows abrupt change in dispersion due to small change in pitch, Λ . Figures 4.7, 4.8, 4.9, 4.10 and 4.11 show the dispersion properties of the proposed dd-SPCF for changing in diameters d_1 , d_2 , d_3 and d_4 respectively. It is obvious that the shape of dispersion curve is mostly dependent on the first air hole ring diameter, d_1 . However, there is a little effect of changing outer diameters d_3 and d_4 on dispersion parameter and even variation in dispersion due to tuning d_4 is found negligible up to 1550 nm.

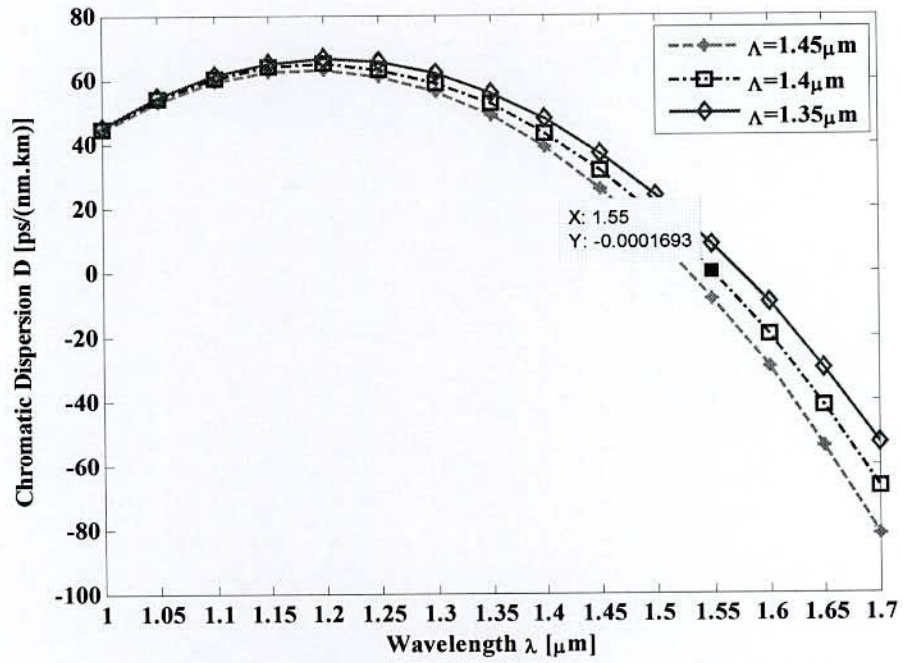


Fig.4.5 Dispersion properties of dd-SPCF and effects of changing pitch, Λ keeping all others parameters constant

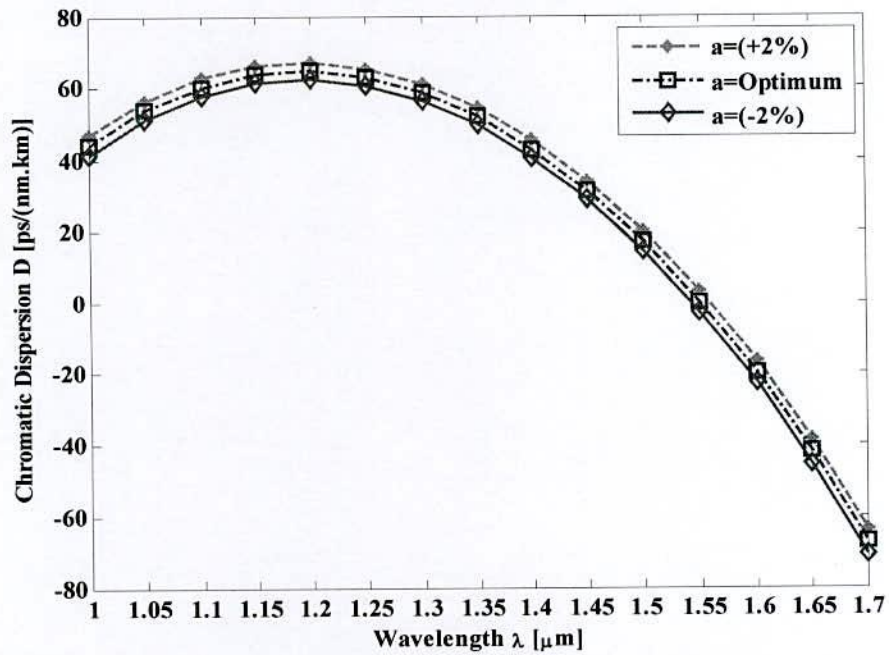


Fig. 4.6 Dispersion properties of dd-SPCF: optimum dispersion and effects of changing a

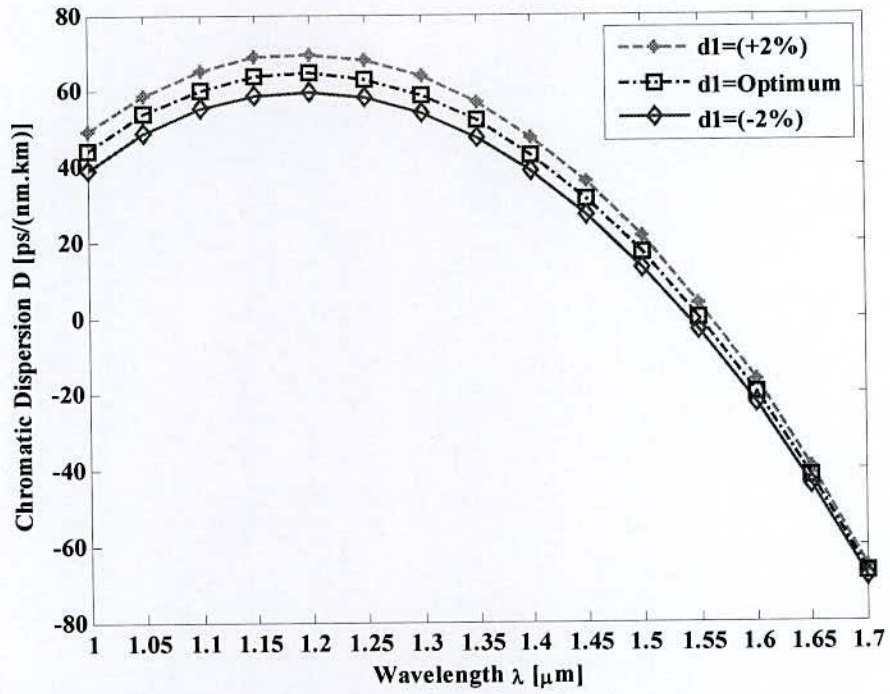


Fig. 4.7 Dispersion properties of dd-SPCF: optimum dispersion and effects of changing d_1

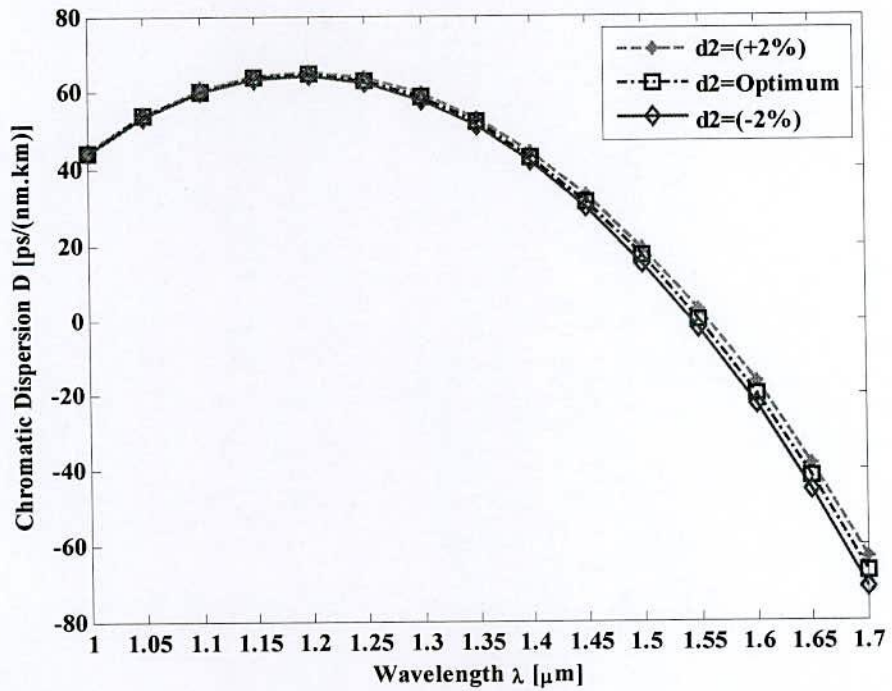


Fig. 4.8 Dispersion properties of dd-SPCF: optimum dispersion and effects of changing d_2

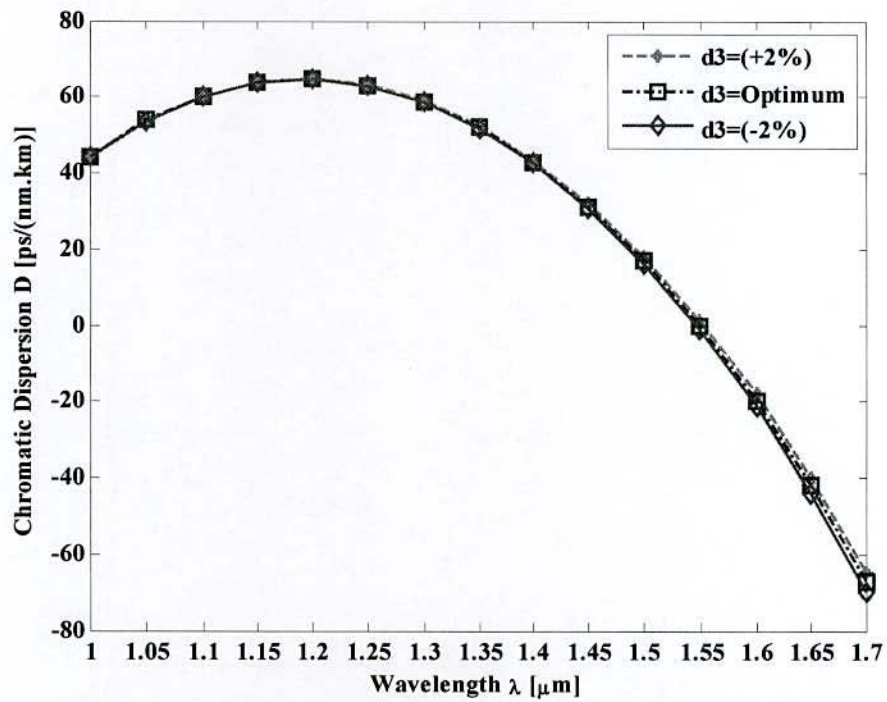


Fig. 4.9 Dispersion properties of dd-SPCF: optimum dispersion and effects of changing d_3

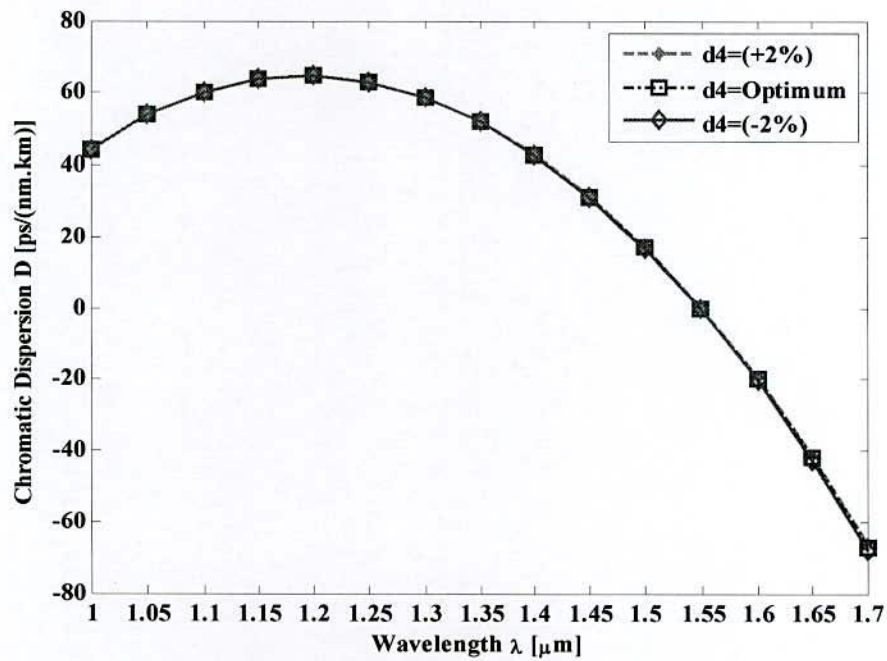


Fig. 4.10 Dispersion properties of dd-SPCF: optimum dispersion and effects of changing d_4

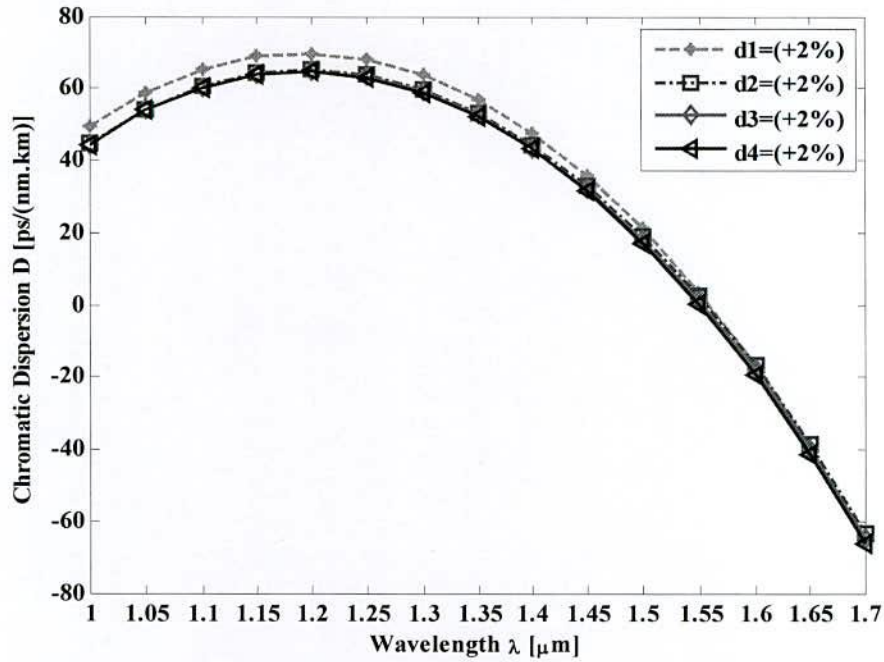


Fig. 4.11 Comparison of dispersion properties of dd-SPCF and effects of changing d_1 , d_2 , d_3 and d_4

According to equation 4.5, Fig. 4.12-4.14 shows effective areas of the fiber for optimum design parameters and for global diameter variations of order $\pm 2\%$. The effective area of the fiber at 1550 nm is $2.6516 \mu\text{m}^2$. From the Fig.4.13, it is clear that, the effective area of the proposed dd-SPCF is mostly dependent on the first air hole ring diameter, d_1 . However, there is a little effect of changing outer diameters d_2 to d_4 on effective area beyond 1550 nm. Moreover, effective area remains constant due to change in pitch, Λ is shown in Fig.4.15. When the dispersion is close to zero, the four-wave mixing efficiency becomes its maximum. Through adjusting the parameters of our dd-SPCF slightly, the fiber can meet different applications. We can design the dd-SPCF with a small dispersion value for transmission medium, and with the nearly zero dispersion for nonlinear medium. Moreover, when we select the doped silica with high nonlinear index as fiber core, the dd-SPCF is beneficial for emphasizing the nonlinear effect such as supercontinuum generation [15-18]. So the dd-SPCF can be applied to not only transmission medium but also nonlinear medium. In practical applications however only the near-zero dispersion characteristics may not be enough for justifying the usefulness of the fiber. Our proposed PCF structure has small effective mode area and high nonlinear gain for nonlinear applications. Nonlinear coefficient of the fiber corresponding to effective area $2.6516 \mu\text{m}^2$ is $76.4391\text{W}^{-1}\text{km}^{-1}$. The following equation is used to calculate the nonlinear coefficient [17]. Fig.4.16-4.18 shows

non-linear coefficient with respect to changing parameter d , a and Λ and it is clear that changing of each parameters show the same effect on nonlinear coefficient just like as effective area.

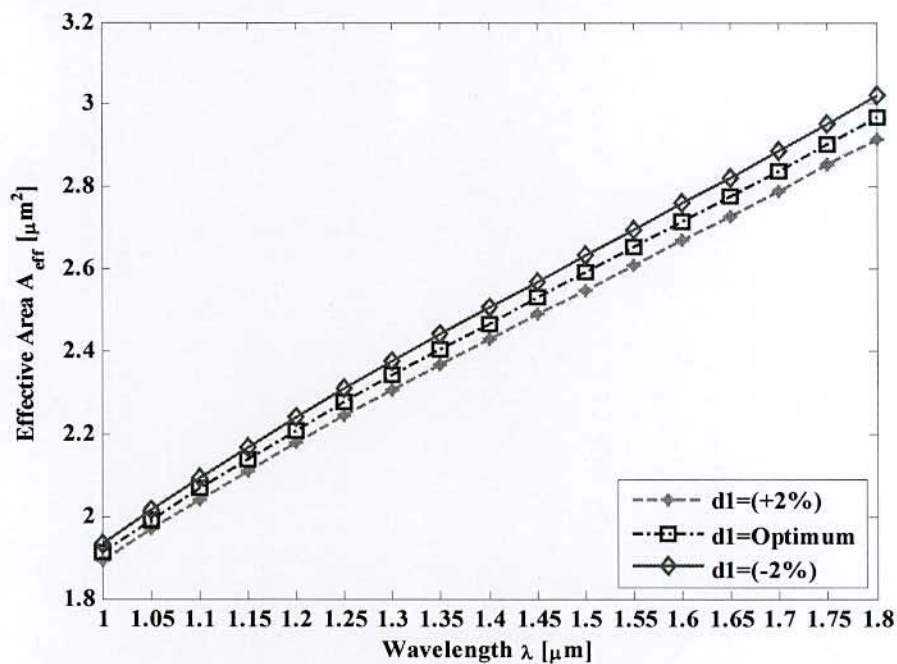


Fig. 4.12 Effective area of the proposed dd-SPCF for optimum design parameters and $\pm 2\%$ variation of d_1

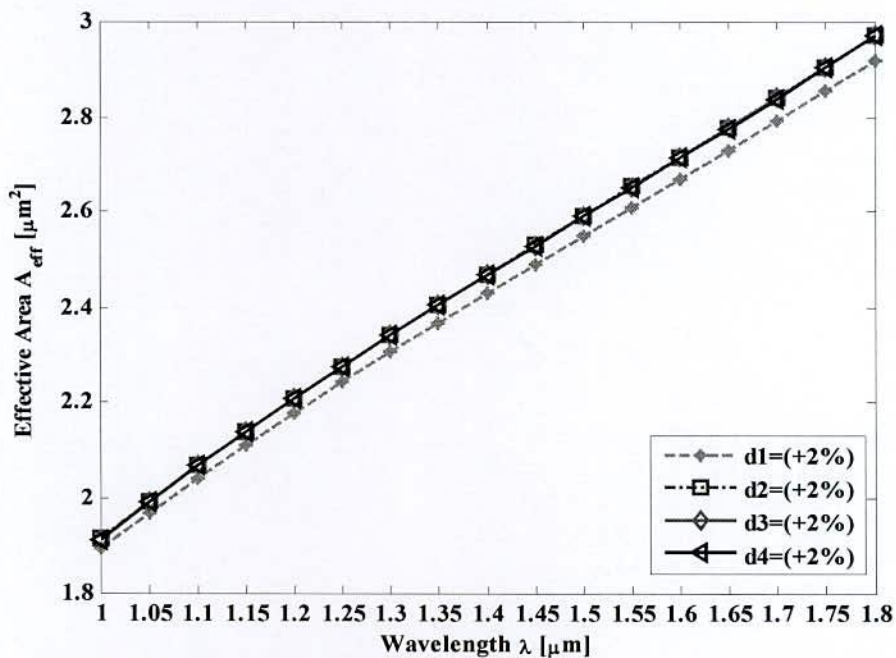


Fig. 4.13 Effective area of the proposed dd-SPCF for optimum design parameters and $+2\%$ variation of d_1 , d_2 , d_3 and d_4

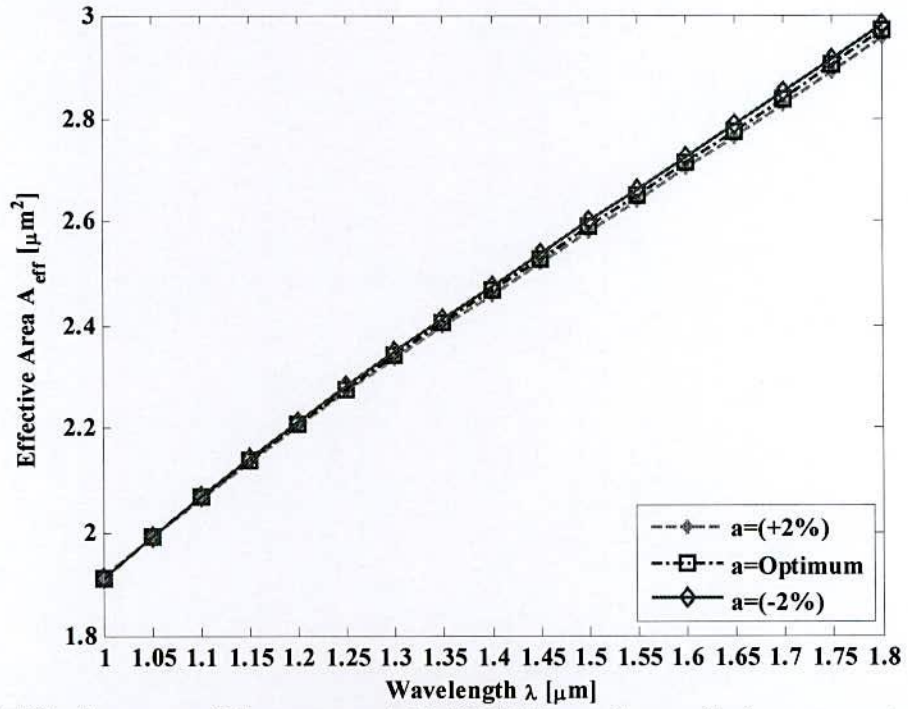


Fig. 4.14 Effective area of the proposed dd-SPCF for optimum design parameters and $\pm 2\%$ variation of a

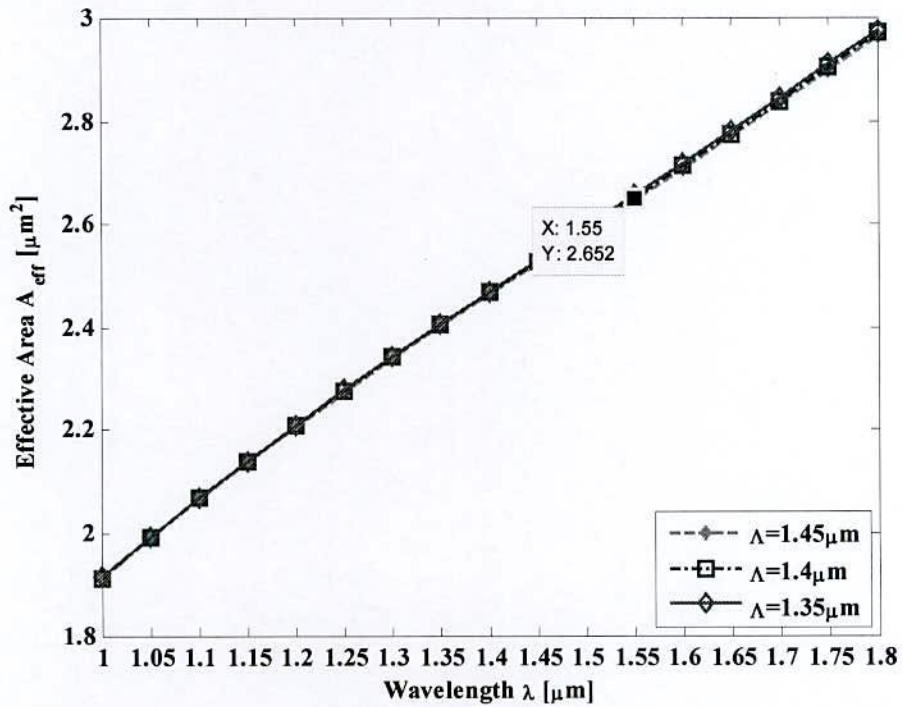


Fig. 4.15 Effective area of the proposed dd-SPCF for optimum design parameters in changing parameter Λ

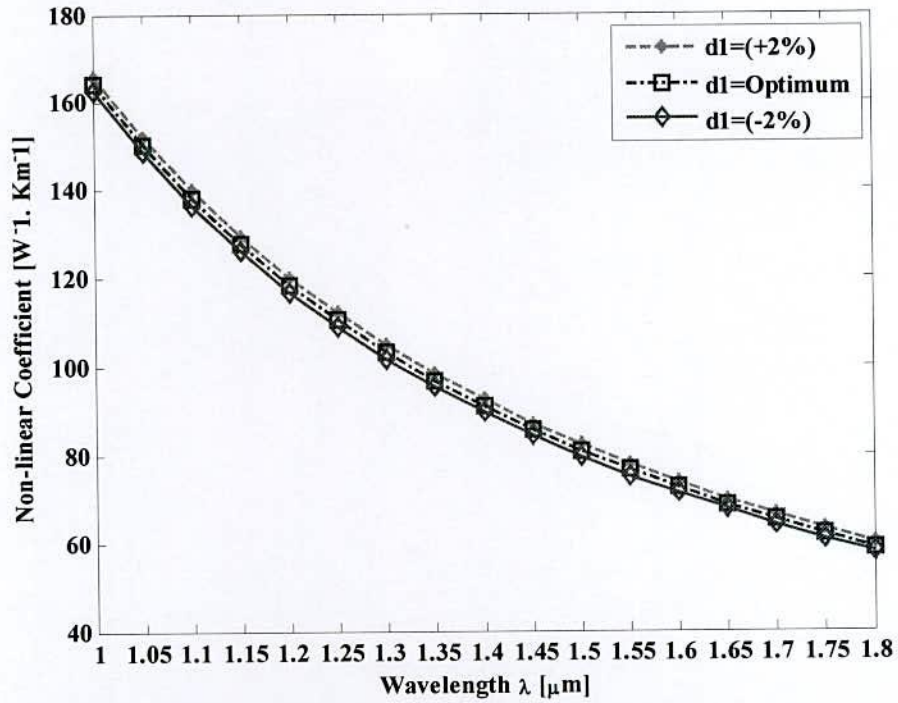


Fig. 4.16 Non-linear coefficient of the proposed dd-SPCF for optimum design parameters and $\pm 2\%$ variation of d_1

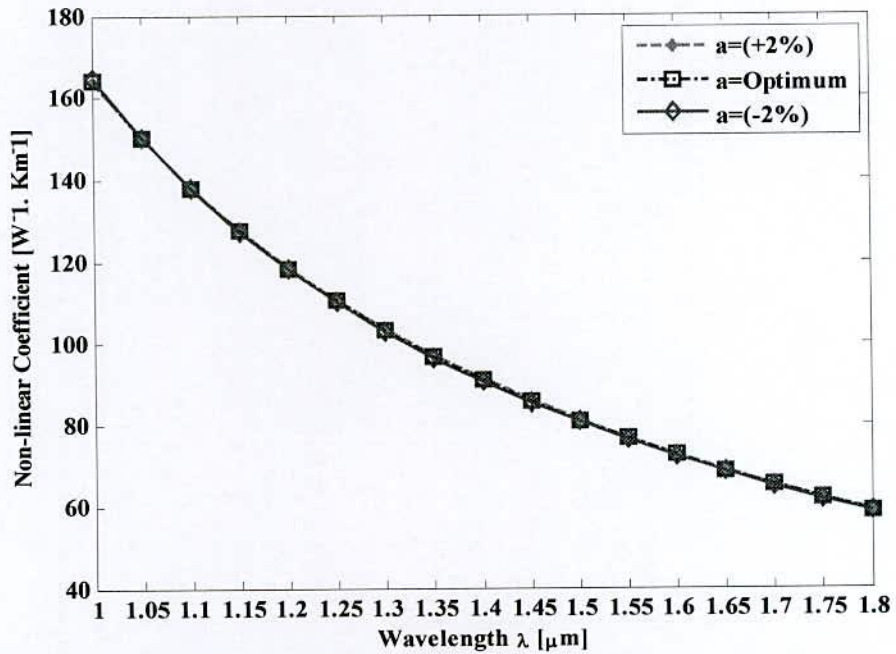


Fig. 4.17 Non-linear coefficient of the proposed dd-SPCF for optimum design parameters and $\pm 2\%$ variation of a

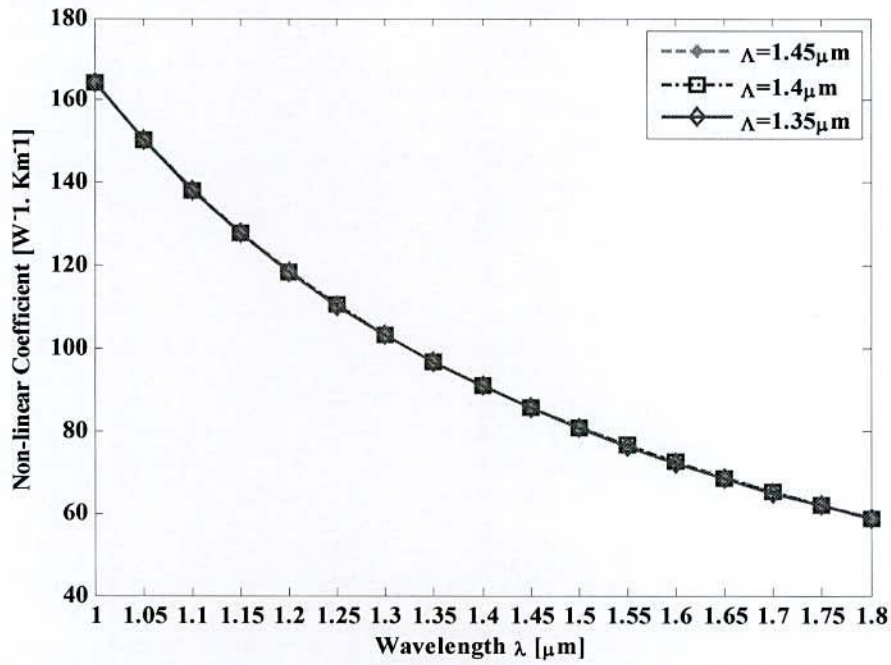


Fig. 4.18 Non-linear coefficient of the proposed dd-SPCF for optimum design parameters in changing parameter Λ

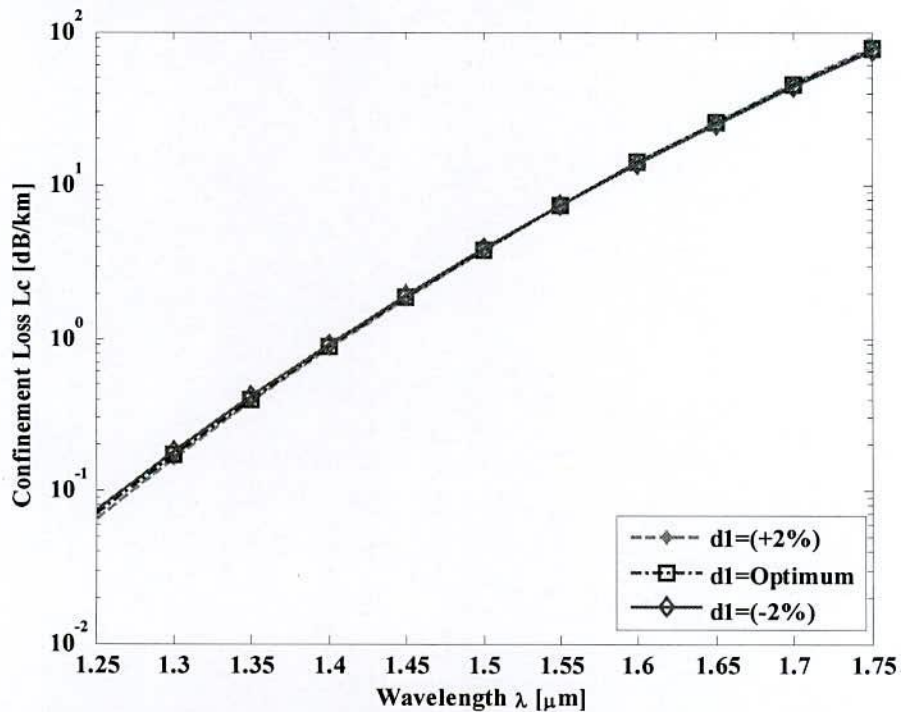


Fig. 4.19 Confinement loss of the proposed dd-SPCF for optimum design parameters and $\pm 2\%$ variation of d_1

Fig. 4.19 shows wavelength dependence of fiber's confinement losses for optimum design parameters and also for fiber's global diameter variations of order $\pm 2\%$. Note that the loss

is increasing smoothly with the wavelength and there is no evidence of abrupt change in leakage. Again increasing losses due to corresponding decrease in air-hole diameters are also consistent. Confinement loss at 1550nm is about a 7.4608dB/km.

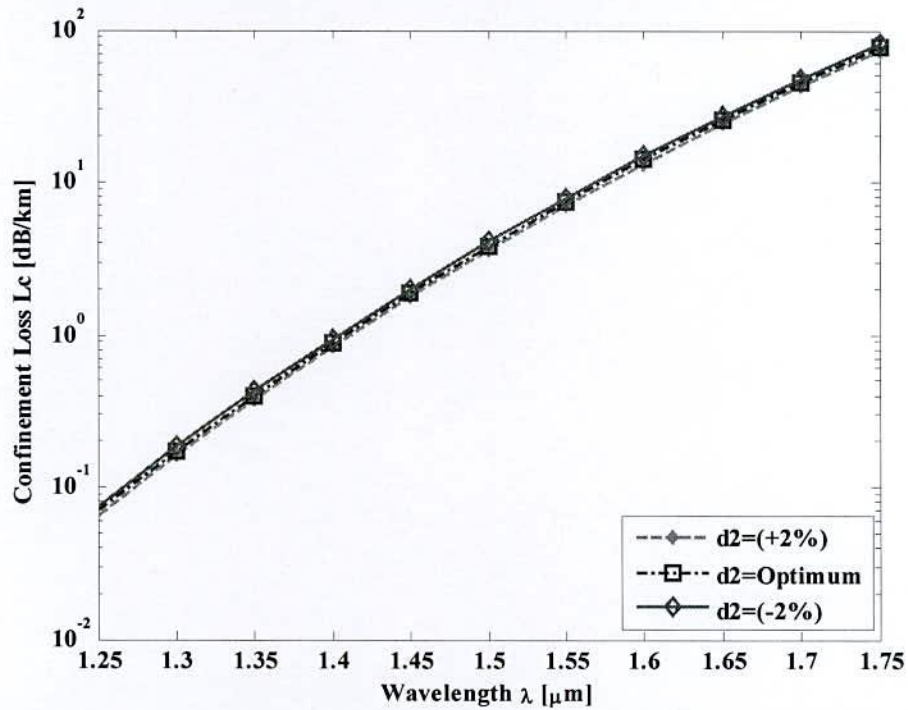


Fig. 4.20 Confinement loss of the proposed dd-SPCF for optimum design parameters and $\pm 2\%$ variation of d_2

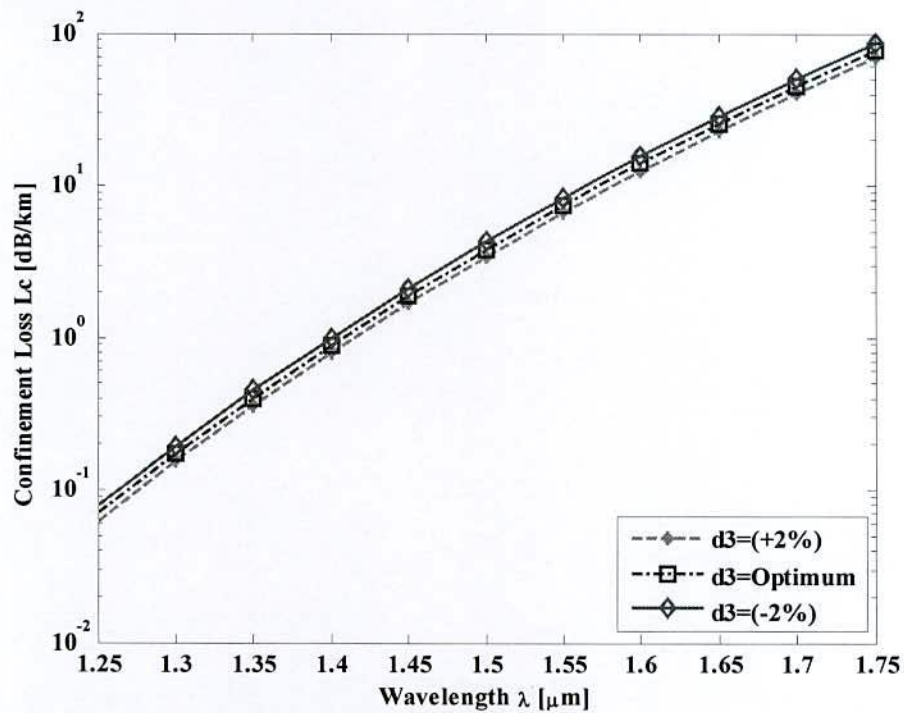


Fig. 4.21 Confinement loss of the proposed dd-SPCF for optimum design parameters and $\pm 2\%$ variation of d_3

It is also evident from Fig.4.20-4.23 that changes in design d_2 , d_3 , d_4 and a parameters up to $\pm 2\%$ have an insignificant effect on the confinement losses but d_1 and d_2 is used as tuning parameter. Pitch, Λ has an effect on confinement loss is shown in Fig.4.24.

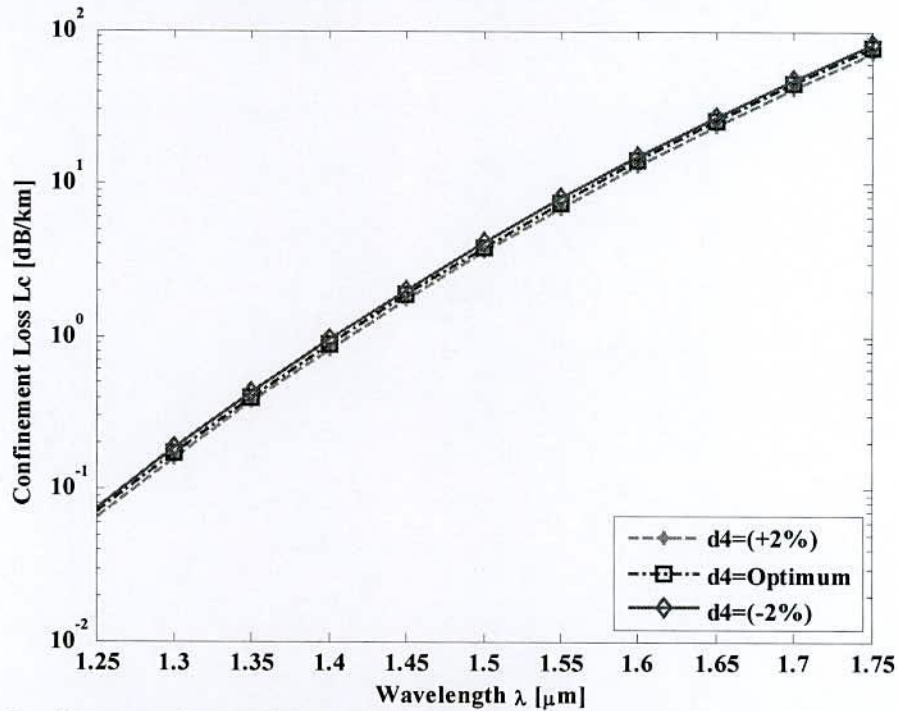


Fig. 4.22 Confinement loss of the proposed dd-SPCF for optimum design parameters and $\pm 2\%$ variation of d_4

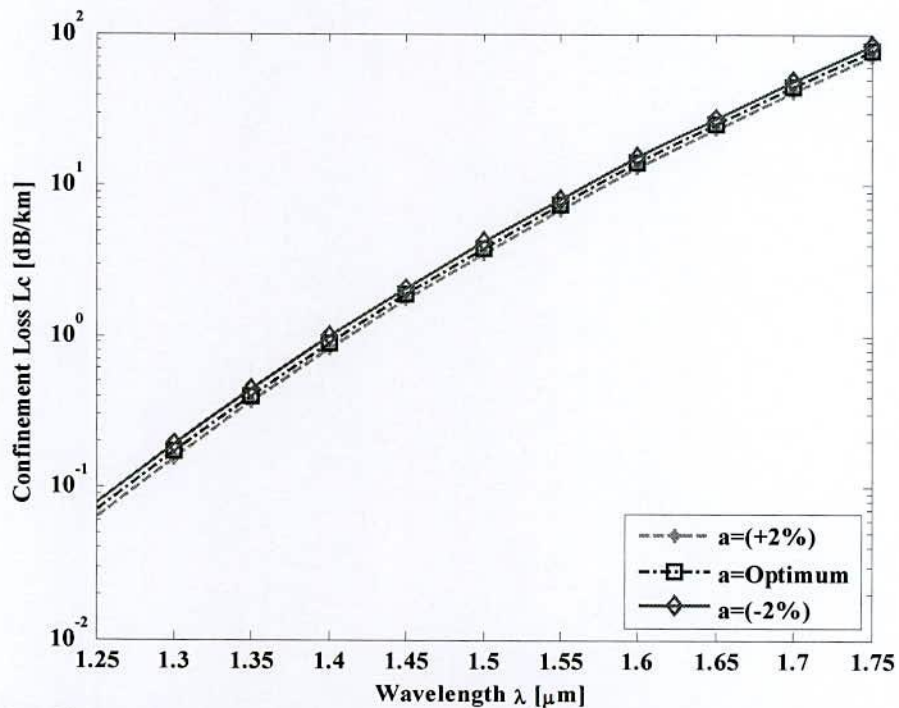


Fig. 4.23 Confinement loss of the proposed dd-SPCF for optimum design parameters and $\pm 2\%$ variation of a

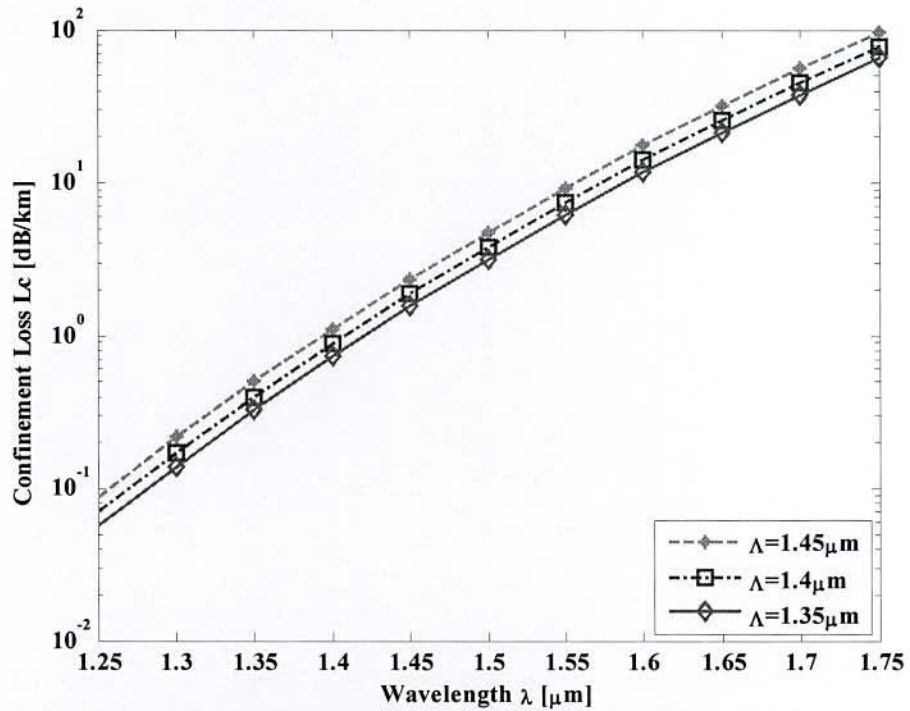


Fig. 4.24 Confinement loss of the proposed dd-SPCF for optimum design parameters in changing parameter Λ

Finally, a comparison is made between properties of the dd-SPCF and some other fibers designed for dispersion managed applications. Table II compares those fibers taking into account near zero dispersion, effective area and nonlinear coefficient at operating wavelength and number of design parameters including number of rings in the cladding.

Table II: Comparison between properties of the proposed NZDF and other NZDFs

PCFs	Dispersion (ps/km-nm)	Wavelength (nm)	Effective area (μm^2)	Nonlinear coefficient ($W^{-1} km^{-1}$)	Number of design parameters
dd-SPCF	-0.000169	1550	2.6516	76.4391	4
Ref.[9]	0.0001787	1550	3.03	67.23	4
Ref.[15]	0.304	1550	>3.03	-	-

These results Fig.4.6-4.18 show that the newly proposed structure is indeed sensitive to the design parameter X , Λ , d and a . The advantage of our structure is the fact that is much simpler from the design point of view, in comparison to previous designs because it contains less number of design parameters.

4.5 Conclusion

This thesis presents an optimized design of a GeO₂ doped SiO₂ square defected core SPCF. Based on full vectorial model, the finite element method is adopted to analyze and compute the characteristics of the dd-SPCF such as dispersion properties, effective mode area, nonlinear coefficient and confinement loss. The effective mode area of the dd-SPCF is comparable to the conventional single-mode fiber is low. It is found that at GeO₂ doping concentration 45.47% in defected core with lattice constant $\Lambda=1.4\mu\text{m}$ and $a=\mu\text{m}$, the NZDF shows dispersion coefficient of $-0.000169\text{ ps}/(\text{km}\cdot\text{nm})$ with small effective area $2.6516\mu\text{m}^2$ and high nonlinear gain $76.4391\text{ W}^{-1}\text{ km}^{-1}$ at operating wavelength. So this fiber is a suitable candidate for telecommunication application.

References

- [1] J. K. Ranka, R. S. Windeler, and A. J. Stentz, "Visible continuum generation in air silica microstructure optical fibers with anomalous dispersion at 800 nm," *Opt. Lett.*, vol. 25, no. 1, pp. 25–27, Jan. 2000.
- [2] J. M. Dudley, G. Genty, and S. Coen, "Supercontinuum generation in photonic crystal fiber," *Rev. Mod. Phys.*, vol. 78, no. 4, pp. 1135–1184, Oct. 2006.
- [3] K.,G. Bouwmans, M. Douay, M. Taki, and A. Mussot, "Dispersion-engineered photonic crystal fibers for cw-pumped supercontinuum sources," *J. Lightwave Technol.*, vol. 27, no. 11, pp. 1556-1564, June 2009.
- [4] M. Liao, X. Yan, G. Qin, C. Chaudhari, T. Suzuki, and Y. Ohishi, "A highly nonlinear tellurite microstructure fiber with multi-ring holes for supercontinuum generation," *Opt. Exp.*, vol. 17, no. 18, pp. 15481–15490, Aug. 2009.
- [5] Agrawal, N. Kejalakshmy, J. Chen, B. M. A. Rahman, and K. T. V. Grattan, "Golden spiral photonic crystal fiber: polarization and dispersion properties," *Opt. Lett.*, vol. 33, no. 22, pp. 2716–2718, Nov. 2008.
- [6] A., N. Kejalakshmy, J. Chen, B. M. A. Rahman, and K. T. V. Grattan, "Soft glass equiangular spiral photonic crystal fiber for supercontinuum generation," *IEEE Photon. Technol. Lett.*, vol. 21, no. 22, pp. 1722–1724, Nov. 2009.
- [7] S., and J. Clowes, "Supercontinuum developments—research, exploitation and applications," *Opt. Eng.*, vol. 20, no. 1, pp. 19, Dec. 2009.

- [8] J. Cascante Vindas, S. Torres Peiró, and A. Diez M. V. Andrés, "Supercontinuum generation in highly Ge-doped core Y shaped microstructured optical fiber," *Appl. Phy.*, pp. 3723–3725, Sept. 2009.
- [9] M. Sajjad Hossain, Kishan Neupane, Md. Shihab Bin Hafiz, and Satya Prasad Majumder, "Dispersion and nonlinear characteristics of a photonic crystal fiber (PCF) with defected core and various doping concentration," *8th International Conference on Electrical and Computer Engineering*, 20-22 December, 2014, Dhaka, Bangladesh.
- [10] COMSOL Multiphysics, version 3.2, 2005.
- [11] Ge-SiO₂ dispersion, *Appl Optics*, 1984.
- [12] S. M. A. Razzak, Y. Namihira, F. Begum, S. Kaijage, N. H. Hai, and N. Zou, "Design of a decagonal photonic crystal fiber with ultra-flattened chromatic dispersion," *IEICE Trans. Electron.*, vol. E90-C, no. 11, pp. 2141-2145, Nov. 2007.
- [13] G.P.Agrawal, "Nonlinear fiber optics", Fourth Edition.
- [14] R.T. Bise, and D.J.Trevor "Sol-gel derived microstructured fiber Fabrication and characterization," in *Optical Fiber Comm Conf.(OFC)*, Washington, DC, vol. 3, Optical Society of America, Mar.2005.
- [15] K. Saitoh and M. Koshiba, "Ultra-flattened chromatic dispersion controllability using a defected core photonic crystal fiber with low confinement loss," *Opt. Express*, vol. 13, no. 21, pp. 8365, 2005.
- [16] Arti Agrawal, N. Kejalakshmy, J. Chen, B. M. A. Rahman, and K. T. V. Grattan, "Golden spiral photonic crystal fiber: polarization and dispersion properties," *Opt Letters*, vol. 33, no. 22, 2008.
- [17] Muhammad Nazmul Hossain, M. Shah Alam, Dihan Md. Nuruddin Hasan, and K. M. Mohsin, "A highly nonlinear spiral photonic crystal fiber for tailoring two zero dispersion wavelengths in the visible region," *Photonics letters of poland*, vol. 2 , no. 3, pp.143-145,2010.
- [18] S. Coen, A. H. L. Chau, R. Leonhardt, J. D. Harvey, J. C. Knight, W. J. Wadsworth, and P. S. J. Russell, "White-light supercontinuum generation with 60-ps pump pulses in a photonic crystal fiber," *Opt. Lett.*, vol. 26, no. 17, pp. 1356–1358, 2001.

Design and Characterization of Broadband DC-SPCF

5.1 Introduction

This chapter reveals the design methodology of broadband dispersion compensating fiber (DCF) using PCF and also describes the performance of the designed DCF as a dispersion compensator to compensate the chromatic dispersion of telecom fiber. In addition, this chapter presents the condition of broadband dispersion and dispersion slope compensation. Firstly, spiral shape of photonic crystal fiber (SPCF) with defected elliptical core is designed to achieve the goal of broadband dispersion compensation of SMFs. However, simulation results reveal that although SPCF with defected elliptical core gives high negative dispersion over a wide band but variation of flattened profile was high and the birefringence is not enough to compensate the PMD. In addition, the perfectly matched layer (PML) effect on this design has been disturbed that causes on manufacturing process. As a result, SPCF like as distribution sunflower seeds with defected elliptical core has been extended to achieve flattened profile of large value of negative dispersion and birefringence which leads to PMD compensation as well as nullify the PML effect on boundary. Moreover, simulation results show that it is possible to use SPCF to compensate both chromatic dispersion and PMD over wideband. Besides, SPCF like as nautilus shell has been designed and simulated to observe the performance as dispersion compensator. Finally, a comparison has been made to show the performance of the designed SPCFs.

5.2 Requirements for broadband dispersion and dispersion slope compensation

Dispersion compensation is a technique to nullify the positive dispersion caused by the standard SMFs. To do it, DCF which shows negative dispersion characteristics is added to transmission fiber link of SMFs so as to achieve signal with zero dispersion at the output. However, the uses of negative-slope DCFs offer the simplest solution to dispersion compensation in high capacity WDM systems with a large number of channels. The equation of broadband dispersion compensation is given by [1].

$$D_m(\lambda_m)L_m + D_n(\lambda_n)L_n = D_t \quad (5.1)$$

where $D_m(\lambda_m)$ and $D_n(\lambda_n)$ are dispersion coefficient of SMF and DCF where λ_n is wavelength of n^{th} channel, L_m and L_n are the length of SMF and DCF respectively. For full compensation of the dispersion caused by SMF, the length of the DCF is selected such that

total dispersion coefficient $D_t = 0$ after dispersion compensation. Under this condition, the length of DCF will be as follows.

$$L_n = -\frac{D_m L_m}{D_n} \quad (5.2)$$

The equation clearly shows that the length of DCF will be short only for high negative value of D_n . On the other hand, dispersion compensation over a wideband requires dispersion and dispersion slope compensation at the same time for broadband communication system. Hence, the total dispersion slope DS_t is given as follows [2].

$$DS_t = DS_m L_m + DS_n L_n \quad (5.3)$$

where, DS_m and DS_n are the dispersion slopes of the SMF and the DCF respectively. From Eq. (5.3), it is obvious that a negative dispersion slope of the DCF is necessary in order to achieve slope compensation. Thus, the condition for full slope compensation is that the relative dispersion slope (RDS), which is the ratio of dispersion slope to dispersion, of both fibers would have to be equal.

$$RDS_m = RDS_n \quad (5.4)$$

where RDS_m and RDS_n are the relative dispersion slope of the standard SMF and the DCF. It should be pointed out that standard SMF exhibits RDS value of about 0.0036 nm^{-1} at $\lambda=1.55 \text{ }\mu\text{m}$ [2].

5.3 Proposed DC-PCF models

In order to achieve the goals, I have modeled three SPCF structures for broadband dispersion compensation namely SPCF with defected elliptical core [3], SPCF like as distribution sunflower seeds and SPCF like as nautilus shell with defected elliptical core. All of SPCF model is designed with only circular air holes of different arrangements for different air hole rings in the cladding.

5.3.1 Structure of SPCF with defected elliptical core

Fig.5.1 depicts the proposed three rings SPCF with defected elliptical core. It has 10 arms and the starting air holes of each arm form a single spiral of radius r_0 with equal angular displacement from previous one is increased by θ . The radii of subsequent rings enhance by geometric progression of following manner ($r_0, r_0+2p, r_0+4p, \dots$); where p represents the distance factor to control the pitch. The air-hole pitch is labeled Λ . Each arm contains 6 air holes which are denoted by d_1, d_2, d_3, d_4, d_5 and d_6 respectively. The PCF is composed of

elliptical lattices in having 6 circular air holes have same radius of r_e with ellipticity ratio ($a:b=2:1$) in the central core region to make asymmetry.

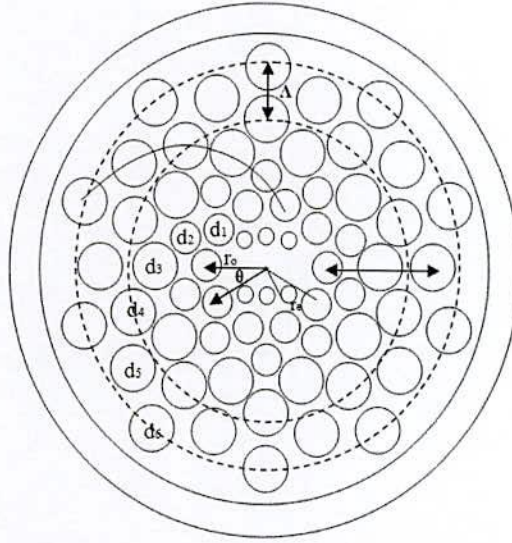


Fig. 5.1 Structure of the proposed three rings SPCF for broadband dispersion compensation

Therefore, the first, second, and third hole of each arm represent the first, second, and third ring, respectively. In the proposed structure, the diameter of the first two air-hole ring d_1 and d_2 is used to obtain large negative dispersion. The diameter of the last two air-hole rings d_5 and d_6 is selected large for keeping low confinement loss level in the targeted region. To analyze, $\Lambda=1.2$, $r_0=1.4\mu\text{m}$, $\theta =18^\circ$, $r_e=0.215\mu\text{m}$, $d_6=d_5=1.2$, $d_4=d_3=0.96$, $d_2=d_1=0.64$, $a=1.3\mu\text{m}$ and $b=0.65\mu\text{m}$ are reported for the optimized structure.

On the other hand, the material of proposed SPCF is taken to be silica except the air holes whose refractive index is 1. Thus, the effective refractive index, n_{eff} of the material is changed with operating wavelength. However, the wavelength dependent refractive index of the material is determined by Sellmeier equation [2].

5.3.2 Structure of SPCF (distribution sunflower seeds) with defected elliptical core

The general structure of the proposed six rings SPCF-distribution sunflower seeds with defected elliptical core in our simulation as illustrated in Fig.5.2. Compared to the conventional circular lattice structure and hexagonal lattice structure, spiral lattices of circular air holes (black dashed lines) with defected elliptical core in Fig.5.3 are introduced as the cladding of the PCF. It has 10 arms and the starting air holes of each arm form a single spiral of radius r_0 with equal angular displacement from previous one is increased by

θ . The radii of subsequent rings enhance by geometric progression of following manner ($r_0, r_0+p, r_0+2p, \dots$); where p represents pitch.

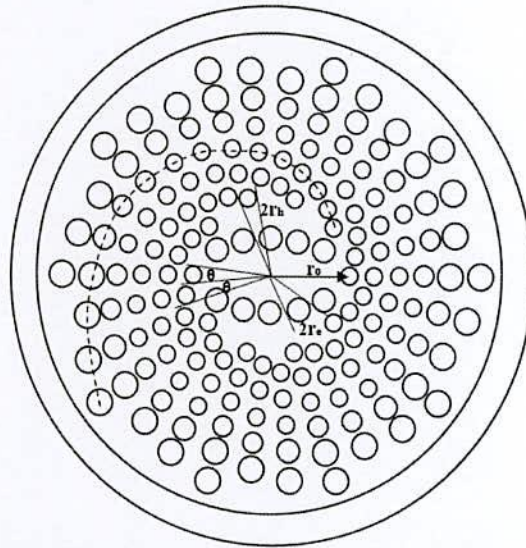


Fig. 5.2 Structure of the proposed six rings SPCF for broadband dispersion compensation

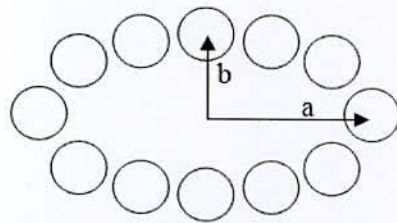


Fig. 5.3 Elliptical core with circular air holes

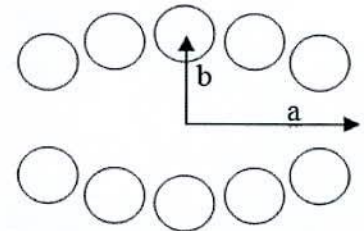


Fig. 5.4 Defected elliptical core in central region

Each arm contains 16 air holes. Among these, first nine air holes have same radius of r_h . The PCF is composed of elliptical lattices in Fig.5.3 having 12 circular air holes have same radius of r_e with ellipticity ratio ($a: b=2:1$) in the central core region. However, the position of the air holes is designed with taking into account the center of the core of the proposed PCF as origin of cartesian coordinate system. Then, the position of air holes, (X_{Nn}, Y_{Nn}) in each ring will be determined as follows where N denotes the number of rings and n represents the total number of air holes in that ring. For instance, the position of air holes in 1st ring ($N=1$) can be designed using the following equation. In this case, the total number of air holes in the 1st ring, n would be 9 where $n=0, 1, 2, \dots, 5$.

$$(X_{Nn}, Y_{Nn}) = (r_0 \times N \times \cos(\frac{n\pi}{5}), r_0 \times N \times \sin(\frac{n\pi}{5}))$$

2nd ring.....

$$(X_{Nn}, Y_{Nn}) = ((r_0 + ((N+1) \times p)) \times \cos(\frac{n\pi}{5} + \frac{\pi}{5}), (r_0 + ((N+1) \times p)) \times \sin(\frac{n\pi}{5} + \frac{\pi}{5}))$$

3rd ring.....

$$(X_{Nn}, Y_{Nn}) = ((ro + (N \times 2 \times p)) \times \cos(\frac{n\pi}{5} + \frac{\pi}{2.5}), (ro + (N \times 2 \times p)) \times \sin(\frac{n\pi}{5} + \frac{\pi}{2.5}))$$

4th ring.....

$$(X_{Nn}, Y_{Nn}) = ((ro + ((N \times 2 + 1) \times p)) \times \cos(\frac{n\pi}{5} + \frac{\pi}{1.875} + \frac{\pi}{15}), ((ro + ((N \times 2 + 1) \times p)) \times \sin(\frac{n\pi}{5} + \frac{\pi}{1.875} + \frac{\pi}{15})))$$

5th ring.....

$$(X_{Nn}, Y_{Nn}) = ((ro + ((N \times 2 + 2) \times p)) \times \cos(\frac{n\pi}{5} + \frac{\pi}{1.25}), ((ro + ((N \times 2 + 2) \times p)) \times \sin(\frac{n\pi}{5} + \frac{\pi}{1.25})))$$

6th ring.....

$$(X_{Nn}, Y_{Nn}) = ((ro + ((N \times 2 + 3) \times p)) \times \cos(\frac{n\pi}{5} + \frac{\pi}{1}), ((ro + ((N \times 2 + 3) \times p)) \times \sin(\frac{n\pi}{5} + \frac{\pi}{1})))$$

To make extra large asymmetry, 1 and 7 position air holes are omitted in elliptical core, shown in Fig.5.4. The spiral-shape structure is compact for tight light confinement and large nonlinearity; the defected elliptical arrangement of circular air holes provides high birefringence as well as large negative chromatic dispersion. We use circular air holes to facilitate easy fabrication.

5.3.2 Structure of SPCF (nautilus shell) with defected elliptical core

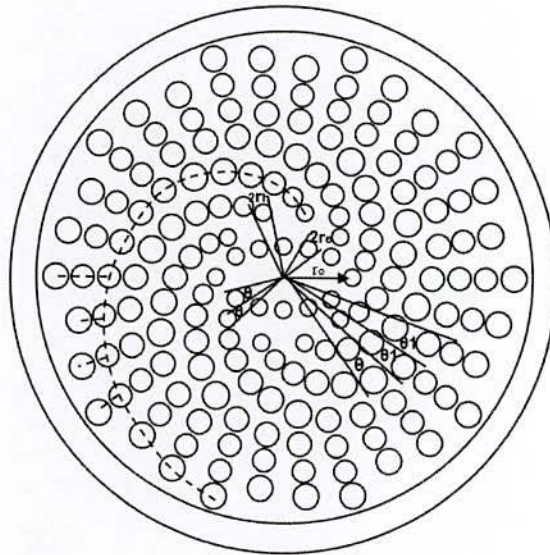


Fig.5.5 Structure of the proposed SPCF (nautilus shell) for broadband dispersion compensation

Fig. 5.5 shows the model of the proposed SPCF -nautilus shell with defected elliptical core with optimized air-hole diameters $d_1, d_2, d_3, \dots, d_{16}$, pitch p , and with ellipticity ratio (a :

$b=2:1$) in the central core region to make asymmetry. Compared to the conventional circular lattice structure and hexagonal lattice structure, spiral lattices of circular air holes (black dashed lines) with defected elliptical core in Fig.5.5 are introduced as the cladding of the PCF. It has 10 arms and the starting air holes of each arm form a single spiral of radius r_0 with equal angular displacement from previous one is increased by θ for first seven holes of the arms. The radii of subsequent rings for first seven holes enhance by geometric progression of following manner ($r_0, r_0+1.5 \times p, r_0+2 \times 1.5 \times p, \dots$ to $r_0+6 \times 1.5 \times p$) with air hole diameter ratio 1.11 to periphery. After first seven holes, the geometric progression of following manner ($r_0+10 \times p, r_0+11 \times p, \dots$ to $r_0+18 \times p$) with angular displacement 12° at starting 156° for eight number holes of the arms; where p represents pitch. Among these, last nine air holes have same radius of r_h . The PCF is composed of elliptical lattices in Fig.5.5 having 12 circular air holes have same radius of r_e with ellipticity ratio ($a: b=2:1$) in the central core region. However, the position of the air holes is designed with taking into account the center of the core of the proposed PCF as origin of cartesian coordinate system. To make extra large asymmetry, 1 and 7 position air holes are omitted in elliptical core to achieve high birefringence property, shown in Fig.5.5. This results in a higher air-filling ratio and a lower refractive index around the core, thereby providing strong confinement ability. It is known that the size of the air-holes near the PCF core affects the dispersion characteristics [4].

5.4 Numerical simulation using COMSOL Multiphysics 4.2

COMSOL Multiphysics (formerly FEMLAB) 4.2 is a versatile simulation software based on FEM. It is a flexible platform that allows even novice users to model all relevant physical aspects of their designs. COMSOL Multiphysics also offers an extensive interface to MATLAB. Simulation of a DC-SPCF model using COMSOL Multiphysics 4.2 software requires a high configuration computer. In this thesis, all simulations are performed with a notebook of HP brand (ProBook 4440s). The detail configuration of used notebook is as follows:

Processor	Intel(R) core(TM) i5, 3230M CPU@2.60GHz
RAM (Installed)	4GB
Operating System	Windows 7 Ultimate, 64 bit
Cache memory RAM, (built into the processor)	3MB

5.4.1 Simulation results of three rings SPCF

Fig. 5.6 shows the variation of chromatic dispersion against PML for the three rings SPCF with defected elliptical core. To ensure accurate calculations, we verify the convergence of the calculated chromatic dispersion values under different thickness of PML in the elliptical core region. For evaluating the dependency on thickness of perfectly matched layer (PML) has been reported [5]. However, we change the PML value from 0.6 to 1.5 μm in shown in Fig.5.6.

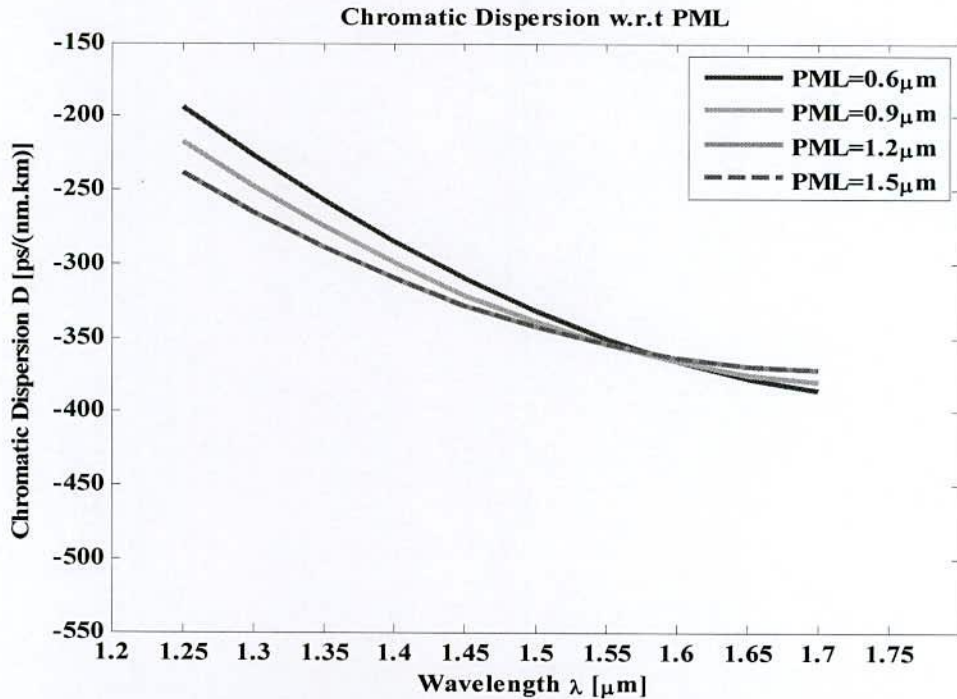


Fig.5.6 Dispersion as functions of thickness of PML in core region

It can be clearly seen that the chromatic dispersion values change fast and then vary slowly with the increase in the thickness of PML. In particular, when the thickness of PML is greater than 1 μm , the chromatic dispersion values keep constant. Hence, a 1.2 μm -thick PML is employed when calculating chromatic dispersion values as shown in Fig. 5.6.

According to simulation result, the proposed structure shows the average negative dispersion coefficient equal to -355.898 ps/nm-km with a dispersion variation of 11.8 ps/nm-km over S to U-bands for X-polarization. The dispersion value of the proposed PCF at 1550 nm is about -354.307 ps/nm-km.

In our work, all the dispersion curves are presented only for fundamental mode and the optimum parameter of the proposed SPCF is ($d_6/\Lambda=d_5/\Lambda=1$; $d_4/\Lambda=d_3/\Lambda=0.8$, $\Lambda=1.2\mu\text{m}$, $d_2=0.64$, $d_1=0.64$). In this consideration, the values of air hole diameters and the pitches are varied in $\pm 2\%$ from their optimum value is shown in fig.5.7.

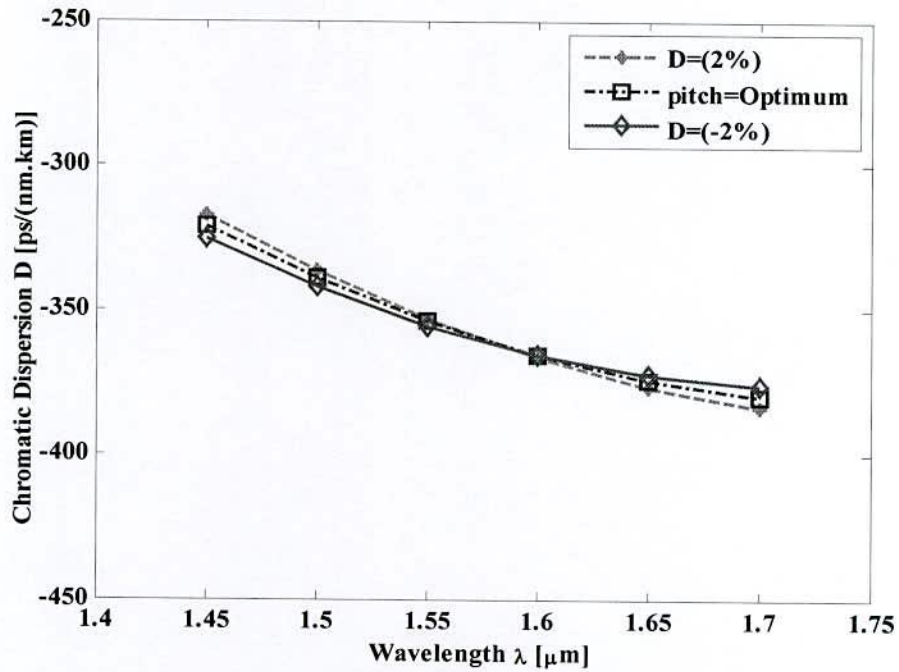


Fig. 5.7 Dispersion of the three rings SPCF with a variation of $\pm 2\%$ for all parameters

We then investigate the dependence of chromatic dispersion on the wavelength under different r_e of elliptically circular air holes. With the increase of r_e , dispersion for X polarizations also increases as demonstrated in Fig.5.8.

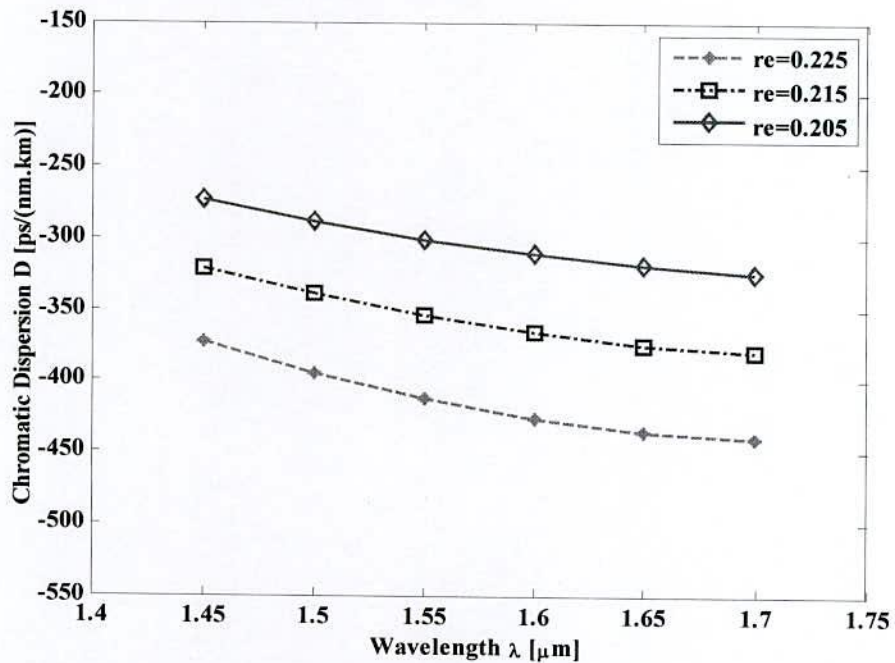


Fig.5.8 Chromatic dispersion for X-polarization of variation of r_e of three rings SPCF

From fig, it can be explained that negative dispersion is more flatness near about 1550nm to 1650nm for X-polarization. Thus the proposed fiber can be used to compensate the accumulated dispersion of SMF currently deployed in WDM systems as it possesses large negative dispersion over a wide range of wavelength.

Thus, it is clearly understood that our proposed three rings SPCF with optimized parameters is suitable for systems with high bit rates transmission systems covering entire S to U band effectively. Besides, our proposed three rings SPCF exhibits a modal birefringence of about 0.0175 at 1550 nm as shown in Fig. 5.9 with a variation of $\pm 2\%$ for all parameters. However, this value of birefringence is enough to eliminate the effect of PMD.

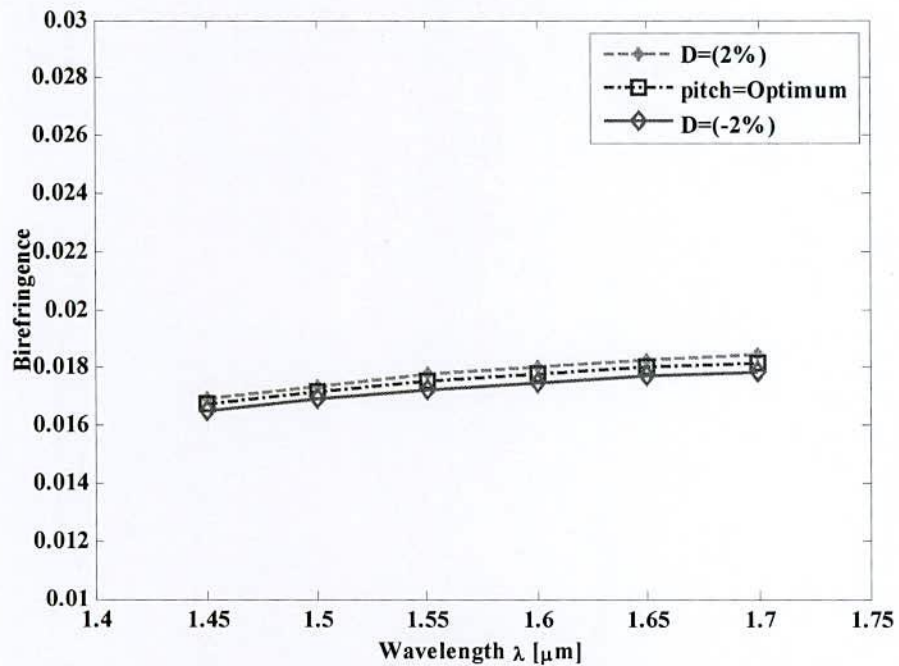


Fig. 5.9 Birefringence of three rings SPCF with a variation of $\pm 2\%$ for all parameters

As a result, the proposed three rings SPCF although capable enough to compensate broadband dispersion but dispersion variation is large. Fig.5.10 shows the dependence of birefringence on the diameter of elliptically circular air holes. The birefringence increases with the increase of the diameter of r_e because the fiber cross-section is more asymmetric. It can be demonstrated that the birefringence is about 0.0175 at 1550nm when $r_e=0.215 \mu\text{m}$. A maximum birefringence of 0.0201 is achieved when r_e enhances up to $0.225 \mu\text{m}$.

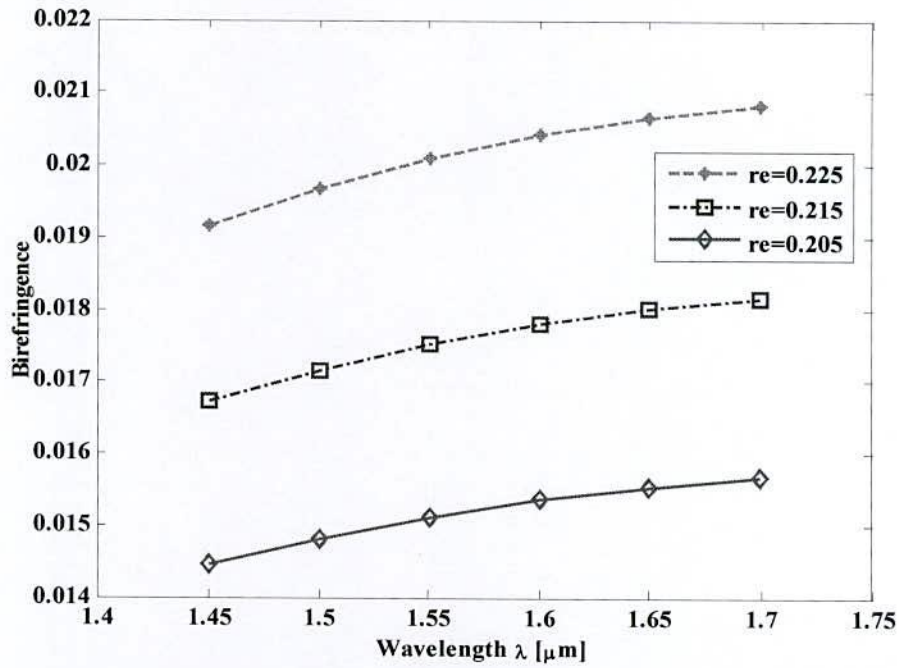


Fig.5.10 Birefringence variance with respect to r_e of three rings SPCF

Chromatic dispersion of both polarization states is shown in Fig. 5.11. From fig. it can be explained that chromatic dispersion for Y-polarization is changing almost linearly but for X-polarization it is very small change and goes to flattened profile beyond 1450 nm. Beyond U- band, dispersion variation is very low. Fig. 5.12 shows the electric field distributions at $\lambda = 1550$ nm for each polarization state.

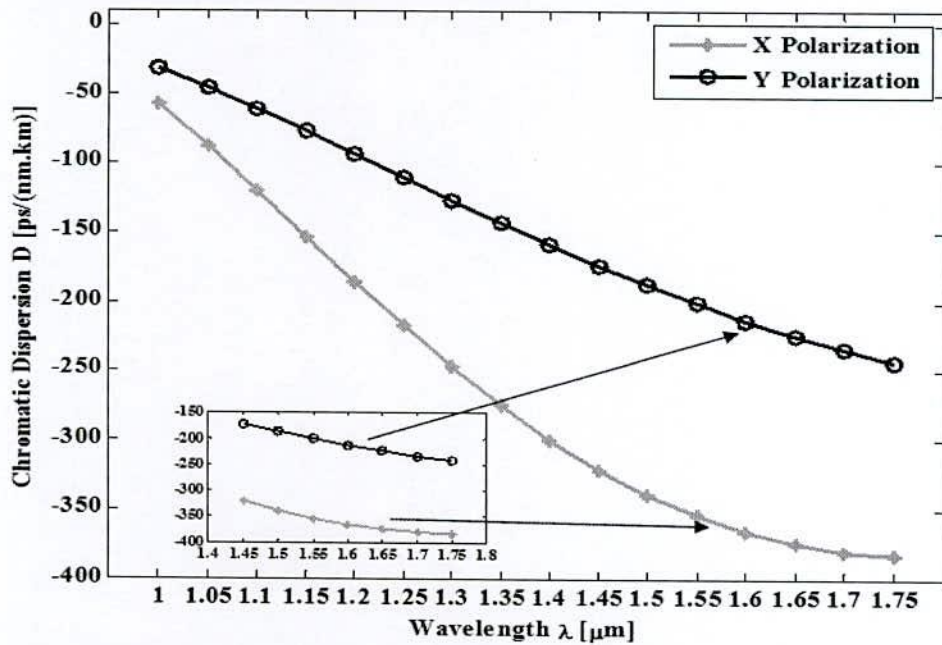


Fig.5.11 Wavelength response of chromatic dispersion of the proposed three rings SPCF for both x- and y-polarization for the optimum design parameters

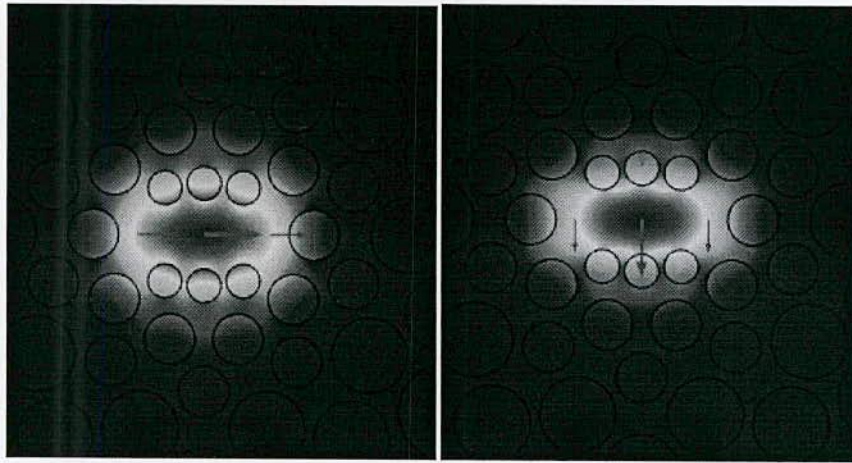


Fig. 5.12 Electric field for X-polarization and Y-polarization at 1500nm of the proposed three rings SPCF

Fig. 5.13 represents the effective area of the proposed three rings SPCF which increases with wavelength for optimum design parameters and also for elliptical air hole diameter, r_e variation. In particular, the effective area at $\lambda=1550$ nm is $2.3348 \mu\text{m}^2$ for the optimum parameters which is higher than that obtained for MS-MOF [6] and [7]. However, low effective area causes splice loss and as a solution, tapered intermediate PCF can be used for interfacing between proposed SPCF and SMF successfully [8]. So, we believe that our proposed SPCF can be interconnected with SMF without any major complications.

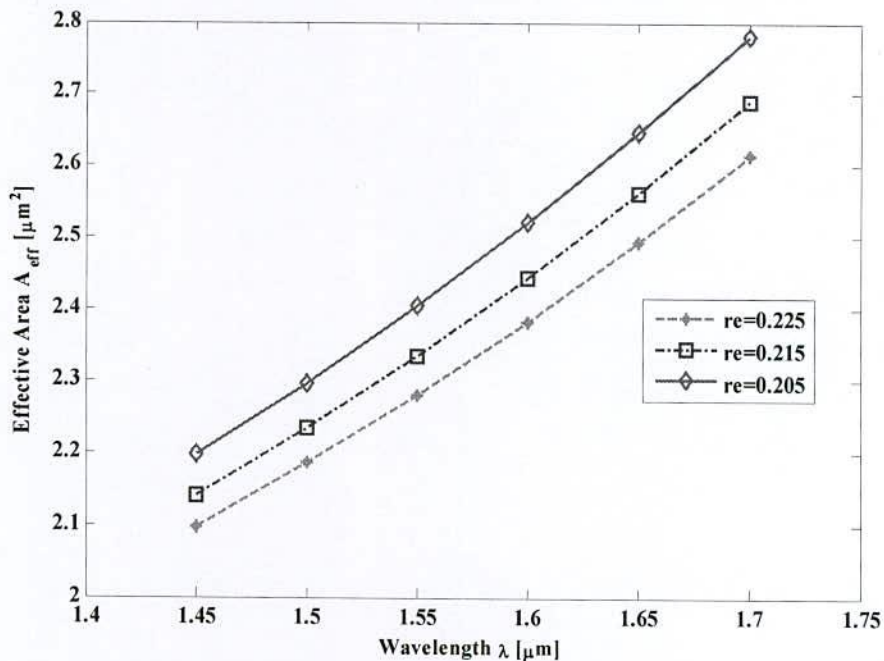


Fig. 5.13 Effective area of the proposed three rings SPCF for r_e optimum design parameters

One can observe that the non-linear coefficient is $39.9333 \text{ W}^{-1}\text{km}^{-1}$ at 1550nm which is very high. Nonlinear coefficient of the three rings SPCF with a variation of $\pm 2\%$ for all parameters is shown in Fig.5.14.

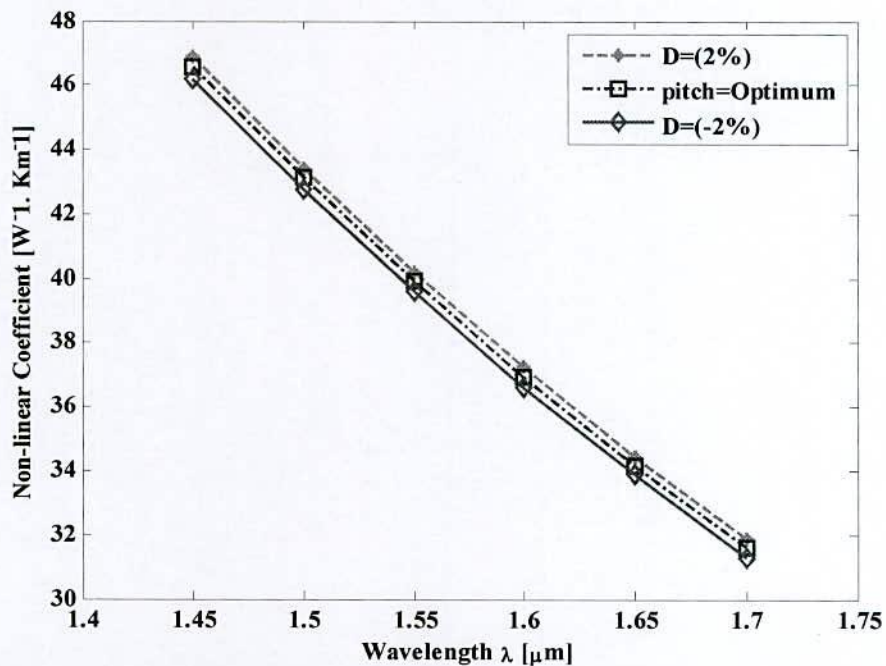


Fig. 5.14 Nonlinear coefficient of the three rings SPCF with a variation of $\pm 2\%$ for all parameters

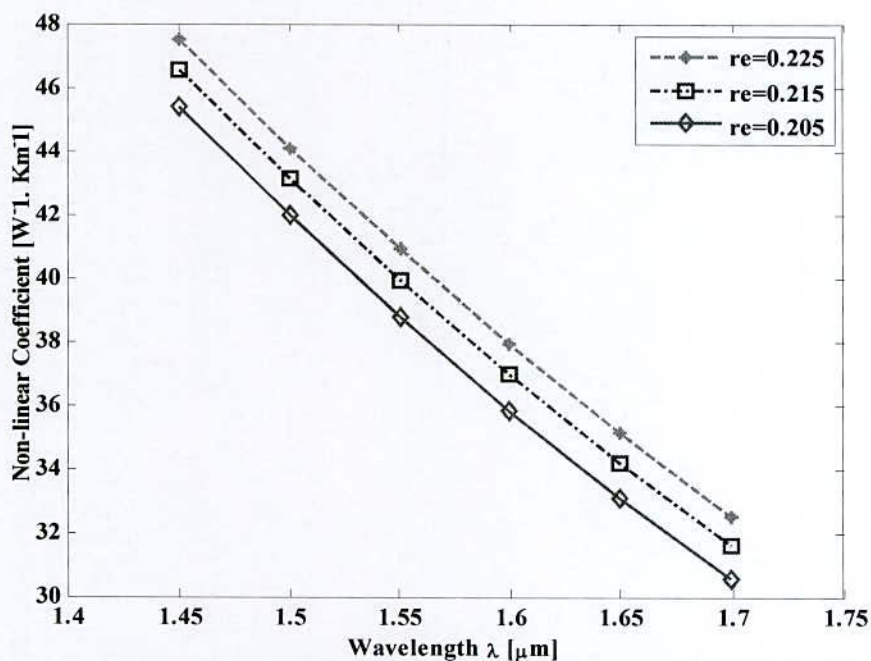


Fig.5.15. Influence of r_e on non-linearity of the proposed three rings SPCF

The nonlinear coefficient does not change significantly increasing with elliptically circular air holes radius, but reducing almost linearly with increasing wavelengths is shown in Fig.5.15. Dispersion slope, dispersion compensation ratio and effective dispersion are presented against wavelength for the proposed three rings SPCF in Figures 5.16- 5.18 respectively.

Moreover, the dispersion slope curve possesses negative slope and variation in magnitude is less than that of which presented in [1]. Effective dispersion after compensating the positive dispersion of 40 km SMF by the proposed SPCF for optimum parameters is shown in Fig. 5.18. It is to be mentioned here that the residual dispersion should be lower than $8.0 \pm$ ps/(nm.km) [9] to compensate for a 40 Gbps signal. However, the maximum value of effective dispersion in usable bandwidth (1450-1700 nm) for the proposed SPCF after compensating the dispersion of SMF is about ± 4 ps/(nm.km) and particularly at 1450 and 1700 nm, effective dispersion is zero.

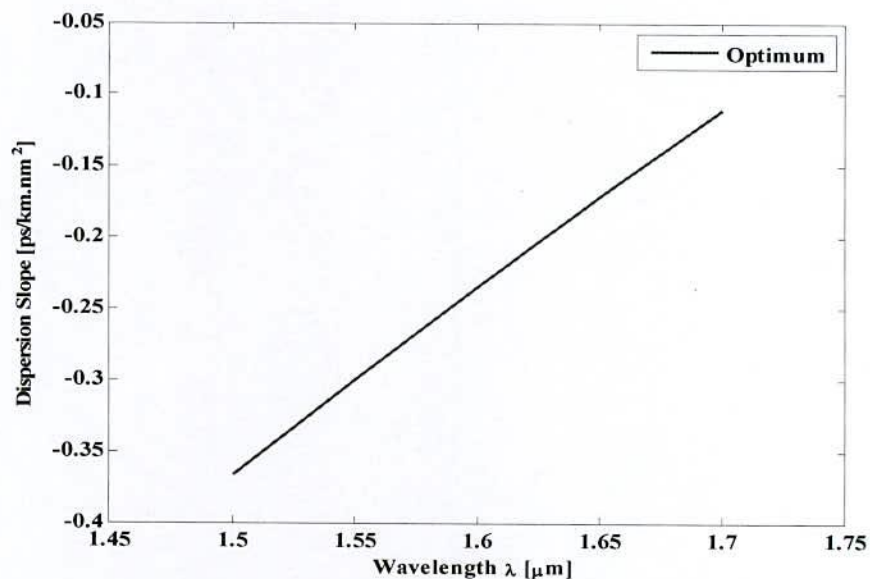


Fig. 5.16 Dispersion slope of three rings SPCF for optimum design parameters

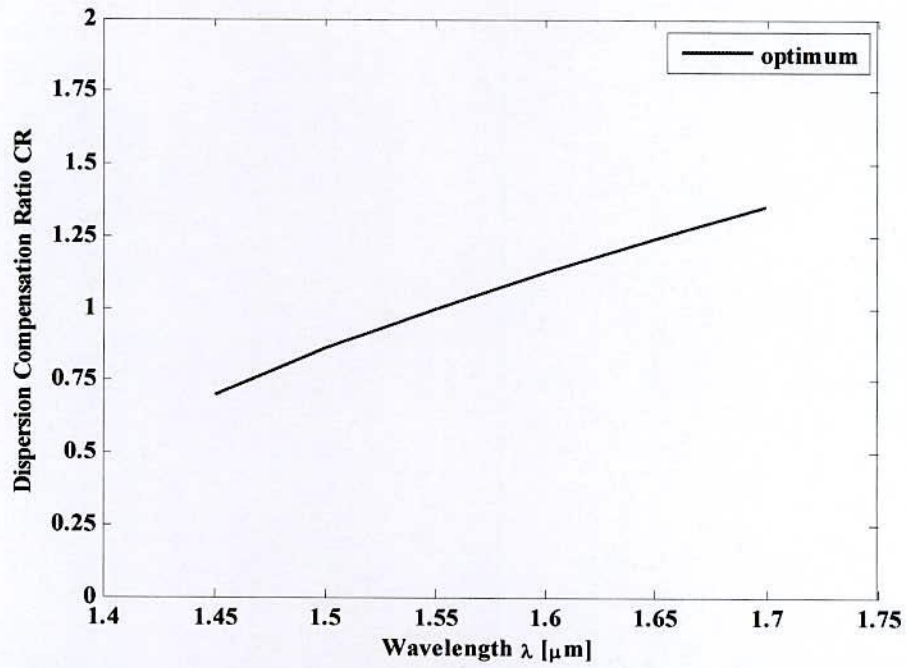


Fig. 5.17 Dispersion compensation ratio of three rings SPCF for optimum design parameters

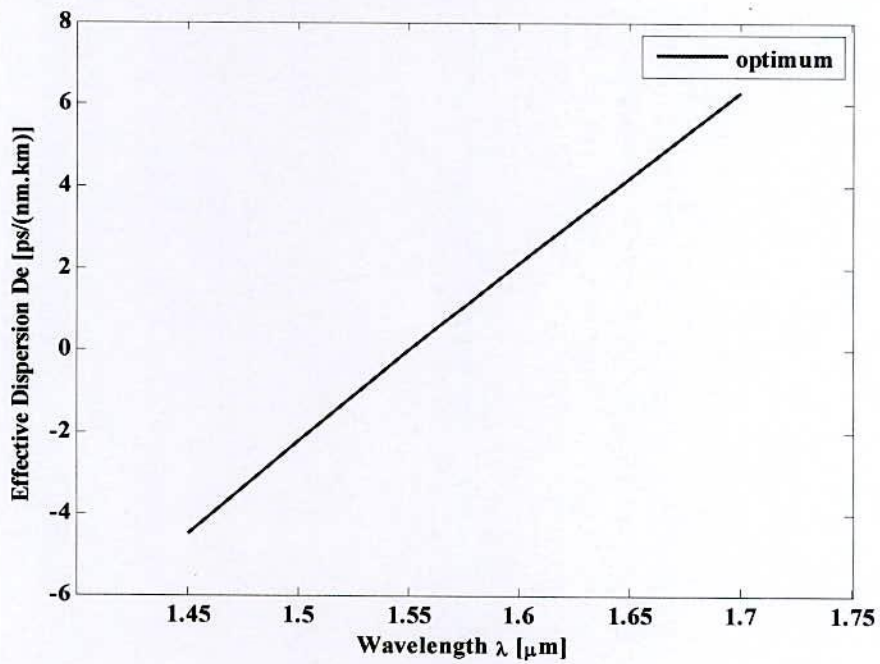


Fig. 5.18 Variation of effective dispersion against wavelength of 1.825 km long optimized three rings SPCF to compensate for a 40 km long standard SMFs

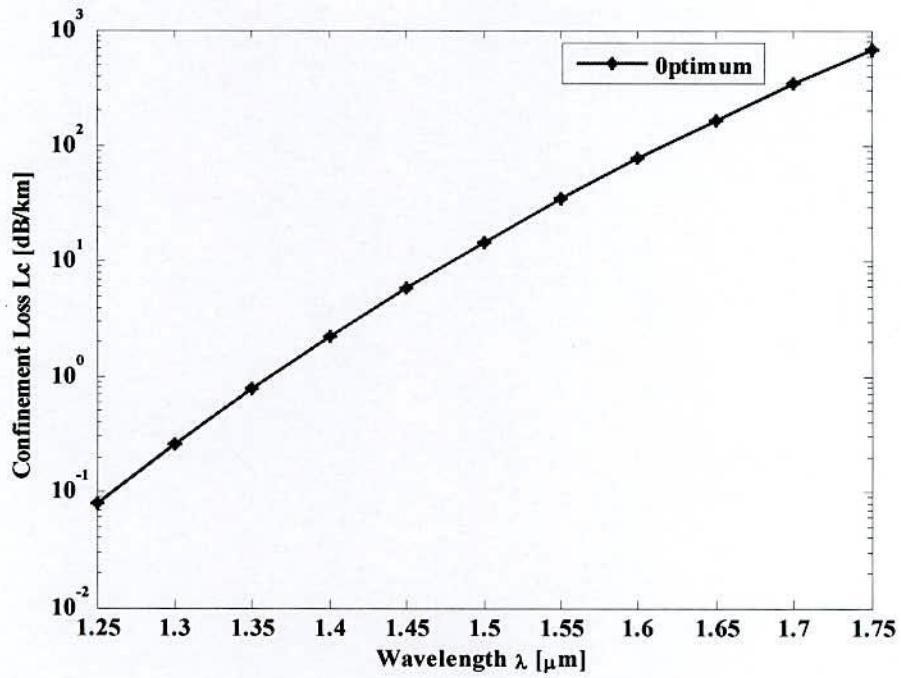


Fig. 5.19 Confinement loss of the proposed three rings SPCF for the optimum parameters

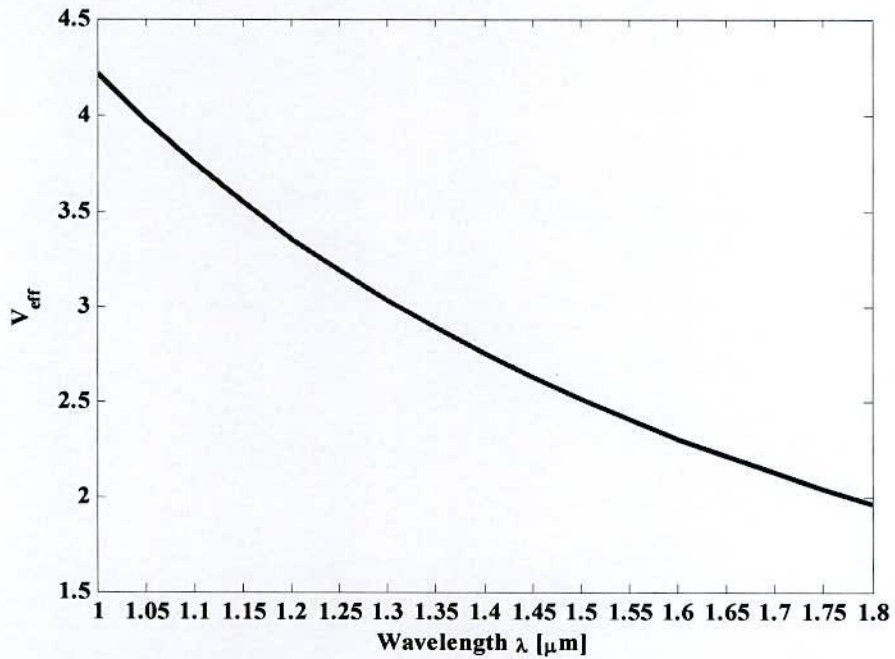


Fig. 5.20 Variation of effective V-parameter of the proposed three rings SPCF for optimum design parameters

Fig. 5.19 describes the wavelength dependence properties of the confinement loss of the proposed SPCF only for optimum parameters. From figure, it is observed that the confinement loss is about 0.0346 dB/m at $\lambda=1550$ nm which are the acceptable level for the transmission fiber. The above confinement loss covers wavelength ranging from 1.45 to 1.7 μm [1, 10]. Therefore, the design complexity of the proposed SPCF is lower than mentioned [11]. The effective V-parameter, V_{eff} for the proposed SPCF has been presented in Fig. 5.20 for the entire band of interest ranging from 1450-1700 nm wavelengths. However, simulation results show that the maximum value of V_{eff} is 2.627581 at 1450 nm and obviously the presented figure satisfies the condition $V_{\text{eff}} < \pi$ for the entire band of interest. Thus, our proposed SPCF will support only a single mode rather than multimode within that range of wavelength.

5.4.2 Simulation results of SPCF (distribution sunflower seeds)

To analyze the variation of chromatic dispersion against wavelength of the six rings SPCF, $r_o=1.4 \mu\text{m}$, $\theta=12^\circ$, $r_h=0.154 \mu\text{m}$, $r_e=0.21 \mu\text{m}$, $a=1.3 \mu\text{m}$ and $b=0.65 \mu\text{m}$ are reported for the optimized structure. Our proposed design shows an average value of chromatic dispersion for X-polarization which is equal to -609.32 ps/nm-km with a dispersion variation of 14.26 ps/nm-km (between -598.15 ps/nm-km and -582.75 ps/nm-km) in the wavelength range 1350nm-1600nm (250 nm band) which is equal to -396.33 ps/nm-km for Y-polarization with a dispersion variation of 9.34 ps/nm-km (between -356.25 ps/nm-km and -388.60 ps/nm-km) in the wavelength range 1350nm-1800nm(450nm band). In particular, the negative dispersion at 1550 nm is -626.091650 ps/(nm.km) for the six rings SPCF which is larger than what obtained at 1550 nm for three rings SPCF. We have compared our result of chromatic dispersion with those obtained by Franco et. al. [11], Da Silva et. al. [12] and M Islam et.al. [13], shown in Fig.5.21. But our proposed design has been provided better negative dispersion than those of Franco et. al. Da Silva et. al. and M Islam et.al.

For evaluating the dependency on thickness of perfectly matched layer (PML) has been reported [5]. However, we change the PML value from 0.6 to 1.6 μm in shown in Fig.5.22. It can be clearly seen that the chromatic dispersion remains unchanged for six rings SPCF with wavelength but comparison with Fig. 5.6 of three rings SPCF that have PML effect less than 1 μm . For that case, six rings SPCF would be afforded to fabricate the PCF design easily.

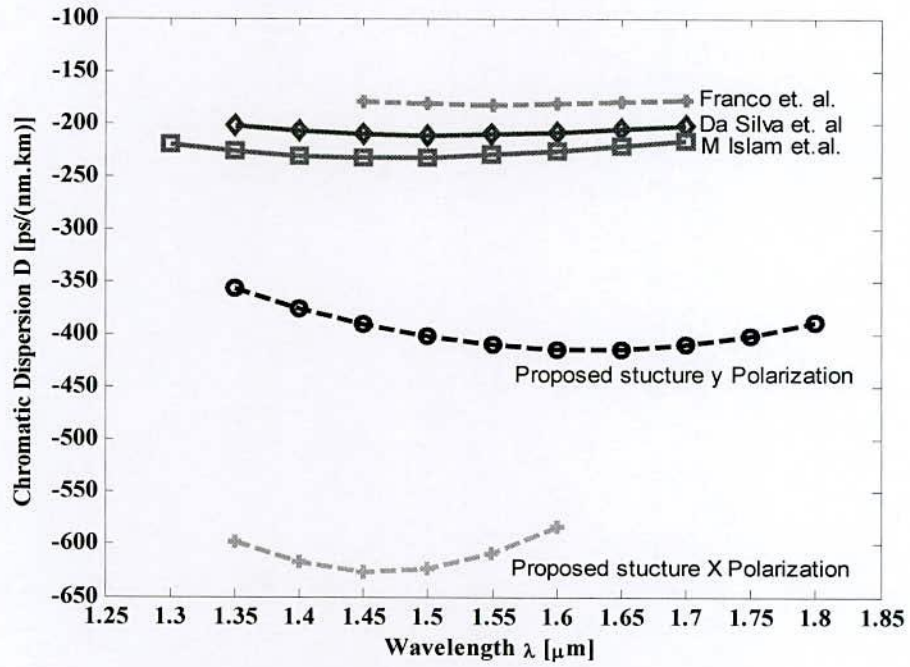


Fig.5.21 Comparison between chromatic dispersion

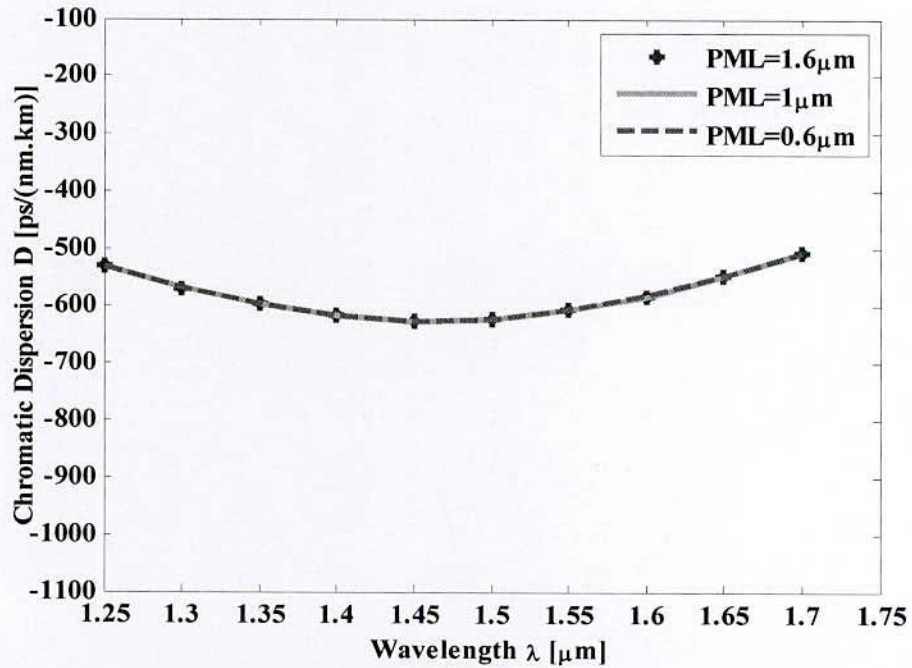


Fig.5.22 Dispersion with respect to thickness of PML of the proposed six rings SPCF

However, for the flattened profile of negative dispersion coefficient and dispersion slope over the entire band of interest provides good dispersion compensating ability. Thus, the proposed fiber can be used to compensate accumulated dispersion of SMF currently

deployed in WDM systems as it possesses large negative dispersion over a wide range of wavelength.

We then investigate the dependence of chromatic dispersion on the wavelength under different r_e of elliptically circular air holes keeping constant all others parameters. With the increase of r_e , dispersion for X and Y polarizations also increases in both case as demonstrated in Fig.5.23 and Fig.5.24 respectively. From Fig, it can be explained that 1) negative dispersion for Y-polarization is flatter than X-polarization at r_e equal to $0.21\mu\text{m}$ and 2) dispersion for X-polarization is varied dramatically which can be achieved up to $-1037.49\text{ ps/nm}\cdot\text{km}$ at 1400nm for r_e of $0.23\mu\text{m}$ and 3) more flatness portion is lower than 1550nm (1400nm to 1500nm) for X-polarization which near to 1550nm and above (1550nm to 1700nm) for Y-polarization. In both cases, variation of flat portion is increased from radius $0.21\mu\text{m}$ to $0.23\mu\text{m}$ because field interacts with silica cladding of spiral ring is more for X-polarization than Y-polarization beyond the defected elliptical air holes as illustrated in Fig.5.25 and Fig.5.26.

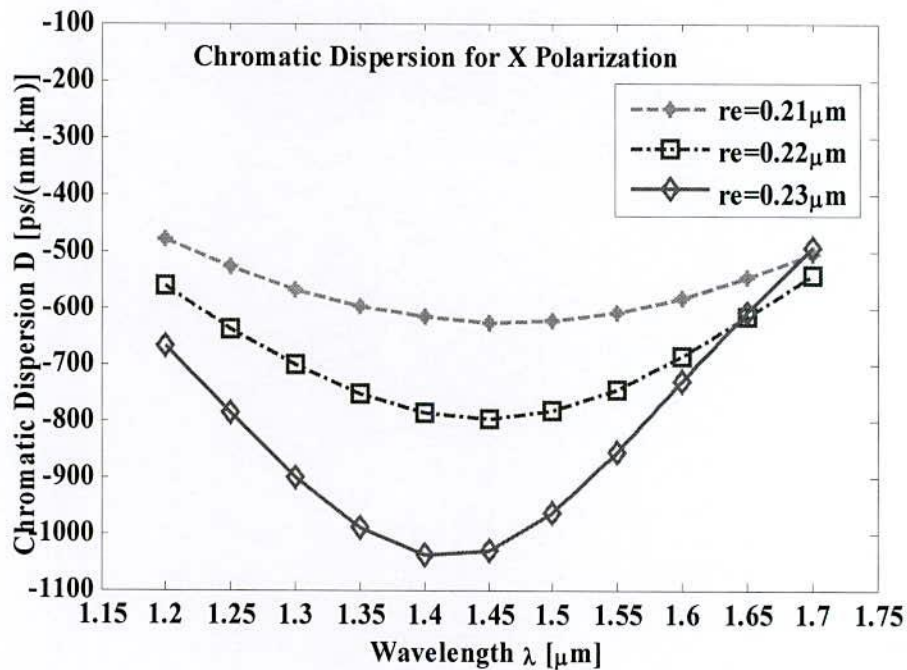


Fig.5.23 Chromatic dispersion for X-polarization of the proposed six rings SPCF

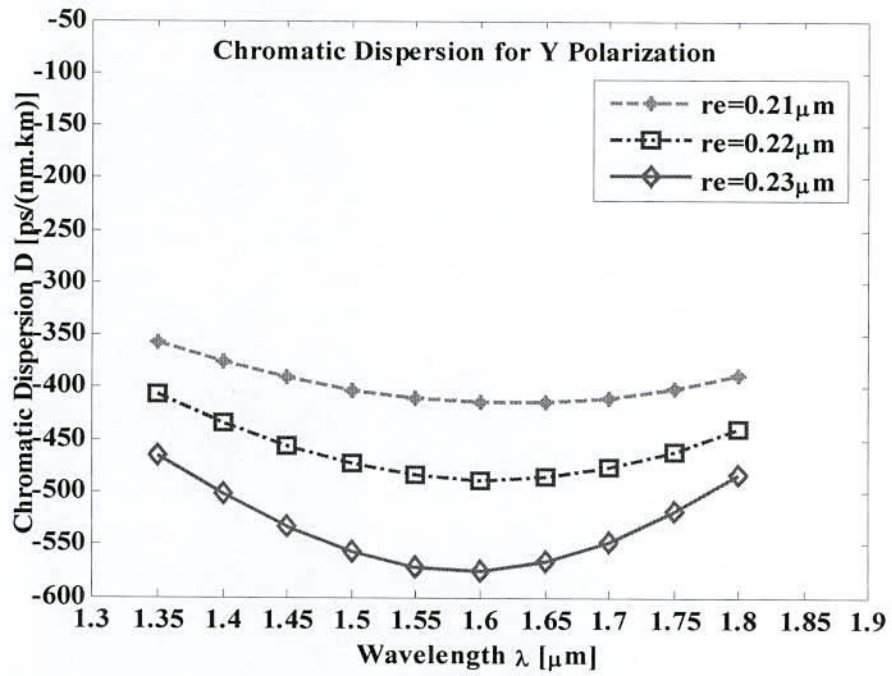


Fig.5.24 Chromatic dispersion for Y-polarization of the proposed six rings SPCF

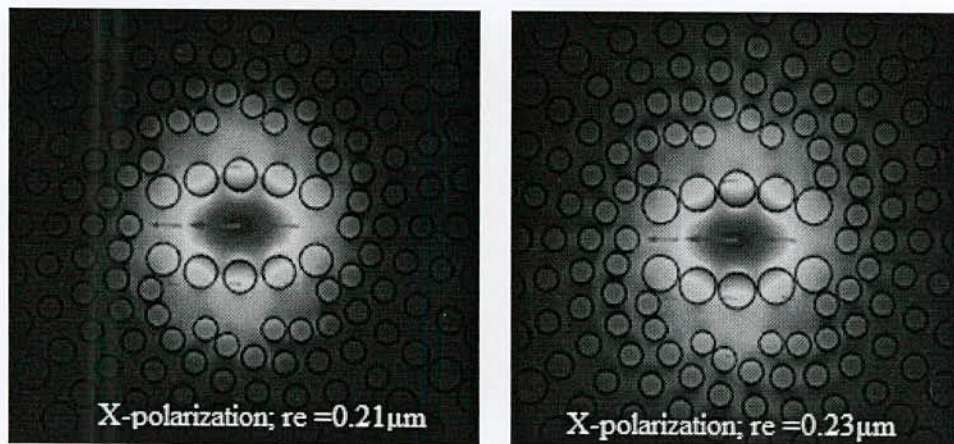


Fig.5.25 Electric field for X-polarization at r_e of 0.21 μm and 0.23 μm

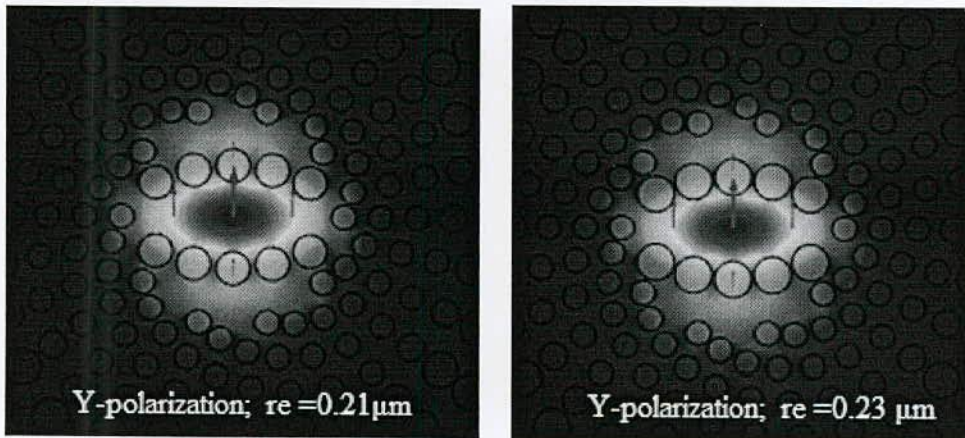


Fig.5.26 Electric field for Y-polarization at r_e of 0.21 μm and 0.23 μm

We further examine the dependence of birefringence and non-linearity on the diameter of elliptically circular air holes. After fixing the ellipticity ratio at 2, the birefringence as a function of the diameter of r_e is depicted in Fig.5.27. The birefringence increases with the increase of the diameter of r_e because the fiber cross-section is more asymmetric. It can be examined that the birefringence is about 0.0170 at 1550nm when $r_e=0.21\mu\text{m}$. A maximum birefringence of 0.0223 is achieved when r_e enhances up to $0.23\mu\text{m}$, manifested in the insets in Fig.5.27.

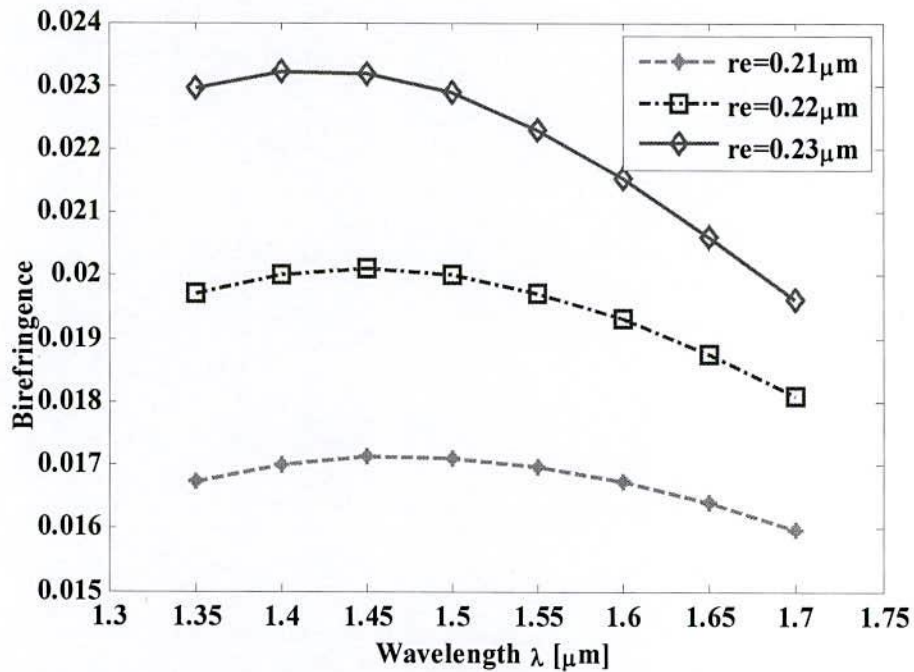


Fig.5.27 Birefringence variance with respect to r_e of the proposed six rings SPCF

Fig 5.28 shows the variation of effective area with wavelength for optimum parameters. To obtain small effective area number of elliptical air hole is placed in core region. The effective area of the proposed fiber is about $2.1014 \mu\text{m}^2$ at 1550 nm wavelength. However, the effective area is increasing with increase in wavelength and elliptical air hole radius r_e . Moreover, the effective area of the six rings SPCF is not even small but still smaller than that obtained for the three rings SPCF.

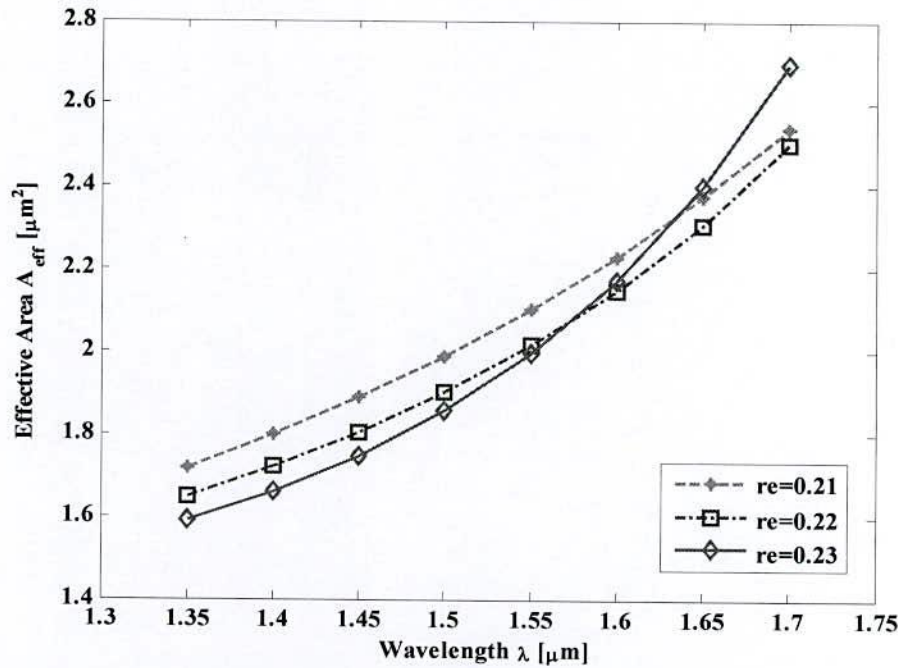


Fig. 5.28 Effective area of the proposed six rings SPCF for r_e optimum design parameters

With the evidence of Fig.5.29, one can observe that the nonlinear coefficient of our designed PCF is very high, and the nonlinear coefficient does not change significantly increasing with elliptically circular air holes radius, but reducing almost linearly with increasing wavelengths. The non-linear coefficient is $44.3679 \text{ W}^{-1}\text{km}^{-1}$ at 1550nm which is greater than that obtained three rings SPCF.

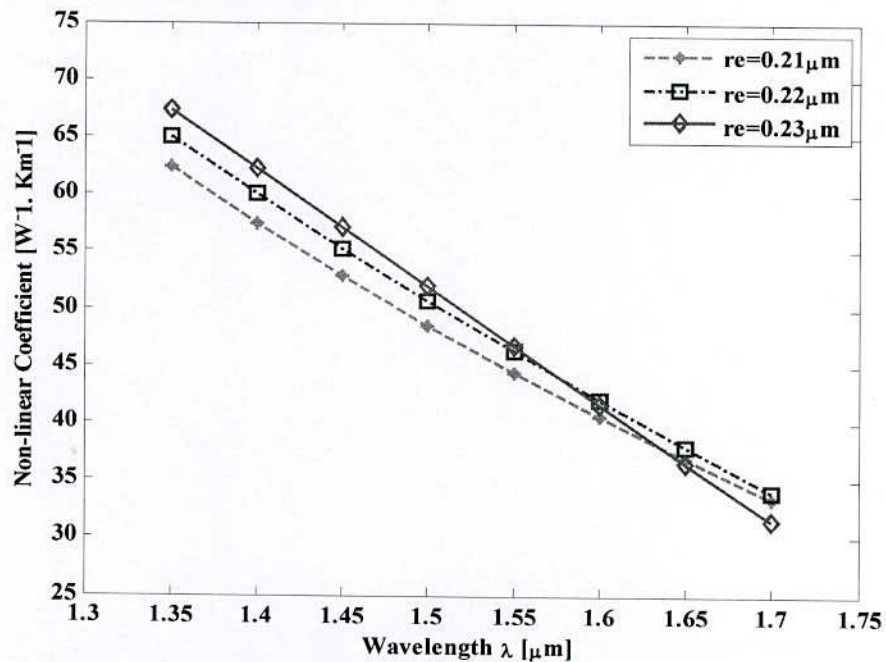


Fig.5.29 Influence of r_e on non-linearity of the proposed six rings SPCF

The birefringence and non-linearity in comparison with values presented former in the literature [13] and [14] respectively. Here, it has been possible to trade off high chromatic dispersion, high birefringence and large non-linearity by using our optimized design.

The dispersion slope and dispersion compensation ratio of the proposed six rings SPCF has been illustrated in Fig.5.30 and Fig.5.31 respectively. It is clearly observed from the figure that it possesses the dispersion slope from -1 to +1 contains more flattened profile than three rings SPCF in Fig.5.16 over the wavelength band ranging from 1250 to 1700 nm and thus complies with the requirement of broadband dispersion compensation. Moreover, the variation in dispersion slope is low and even negligible particularly at 1500 nm wavelength. Fig. 5.32 shows the variation of effective dispersion against wavelength of 1.1427km long optimized SPCF to compensate for a 40 km long standard SMFs. However, the effective dispersion of the proposed SPCF is zero 1550 nm. Thus, it is seen that the optimized six rings SPCF is capable of compensating dispersion with lower dispersion variation over E+S+C+L+U band.

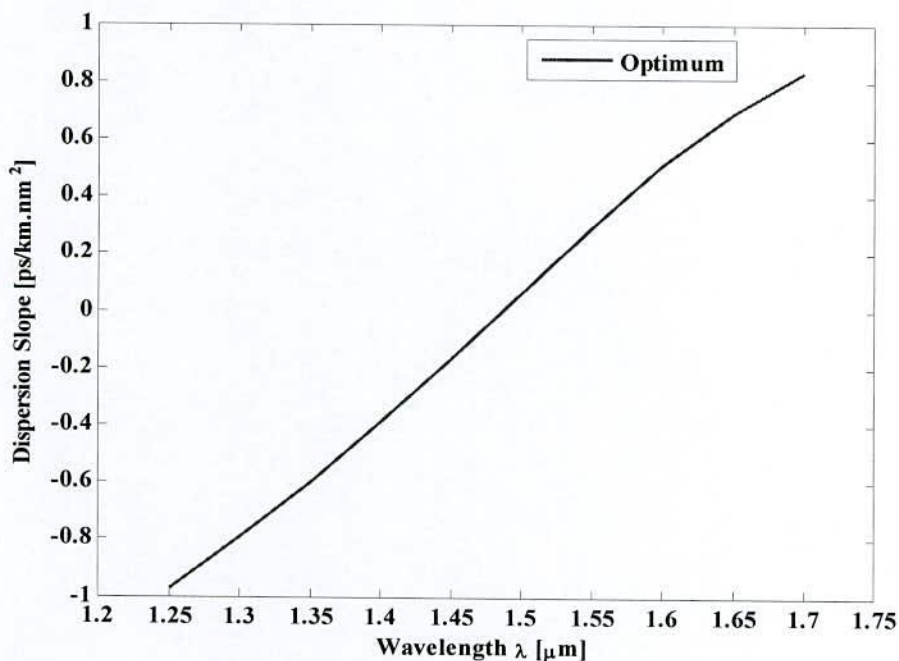


Fig. 5.30 Dispersion slope of six rings SPCF for optimum design parameters

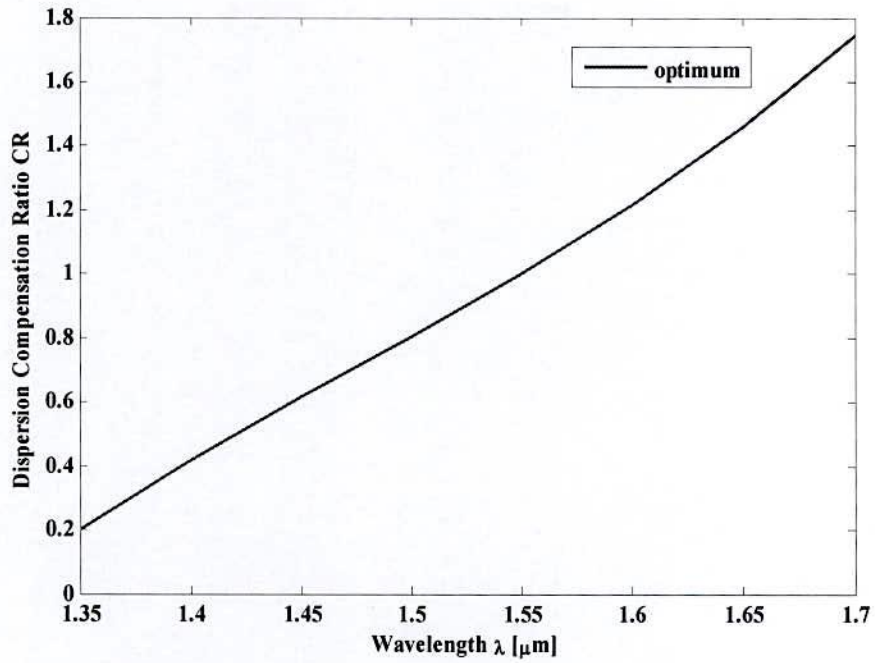


Fig. 5.31 Dispersion compensation ratio of six rings SPCF for optimum design parameters

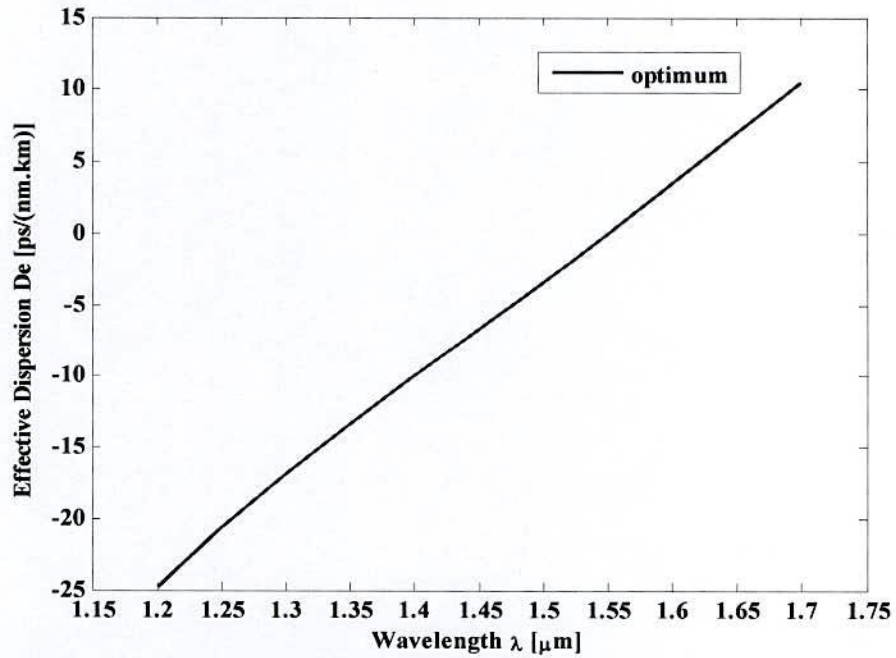


Fig. 5.32 Variation of effective dispersion against wavelength of 1.1427km long optimized six rings SPCF to compensate for a 40 km long standard SMFs

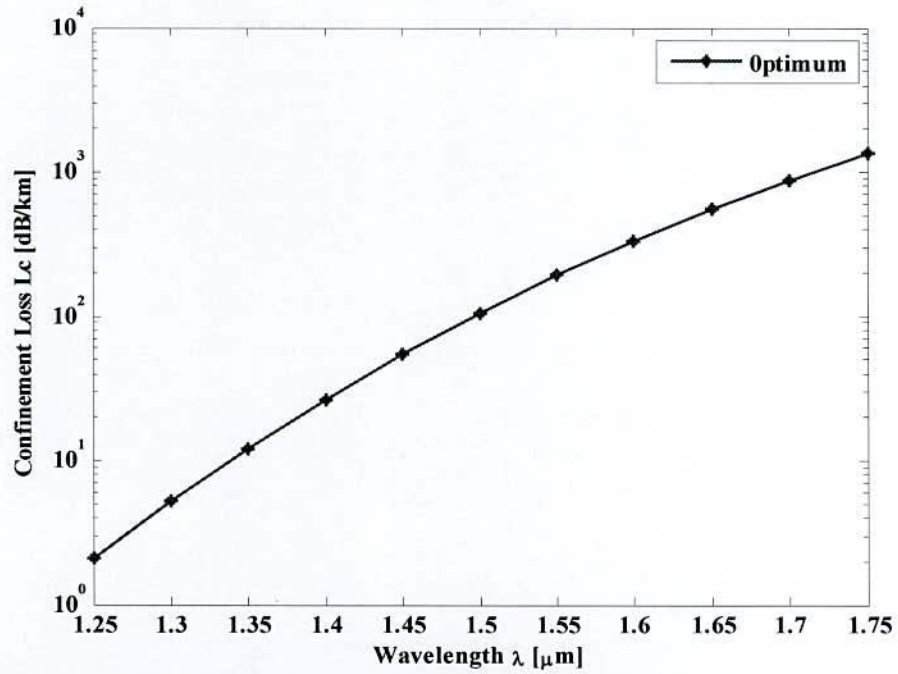


Fig. 5.33 Confinement loss of the proposed six rings SPCF for the optimum parameters

Fig. 5.33 shows the confinement of the proposed six rings SPCF. It is observed from the figure that the confinement loss is 0.1926 dB/m at $\lambda=1550$ nm. The effective V-parameter has been shown in Fig. 5.34. From the figure, it is clear that all values of $V_{eff} < \pi$ and thus the proposed six rings SPCF will only support single mode rather multimode.

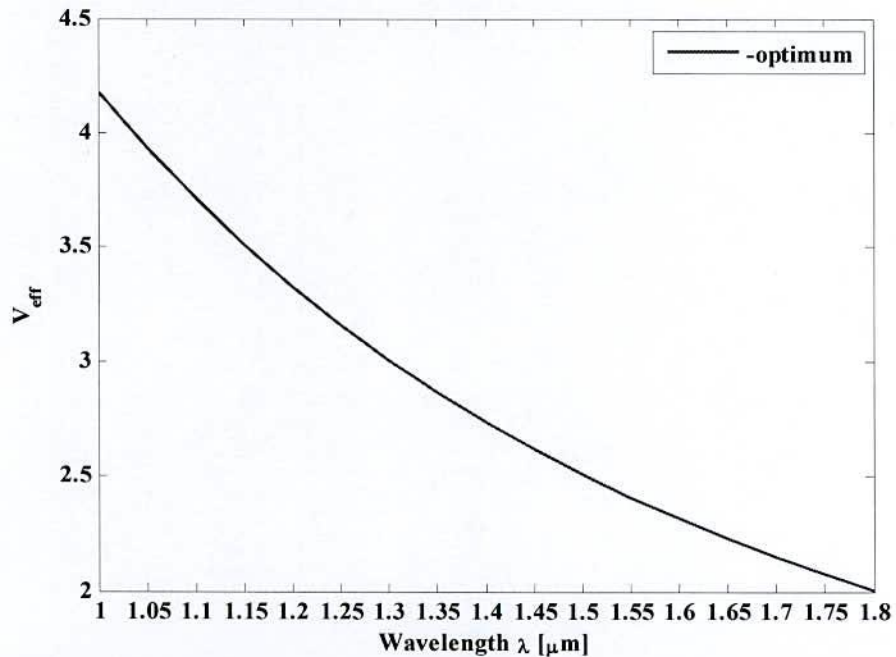


Fig. 5.34 Variation of effective V-parameter of the proposed six rings SPCF for optimum design parameters

5.4.3 Simulation results of SPCF (nautilus shell)

Fig. 5.35 shows wavelength response of chromatic dispersion of the proposed nautilus shell-SPCF for optimum design parameters ($r_0 = 1.4 \mu\text{m}$, $\theta = 12^\circ$ up to seven holes then starting 156° , $r_1 = 0.18 \mu\text{m}$, $r_2 = 0.198 \mu\text{m}$, $r_3 = 0.216 \mu\text{m}$, $r_4 = 0.234 \mu\text{m}$, $r_5 = 0.252 \mu\text{m}$, $r_6 = 0.216 \mu\text{m}$, $r_7 = r_8 = r_9 = r_{10} = r_{11} = r_{12} = r_{13} = r_{14} = r_{15} = r_{16} = 0.237 \mu\text{m}$, $r_e = 0.21 \mu\text{m}$, $a = 1.3 \mu\text{m}$ and $b = 0.65 \mu\text{m}$) from the optimum value. It can be seen that for the optimized set of parameters and air-hole configurations, a flat negative chromatic dispersion of high magnitude over E to U band is obtained. Our proposed design shows an average value of chromatic dispersion for Y-polarization which is equal to -341.73 ps/nm-km with a dispersion variation of 5.02 ps/nm-km (between -328.16 ps/nm-km and -334.96 ps/nm-km) in the wavelength range 1350 to 1700 nm. For considering S to L band, the average value of negative chromatic dispersion is $-347.969 \text{ ps/nm-km}$ and only 2.03 ps/nm-km dispersion variation which is very close to $-348.822048 \text{ ps/nm-km}$ at 1550 nm.

Keeping constant all others parameters, the influence of different r_e of elliptically circular air holes on chromatic dispersion has been shown in Fig.5.35. With the increase of r_e , dispersion for Y and X polarizations also increases in both cases as demonstrated in Fig.5.35 and Fig.5.36 respectively. From Fig, it can be explained negative dispersion for Y-polarization and X-polarization is varied simultaneously which is differ from distribution sunflower seeds-SPCF has been shown in Fig.5.25 and Fig.5.26 for X and Y-polarization respectively. Dispersion for X-polarization can be achieved up to -785.60 ps/nm-km at 1400nm for r_e of $0.23 \mu\text{m}$ and more flatness portion is at 1400nm and for Y-polarization, dispersion is -466.54 ps/nm-km which also large and more flatter at 1550nm than X-polarization. From the above results, it is clear that a large negative dispersion is obtained and the dispersion value of the proposed nautilus shell-SPCF at 1550 nm is higher than [9] and far exceeding the dispersion values of conventional dispersion compensating fibers which is typically -100 ps/(nm.km) [15].

Fig. 5.37 shows the wavelength response of birefringence property for the optimum design parameters. The optimum design parameters give a value of birefringence of 0.0168 at 1550 nm wavelength which is a very high value, two orders of magnitude higher than that of conventional PM fibers [16]. A maximum birefringence of 0.0231 is achieved when r_e enhances up to $0.23 \mu\text{m}$, manifested in the insets in Fig.5.37. Also, a high birefringence fiber could be very useful in a polarization maintaining transmission system [17] and can be used to eliminate the effect of PMD in transmission systems. Therefore, the proposed nautilus

shell-SPCF could be a potential candidate for optical fiber sensing and polarization maintaining transmission system.

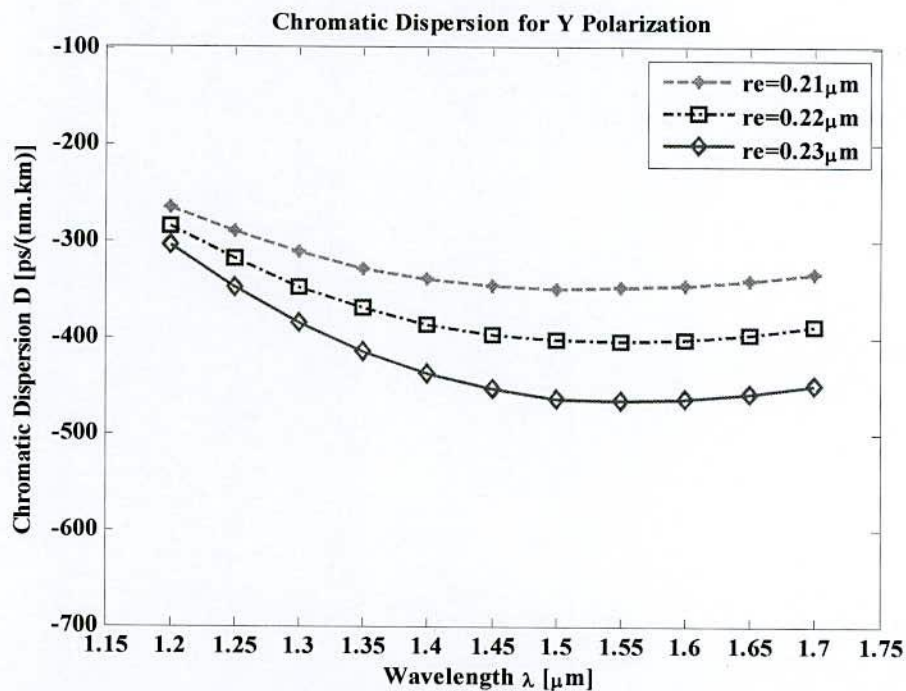


Fig.5.35 Chromatic dispersion for Y-polarization of the proposed nautilus shell-SPCF

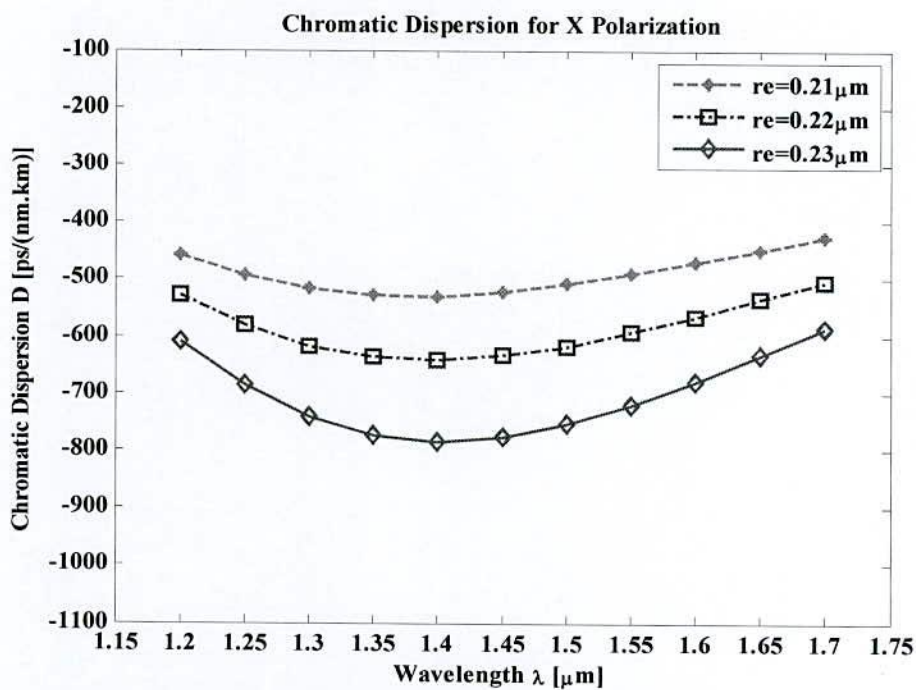


Fig.5.36 Chromatic dispersion for X-polarization of the proposed nautilus shell-SPCF

Fig. 5.38 shows fundamental electric field properties of the proposed nautilus shell-SPCF for X and Y-polarization at $\lambda=1550$ nm. The asymmetrical design of the core of the proposed nautilus shell-SPCF causes a considerable increase in linear birefringence properties, which is suitable for PM applications.

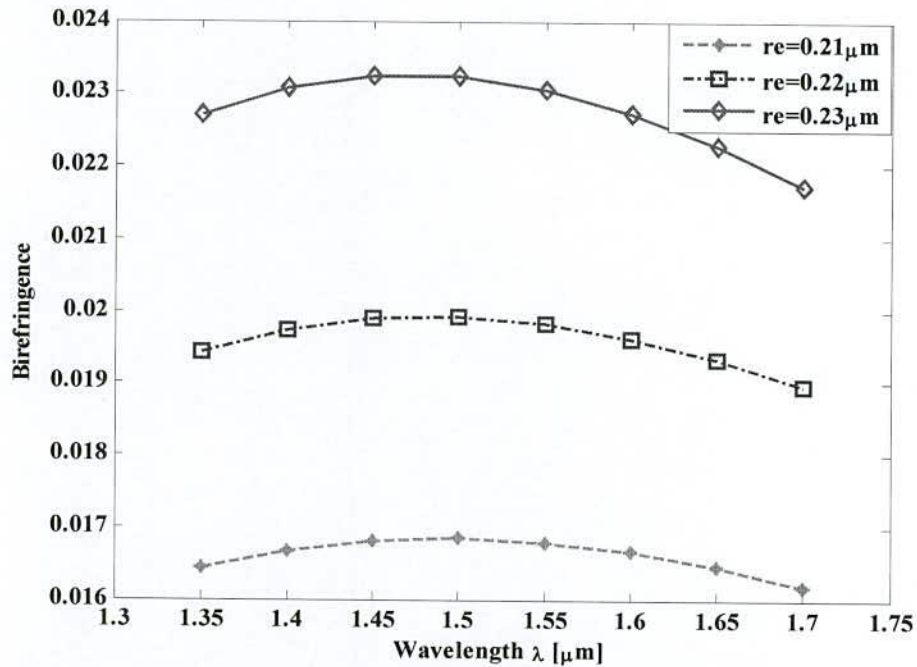


Fig.5.37 Birefringence variance with respect to r_e of the proposed nautilus shell-SPCF

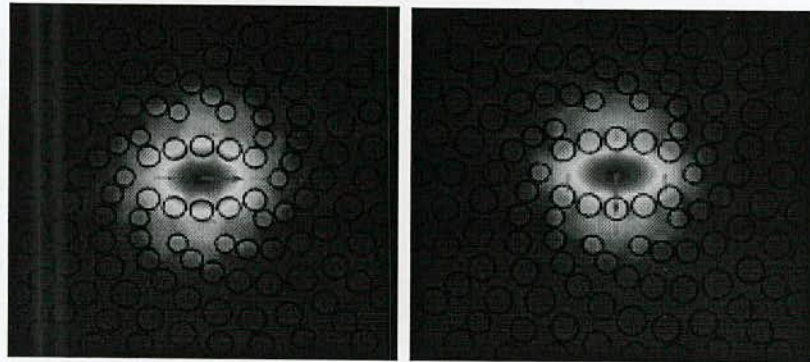


Fig.5.38 Electric field for X and Y-polarization at 1550nm of the proposed nautilus shell-SPCF

Fig. 5.39 corresponds to variation of effective area for optimum design parameters. It can be clearly seen that effective area is $2.13 \mu\text{m}^2$ same as distribution sunflower seeds-SPCF at 1550 nm for the optimum design parameters which is almost same as reported [18]. The non-linear coefficient is $43.724 \text{ W}^{-1}\text{km}^{-1}$ at 1550nm which is obtained up to $47.063 \text{ W}^{-1}\text{km}^{-1}$ with increasing elliptical hole radius r_e has been shown in Fig. 5.40.

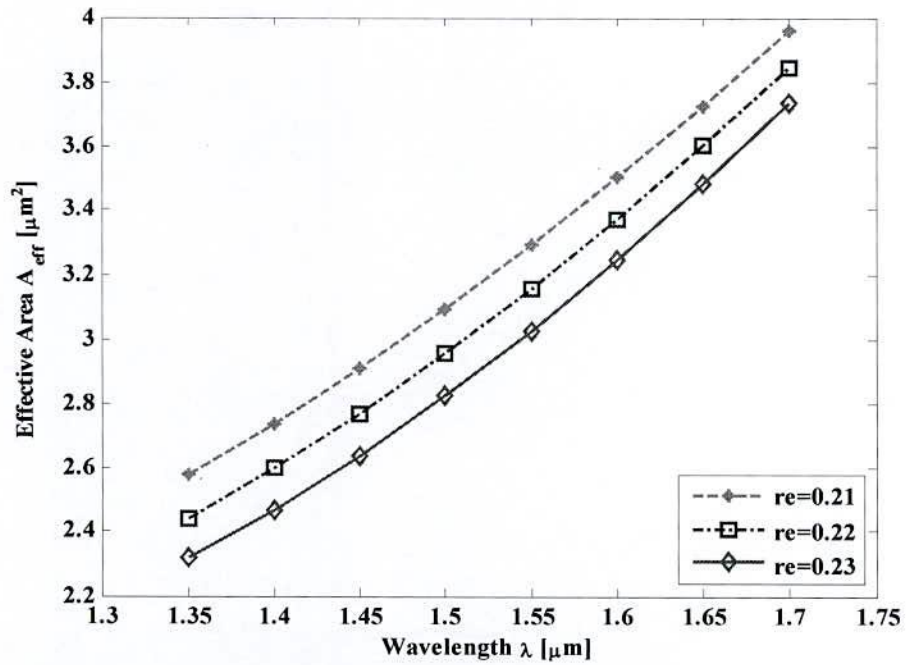


Fig. 5.39 Effective area of the proposed nautilus shell-SPCF for r_e optimum design parameters

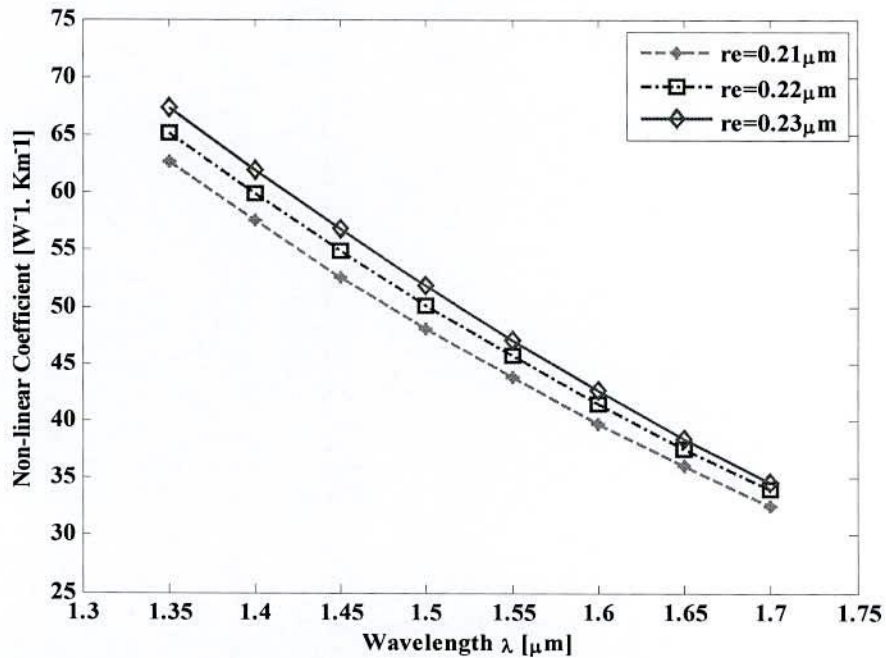


Fig.5.40 Influence of r_e on non-linearity of the proposed nautilus shell-SPCF

The dispersion slope and dispersion compensation ratio of the proposed nautilus shell-SPCF has been illustrated in Fig. 5.41 and Fig. 5.42 respectively. It is clearly observed from the figure that it possesses the negative to positive dispersion slope over the wavelength band

ranging from 1350 to 1700 nm which is more flatness than distribution sunflower seeds-SPCF and thus complies with the requirement of broadband dispersion compensation.

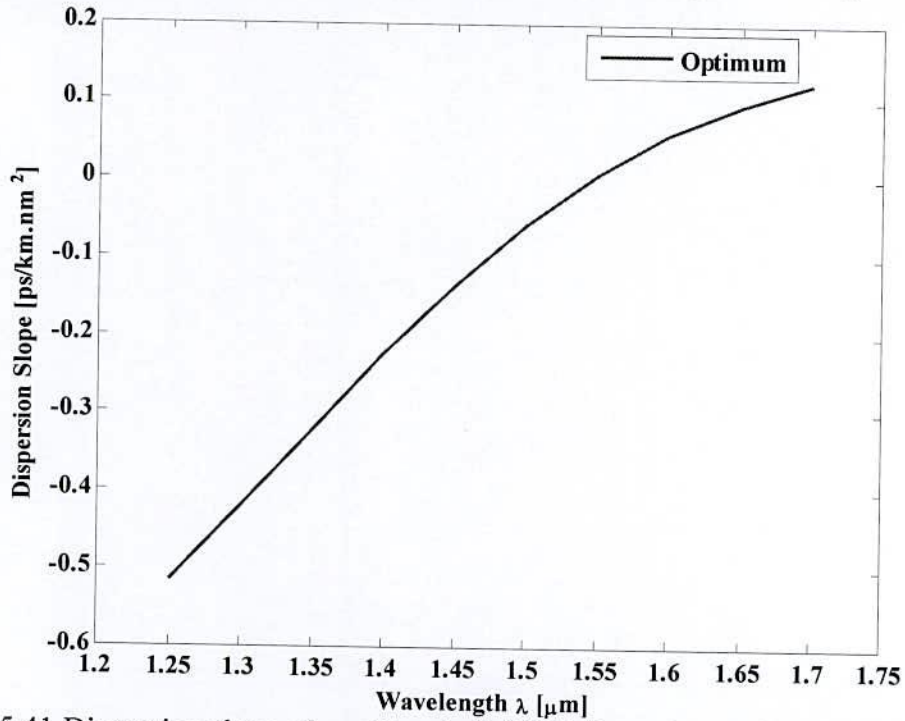


Fig. 5.41 Dispersion slope of nautilus shell-SPCF for optimum design parameters

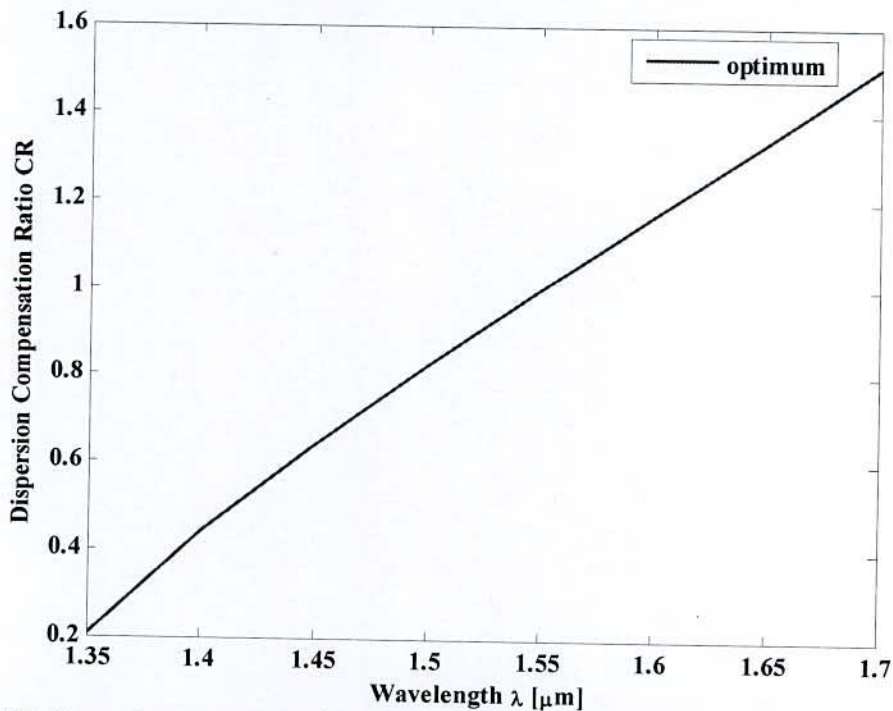


Fig. 5.42 Dispersion compensation ratio of nautilus shell-SPCF for optimum design parameters

Fig. 5.43 correspond effective dispersion obtained after the dispersion compensation by 1.9927 km long nautilus shell-SPCF for the dispersion accumulated in one span (40 km) of

SMF for the optimum design parameters. From the figure, effective dispersion is found within $\pm 8\text{ps}/(\text{nm}\cdot\text{km})$ range and thus, it is clearly proved that our proposed nautilus shell-SPCF with optimized parameters is suitable for systems with high bit rates 40Gb/s covering E to U communication bands.

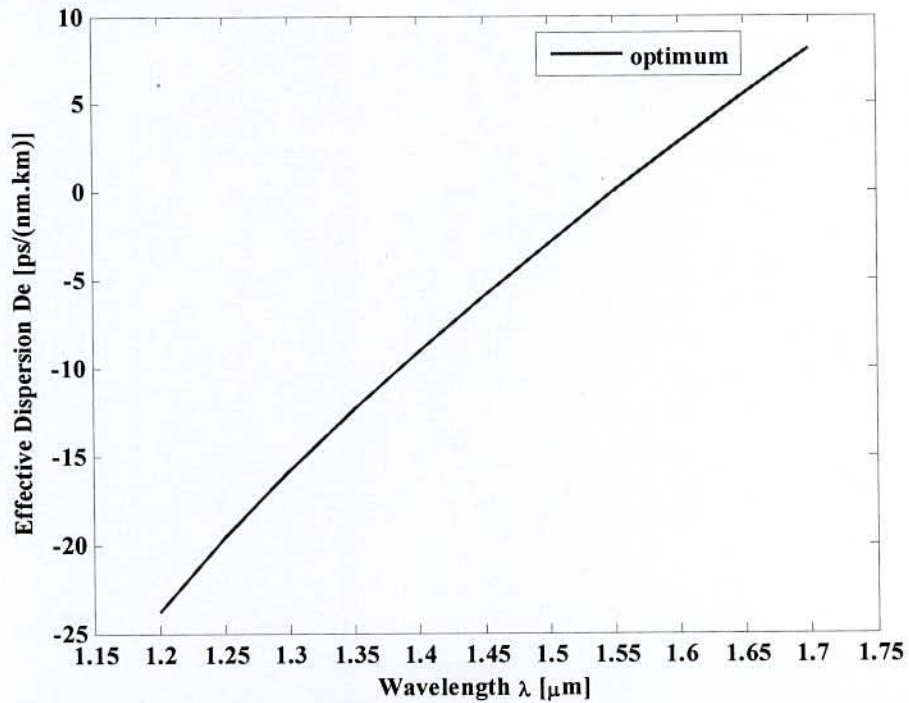


Fig. 5.43 Variation of effective dispersion against wavelength of 1.9927 km long optimized nautilus shell-SPCF to compensate for a 40 km long standard SMFs

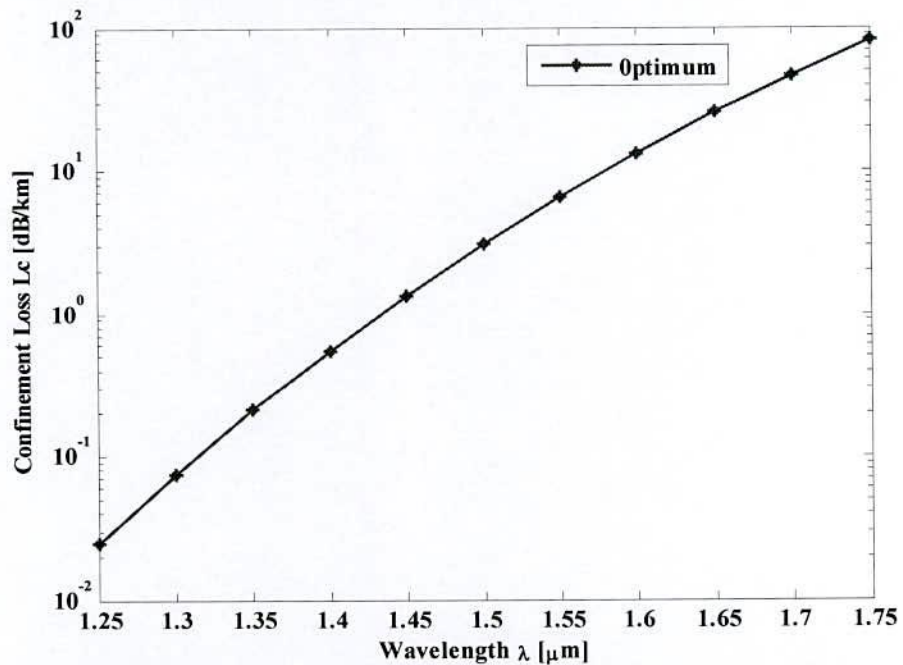


Fig. 5.44 Confinement loss of the proposed nautilus shell-SPCF for the optimum parameters

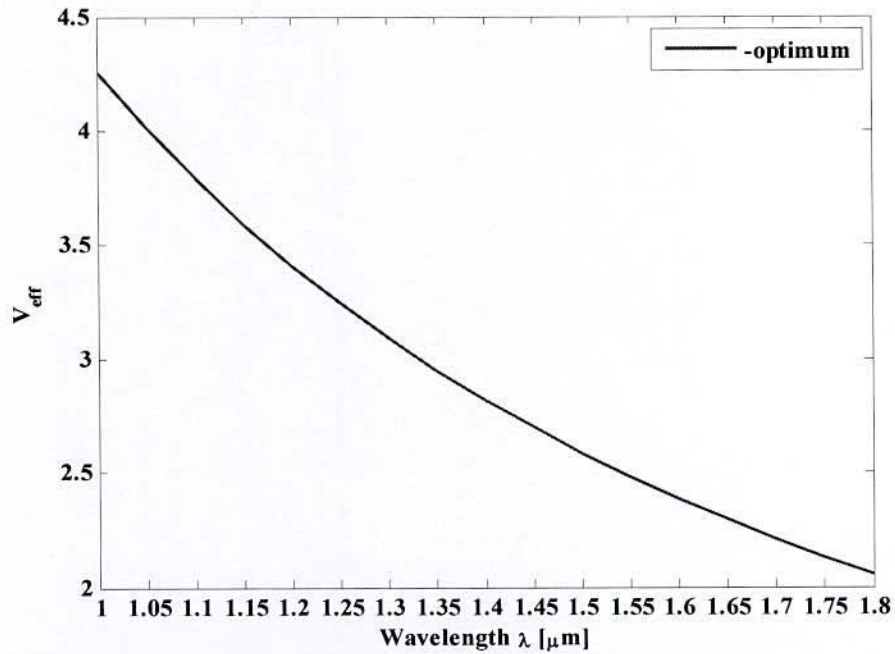


Fig. 5.45 Variation of effective V-parameter of the proposed nautilus shell-SPCF for optimum design parameters

However, wavelength dependence of fiber's confinement loss for optimum design parameters has been shown in Fig. 5.44. Note that the loss is increasing smoothly with the wavelength and there is no evidence of abrupt change in leakage. In particular, confinement loss at 1550 nm is 0.065288 dB/m. It is also evident from. The effective V-parameter is 2.48 has been shown in Fig. 5.45. It is obvious from the figure that the proposed nautilus shell-SPCF will only support single mode rather multimode as $V_{\text{eff}} < \pi$ over the wavelength band ranging from 1350 to 1700 nm.

5.5 Comparison between proposed DC-PCFs and some other DC-PCFs

Finally, a comparison is made between properties of the proposed SPCFs for broadband dispersion compensation and some other PCFs designed for the same. The comparison between these fibers are presented in Table III which takes into account the magnitude of average negative dispersion, dispersion variation, birefringence, effective area, non-linear co-efficient, the length of dispersion compensating fiber to compensate the accumulated dispersion of the SMF and the number of design parameters (NDP). The proposed DC-PCFs exhibit the higher value of the average negative dispersion with lower dispersion variation than those presented before. However, the three rings SPCF shows average dispersion higher than that of other proposed SPCF (nautilus shell) and hence it requires small length of DCF to compensate the accumulated dispersion of SMF but the non-linear coefficient is not enough and dispersion variation is high. As a result, it will not be an appropriate candidate to compensate chromatic dispersion at flattened profile and non-linearity at the same time over wide band.

Table III: Comparison between properties of the proposed DC-PCFs and other DC-PCFs

Spiral phenomena	PCFs	Average dispersion ps/(nm.km)	Dispersion variation	Wavelength/ Band(nm)	B (1550nm)	Non-linearity $W^{-1}km^{-1}$	A_{eff} (μm^2)	PML effect	DCF (km)	NDP
convantional	SPCF (three rings)	-355.89(X)	11.8	1450-1700	0.0175	39.9333	2.334	yes $< 1\mu m$	1.825	1 (r_e)
distribution sunflower seeds	SPCF (six rings)	-609.32(X) -396.33(Y)	14.26 9.34	1350-1600 1350-1800	0.0170	44.3679	2.101	no	---- 1.142	1 (r_e)
nautilus shell	SPCF	-341.73(Y) -347.96(Y)	5.02 2.03	1350-1700 1450-1600	0.0168	43.724	2.13	no	1.992	1 (r_e)
Hexagonal	Ref. [11]	-179	2.1	1480-1675	-	-	-	-	-	3(r_h, d, Λ)
Hexagonal	Ref. [12]	-212	11	1350-1675	-	-	-	-	-	3(r_h, d, Λ)
distribution sunflower seeds	Ref. [13]	-227	11	1350-1675	0.017	-	5	-	-	4 (r_o, r_h, d_m, d_n)

On the other hand, six rings SPCF (distribution sunflower seeds) and SPCF (nautilus shell) both show the large magnitude of average negative dispersion with lower dispersion variation as well as high birefringence in comparison with Ref. [11, 12, 13, 19]. In addition, the effective area of the proposed DC-PCFs is lower than that of Ref. [13, 20].

However, the comparison between average negative dispersion of the proposed DC-PCFs has been shown in Fig. 5.46. It is observed that six rings SPCF and nautilus shell SPCF shows more flatness than three rings SPCF over E to U band but considering S to L, nautilus shell SPCF exhibits average dispersion with an absolute dispersion 2.03 ps/(nm.km). The comparison between birefringence in Fig. 5.47 reveals that nautilus shell SPCF provides 0.0231 which is higher than other proposed DC-PCFs.

The comparison between dispersion slopes for the proposed DC-PCFs in Fig. 5.48 reveals that the nautilus shell SPCF is more appropriate than others for dispersion compensation covering entire E to U band and slope is 0.006195 around 1550nm. In addition, there is a tendency to cover above the U band beyond 1675 nm wavelength.

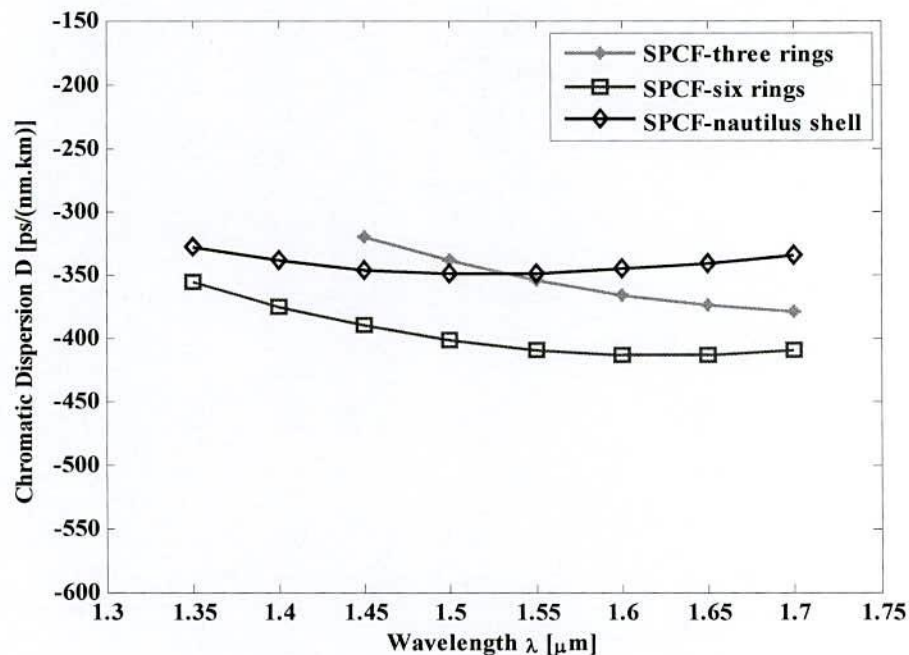


Fig. 5.46 Comparison between relative chromatic dispersion for the proposed DC-PCFs

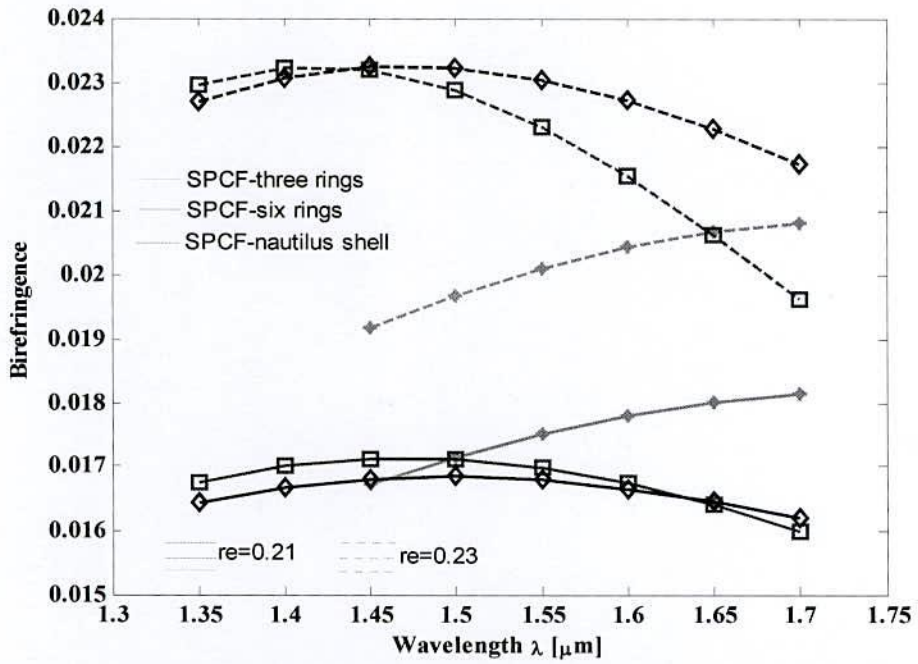


Fig. 5.47 Comparison between birefringence for the proposed DC-PCFs

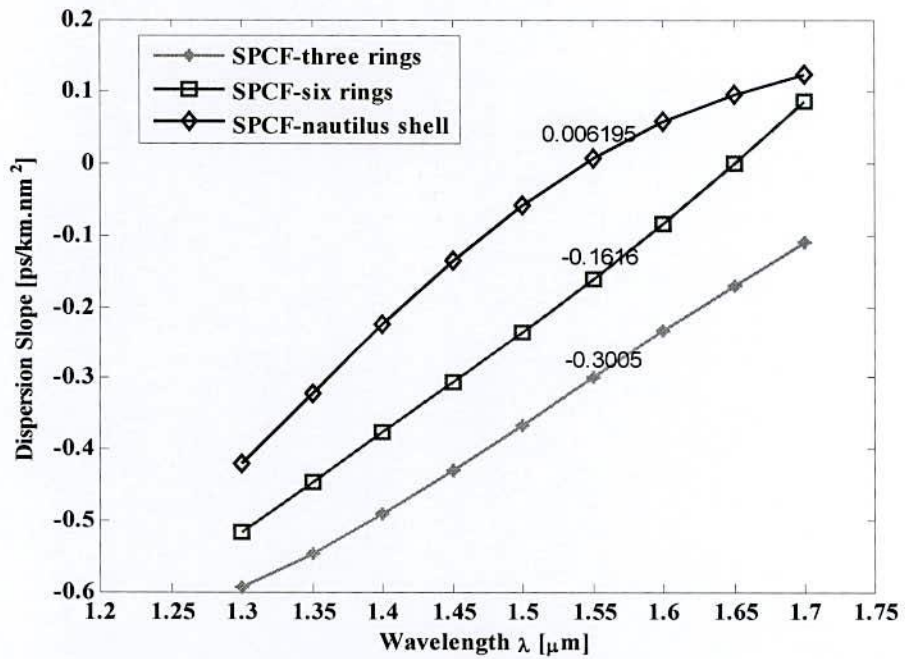


Fig. 5.48 Comparison between dispersion slope for the proposed DC-PCFs

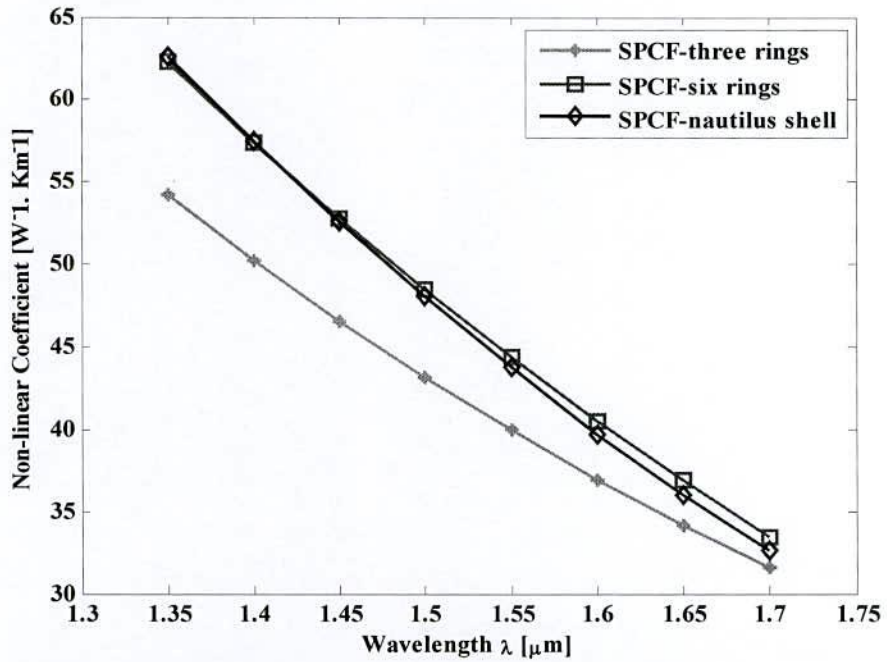


Fig. 5.49 Comparison between non-linear coefficients for the proposed DC-PCFs

A comparison between non-linear coefficients has been presented in Fig. 5.49. Non-linear coefficients are highest for six rings SPCF and nautilus shell SPCF and are about same.

5.6 Conclusion

Some designs of broadband DC-PCFs with high negative dispersion coefficient over a wide band of wavelength for effective dispersion compensation of SMF have been presented based on the FEM. According to numerical results the proposed designs provide high average negative dispersion coefficient with flattened profile. At the same time the proposed DC-PCFs ensure the dispersion slope within negative to positive ranging which allows the designed fibers to be suitable for compensating 40Gbps covering E, S, C, L and U communication bands. The proposed DC-PCFs exhibit high birefringence of order 10^{-2} with the high negative average dispersion characteristics which eliminate the effect of PMD along with chromatic dispersion. The characteristics of broadband dispersion compensation and high birefringence make the proposed fibers potential candidates as its application in the fiber optic communication link in the telecommunication window. It will be a significant design to determine high non-linear coefficients by using only one material that helps to diminish the footprint and power consumption of various optical mechanisms.

References

- [1] F. Begum, Y. Namihira, S. M. A. Razzak, S. F. Kaijage, N. H. Hai, T. Kinjo, K. Miyagi, N. Zou, "Novel broadband dispersion compensating photonic crystal fibers: Applications in high speed transmission," *Optic and Laser Technology*, vol. 41, no. 6, pp. 679-686, Sep. 2009.
- [2] M. Selim Habib, M. Samiul Habib, S. M. A. Razzak, Y. Namihira, M. A. Hossain, and M. A. G Khan, "Broadband dispersion compensation of conventional single mode fibers using microstructure optical fibers," *Optik-International Journal for Light and Electron Optics*, vol. 124, no. 19, pp. 3851-3855, Oct. 2013.
- [3] J. Mondal, M. Shaifur Rahman, "Design of highly birefringent dispersion compensating spiral photonic crystal fiber," *International Conference on Electrical Engineering and Information Communication Technology (ICEEICT 2015)*, 22 May, 2015.
- [4] F. Poli, A. Cucinotta, S. Selleri, and A. H. Bouk, "Tailoring of flattened dispersion in highly nonlinear photonic crystal fibers," *IEEE Photonics Technology Letters*, vol. 16, pp. 1065-1067, 2004.
- [5] Chengcheng Gui and Jian Wang, "Elliptical-Spiral photonic crystal fibers with wideband high birefringence, large nonlinearity, and low dispersion," *IEEE Photonics Journal*, vol. 4, no. 6, pp. 2152-2158, Dec. 2012.
- [6] Md. Samiul Habib, K. M. Nasim, Md. Selim Habib, Md. Imran Hasan and Redwan Ahmad, "Relative dispersion slope matched dispersion compensating highly birefringent spiral microstructure optical fibers using defected core," *Opt. Eng.*, vol. 52, no. 9, pp. 096110-5, Sep. 2013.
- [7] Jianfei Liao, Junqiang Sun, Mingdi Du, and Yi Qin, "Highly nonlinear dispersion-flattened slotted spiral photonic crystal fibers," *IEEE Photonics Technology Letters*, vol. 26, no. 4, Feb. 2014.
- [8] S. G. Leon-Saval, T. A. Birks, N. Y. Joy, A. K. George, W. J. Wadsworth, G. Kakarantzas, and P. St. J. Rusell, "Splice-free interfacing of photonic crystal fibers," *Optics Letters*, vol. 30, pp. 1629-1631, 2005.
- [9] F. Kaijage, Y. Namihira, N. H. Hai, F. Begum, S. M. A. Razzak, T. Kinjo, K. Miyagi, and N. Zou, "Broadband dispersion compensating octagonal photonic crystal fiber for optical communication applications," *Japanese Journal of Applied Physics*, vol. 48, 2009.

- [10] S. K. Varshney, T. Fujisawa, K. Saitoh, and M. Koshiba, "Design and analysis of a broadband dispersion compensating photonic crystal fiber Raman amplifier operating in S-band," *Optics Express*, vol. 14, no. 8, pp. 3528-3540, Apr. 2006.
- [11] M. A. R. Franco, V. A. Serrão, and F. Sircilli, "Microstructured optical fiber for residual dispersion compensation over S+C+L+U wavelength bands," *IEEE Photon. Technol. Lett.*, vol. 20, no. 9, pp. 751-753, May, 2008.
- [12] J. P. Silva, D. S. Bezerra, V. F. R. Esquerre, I. E. Fonseca, and H. E. H. Figueroa, "Ge-doped defect-core microstructured fiber design by genetic algorithm for residual dispersion compensation," *IEEE Photon. Technol. Lett.*, vol. 22, no. 18, pp. 1337-1339, Sep. 2010.
- [13] M. A. Islam and M. S. Alam, "Design of a polarization-maintaining equiangular spiral photonic crystal fiber for residual dispersion compensation over $E + S + C + L + U$ wavelength bands," *IEEE Photon. Technol. Lett.*, vol. 24, no. 11, pp. 930-932, Jun. 1, 2012.
- [14] J. F. Liao, J. Q. Sun, Y. Qin, and M. Du, "Ultra-flattened chromatic dispersion and highly nonlinear photonic crystal fibers with ultralow confinement loss employing hybrid cladding," *Opt. Fiber Technol.*, vol. 19, no. 5, pp. 468-475, Oct. 2013.
- [15] P. J. Roberts, B. J. Mangan, H. Sabert, F. Couny, T. A. Birks, J. C. Knight, and P. St. J. Russell, "Control of dispersion in photonic crystal fibers," *Journal of Optical Fiber Communication Report*, vol. 2 pp. 435-461, 2005.
- [16] S. M. A. Razzak, and Y. Namihira, "Highly birefringent photonic crystal fibers with near zero dispersion at 1550 nm wavelength," *Journal of Modern Optics*, vol. 56, pp. 1188-1193, 2009.
- [17] S. Revathi, Srinivasa Rao Inbathini and Rizwan Ali Saifudeen, "Highly nonlinear and birefringent spiral photonic crystal fiber," *Advances in OptoElectronics*, vol. 2014, Article ID 464391, 6 pages, Jun 2014.
- [18] M. Mejbaul Haque, M. Shaifur Rahman, M. Selim Habib and M. Samiul Habib "A single mode hybrid cladding circular photonic crystal fiber dispersion compensation and sensing applications," *Photonics and Nanostructures-Fundamentals and Applications*, pp.493-500, January 2015.
- [19] M. Mejbaul Haque, M. Shaifur Rahman, M. Samiul Habib, and S. M. A. Razzak. "Design and characterization of single mode circular photonic crystal fiber for broadband dispersion compensation," *Optik-International Journal for Light and Electron Optics*, vol. 125, no.11 pp.2608-2611, 2014.

- [20] M. Selim Habib, M. Mejbaul Haque, M. Samiul Habib, M.I. Hasan and M. Shaifur Rahman and S.M.A. Razzak "Polarization maintaining holey fibers for residual dispersion compensation over S+C+L wavelength bands," *Optik*, vol.125, pp.911–915,2014.

CHAPTER VI

Conclusions and Directions for Future Work

6.1 Conclusion

The broad aims of the work undertaken in this thesis have been reported in two categories: Nearly Zero Dispersion Fiber (NZDF) at operating wavelength at 1550 nm and broadband DC-PCFs by using spiral to design, characterize and optimize Photonic Crystal Fiber (PCF) for practical applications with current optical systems. This was achieved in the work reported and in the examples chosen by implementing the rigorous full vectorial Finite Element Method (FEM) with the conformal transformation and the Perfectly Matched Layer (PML) boundary. Several materials with doping concentration used in the simulations included silica for a wavelength of 1.55 μm . As well as different geometries such as defected and asymmetry core have been proposed which is a new idea.

The research carried out and presented in this thesis to meet NZDF, following objectives have been reported (1) modeling of NZDF for ZDWs using COMSOL Multiphysics 4.2 which is based on FEM, (2) analysis of effective area and hence its potential difficulties in SCG where small effective area is desirable, (3) requirement of better nonlinearity with this smaller effective area may make it easier to invent devices using nonlinear optical fiber effects such as the generation of self-phase modulation (SPM), four-wave mixing, Raman scattering, and soliton generation, (4) investigation of the confinement loss of the proposed designs. The effective refractive index, n_{eff} of the fundamental mode was found by numerical simulation of the proposed dd-SPCF and DC-PCFs using COMSOL Multiphysics 4.2. Subsequently properties mentioned above were determined using some computations presented in section 3.4 and 4.2. However, the proposed spiral NZDE by using dd-SPCF showed a dispersion of about -0.000169 ps/(nm.km) at 1550 nm is a novel design. Although, it experienced a drastic change in dispersion when pitch, Λ and first ring diameter d_1 , is varied up to $\pm 2\%$. Consequently, effective area was small as well as large nonlinearity in particular; at 1550 nm the value of effective area was 2.6516 μm^2 and nonlinearity was 76.44 $W^{-1}\text{km}^{-1}$ respectively. Confinement loss is another important feature was within permissible limit and was further decreased with increasing the third air hole diameter d_3 of the arm. So, the proposed dd-SPCF is beneficial for emphasizing the nonlinear effect such as supercontinuum generation and guiding media.

The proposed novel SPCF designs in this thesis for dispersion compensation, following objectives have been reported: (1) modeling of broadband DC-PCFs for effective dispersion compensation of SMF including three rings SPCF, SPCF- distribution sunflower seeds and SPCF-nautilus shell using COMSOL Multiphysics 4.2 which is based on FEM, (2) requirement of the broadband dispersion compensation, (3) investigation of high negative dispersion phenomenon in the designed DC-PCFs that is needed to compensate the positive dispersion of the SMF during transmission of signals, (4) investigation of the dispersion accuracy of the proposed designs using global diameter variation and individual design parameter variation (5) analysis of high birefringence properties of the proposed fibers to eliminate the effect of PMD, (7) analysis of effective area and hence its potential difficulties in the input coupling and output coupling of light, (8) investigation of the nonlinear coefficient of the proposed designs and its effect on nonlinear mechanism of fiber accessories, (9) effective dispersion to judge the dispersion compensation capability of the proposed DC-PCFs, (10) investigation of the confinement loss of the proposed designs and the length required to compensate the accumulated dispersion of SMF, (11) investigation of the number of modes supported by the proposed DC-PCFs. However, the proposed three rings SPCF showed average high negative dispersion of about -355.89 ps/(nm.km) from S to U band for the optimum design parameters. In addition, it has a PML effect in dispersion that may cause hamper in manufacturing. Although, it experienced a drastic change in X and Y-polarization with wavelength and dispersion variation is high about 11.8 ps/(nm.km) over the wavelength ranging from 1450 to 1700 nm. Hence, three rings SPCF could be applicable for broadband dispersion compensation in a high bit rate transmission systems especially in the S to U communication band. However, the effective area was small and in particular, at 1550 nm the value of effective area was $2.334 \mu m^2$. Consequently, nonlinear coefficient is not enough, about $39.9333 W^{-1} km^{-1}$. In addition, the confinement loss was within permissible limit and was further decreased with increasing the number of air hole rings. Moreover, the most desirable birefringence property that unable to eradicate the effect of PMD was 10^{-2} order and finitely was 0.0175 . With the aim of improving the flattened profile over wideband and enlarging the nonlinearity, the SPCF has been modified. Hence, it was named six rings SPCF just like as distribution sunflower seeds. However, the six rings SPCF showed average high negative dispersion of about -396.33 ps/(nm.km) for Y-polarization with dispersion variation 9.34 ps/(nm.km) which is more flattened than three rings SPCF and -609.32 ps/(nm.km) for X-polarization from E to U band for the optimum

design parameters. The birefringence is nearly equal to three rings SPCF at 1550 nm wavelength. The change in dispersion due to the fiber's structural parameter variation and also for fiber's global diameter variation was found consistent. Additionally, the nonlinearity of six rings SPCF was found $44.3679 \text{ W}^{-1}\text{km}^{-1}$ is high. Thus, the proposed six rings SPCF should be applied for broadband dispersion compensation of SMF. The effective area was also decreased significantly in comparison with three rings SPCF and it was 2.101 at 1550nm wavelength. Nevertheless, the confinement loss for the proposed six rings SPCF is higher than that of other designs. Finally, the SPCF-nautilus shell has been further presented to achieve better results than that of two fibers. However, it demonstrated lower dispersion variation $5.02 \text{ ps}/(\text{nm}\cdot\text{km})$ over E to U band of average negative dispersion of about $-341.73 \text{ ps}/(\text{nm}\cdot\text{km})$ compared to six rings SPCF. The birefringence, effective area and non-linearity of SPCF-nautilus shell were found about same compared to other two proposed fibers. The number of modes supported by the proposed DC-PCFs has been checked with the help of effective V-parameter. However, effective V-parameter V_{eff} was found less than 2.627581 for all three proposed DC-PCFs. Thus, the proposed fiber would have only support single mode and hence no multimode dispersion will be incurred during the operation as broadband DCF. It should also be mentioned that the proposed fiber would be suitable for a number of future application such as PM devices and sensing system due to its high birefringence.

6.2 Directions for future work

There are a number of issues that require further investigations. These include:

- The ring model discussed in this work has been developed for PCFs with spiral hole arrangement such as distribution sunflower seeds and nautilus shell. Extending the modeling effort to other spiral hole arrangements, such as helix and galaxies would be useful.
- Several near zero dispersion, dispersion compensating and large/small effective area of spiral fiber designs made from silica-based and doped silica materials have been analyzed. Investigating other SPCFs designs made from polymers, chalcogenide glasses or non-silica based materials might reveal SPCF designs with attractive transmission properties as well.
- Effective area method can be adopted for detailed characterization of such structures. Since the proposed structure are optimized for short length nonlinear

applications with submicron core sizes dispersion controlling of higher order modes will be necessary for more efficient energy coupling between different wavelengths.

- The present model provides a crude estimate of leakage loss. Appropriate modifications in the outer cladding layer of the ring model is expected to improve the estimation of leakage loss
- To reduce the complexity during fabrication process of the fibers, structural parameter should be minimum. So, efforts should be given to reduce the number of structural parameters.

The research reported in the thesis has opened up scope for further work which could be carried out in this field by prospective students. All areas studied here provide scope for further study to enhance the designs needed for better optical fiber-based devices. Thus overall there is considerable opportunity for on-going research in this field which could positively impact the community.

List of Publications

- [1] **J. Mondal**, M. Shaifur Rahman, "Design of highly birefringent dispersion compensating spiral photonic crystal fiber," *International Conference on Electrical Engineering and Information Communication Technology (ICEEICT), IEEE*, 22 May, 2015.
- [2] **Japatoosh Mondal**, Ashraful Hossain Howlader, Mohammad Shaifur Rahman, "Highly Birefringent Wideband Residual Dispersion Compensating Photonic Crystal Fiber," *Progress in Electromagnetic Research(PIER)*, Submitted, 2015.
- [3] **J. Mondal**, M. S. Hossain, M.S. Rahman, "Dispersion and Nonlinear Characteristics of a Doping Defected Core Spiral Photonic Crystal Fiber," *Journal of Microwaves, Optoelectronics and Electromagnetic Applications, Vol. X, No. Y*, , Submitted,2015.